

แผ่นผ้าไหมวัสดุเสริมแรงทางเลือกสำหรับอีพอกซีคอมพอสิต

นางสาวณัฐริดา ไชยสมคุณ

วิทยานิพนธ์นี้เป็นส่วนหนึ่งของการศึกษาตามหลักสูตรปริญญาวิศวกรรมศาสตรมหาบัณฑิต

สาขาวิชาวิศวกรรมพอลิเมอร์

มหาวิทยาลัยเทคโนโลยีสุรนารี

ปีการศึกษา 2555

**SILK FABRIC AS ALTERNATIVE REINFORCEMENT
FOR EPOXY COMPOSITE**

Nattida Chaisomkul

**A Thesis Submitted in Partial Fulfillment of the Requirements for the
Degree of Master of Engineering in Polymer Engineering
Suranaree University of Technology
Academic Year 2012**

SILK FABRIC AS ALTERNATIVE REINFORCEMENT FOR EPOXY COMPOSITE

Suranaree University of Technology has approved this thesis submitted in partial fulfillment of the requirements for a Master's Degree.

Thesis Examining Committee

(Asst. Prof. Dr. Utai Meekum)

Chairperson

(Asst. Prof. Dr. Wimonlak Sutapun)

Member (Thesis Advisor)

(Asst. Prof. Dr. Nitinat Suppakarn)

Member

(Asst. Prof. Dr. Kasama Jarukumjorn)

Member

(Asst. Prof. Dr. Pranee Chumsumrong)

Member

(Prof. Dr. Sukit Limpijumnong)

Vice Rector for Academic Affairs

(Assoc. Prof. Flt. Lt. Dr. Kontorn Chamniprasart)

Dean of Institute of Engineering

ณัฐธิดา ไชยสมคุณ : ผืนผ้าไหมวัสดุเสริมแรงทางเลือกสำหรับอีพอกซีคอมพอสิต (SILK FABRIC AS ALTERNATIVE REINFORCEMENT FOR EPOXY COMPOSITE)

อาจารย์ที่ปรึกษา : ผู้ช่วยศาสตราจารย์ ดร.วิมลลักษณ์ สุตะพันธ์, 176 หน้า.

งานวิจัยนี้เป็นการศึกษาการใช้ผืนผ้าไหมเป็นวัสดุเสริมแรงสำหรับวัสดุอีพอกซีคอมพอสิตชนิด ไดกรีซิดิล อีเทอร์ ออฟ บิสฟีนอลเอ (DGEBA) โดยผืนผ้าไหมที่ใช้ในการเตรียมอีพอกซีคอมพอสิตที่ใช้มีสองชนิดคือ ผืนผ้าไหมที่ไม่ผ่านการปรับปรุงสภาพพื้นผิว (UT-SF) และผืนผ้าไหมที่ผ่านการปรับปรุงสภาพพื้นผิวด้วยสารกลุ่มควาไซเลนชนิด APTES (ST-SF) และได้ศึกษาสมบัติทางกายภาพและสัณฐานวิทยาของ UT-SF, ST-SF, ผืนผ้าใยแก้วและผืนผ้าเคฟลาร์ อีกทั้งยังศึกษาผลของปริมาณผืนผ้า ผลของการปรับปรุงพื้นผิวของผืนผ้าไหมด้วยสารกลุ่มควาไซเลน APTES ที่มีต่อสมบัติทางกายภาพของอีพอกซีคอมพอสิต อีพอกซีคอมพอสิตที่เตรียมคือ อีพอกซีและ UT-SF คอมพอสิต อีพอกซีและ ST-SF คอมพอสิต อีพอกซีและผืนผ้าใยแก้วคอมพอสิตและอีพอกซีและผืนผ้าเคฟลาร์คอมพอสิต ในการขึ้นรูปอีพอกซีคอมพอสิตใช้เทคนิคการขึ้นรูปด้วยมือ คอมพอสิตที่เตรียมจะใช้สัดส่วนโดยมวลของ UT-SF 0, 0.10, 0.15, 0.18, 0.30 และ 0.35 สัดส่วนโดยมวลของ ST-SF 0, 0.18, 0.30 และ 0.35 สัดส่วนโดยมวลของผืนผ้าใยแก้วและผืนผ้าเคฟลาร์ คือ 0.35 นอกจากนี้ยังได้ทดสอบสมบัติทางกล สมบัติทางความร้อนและสภาวะพื้นผิวแตกหักของอีพอกซีคอมพอสิตที่เตรียมจาก UT-SF, ST-SF, ผืนผ้าใยแก้วและผืนผ้าเคฟลาร์

จากการปรับปรุงสภาพพื้นผิวด้วยสารกลุ่มควาไซเลนพบว่าความทนแรงดึงและค่าความเสถียรต่อความร้อนของผืนผ้า ST-SF มีค่าสูงกว่าของ UT-SF ภาพจากกล้องจุลทรรศน์อิเล็กตรอนแบบส่องกราด แสดงให้เห็นว่า ST-SF มีพื้นผิวที่ขรุขระมากกว่า UT-SF ซึ่งผลจากการวิเคราะห์หุ้มฟังก์ชันด้วยเทคนิคอินฟราเรดสเปกโตรสโคปีและเทคนิคเอ็กซ์เรย์ฟลูออเรสเซนซ์สเปกโตรสโคปี แสดงให้เห็นว่ามีสารกลุ่มควาไซเลนอยู่ที่พื้นผิวของ ST-SF

จากการศึกษาอีพอกซีและ UT-SF คอมพอสิต พบว่า ยังมีมอดูลัส ความทนแรงดึง ความต้านทานต่อแรงกระแทก มอดูลัสตัดโค้ง และ ความทนแรงตัดโค้งของอีพอกซีและ UT-SF คอมพอสิตมีแนวโน้มเพิ่มขึ้นเมื่อปริมาณสัดส่วนโดยมวลของ UT-SF มากกว่า 0.18 เมื่อปริมาณสัดส่วนโดยมวลของ UT-SF เพิ่มขึ้น อุณหภูมิการเกิดโครงสร้างร่างแห (T_{cure}) ของอีพอกซีคอมพอสิตเพิ่มขึ้น ในขณะที่อุณหภูมิการเปลี่ยนสถานะคล้ายแก้ว (T_g) ที่ได้จากการให้ความร้อนครั้งที่หนึ่ง และ T_g ของอีพอกซีคอมพอสิตที่ปฏิกิริยาการเกิดโครงสร้างร่างแหสมบูรณ์ลดลงเมื่อสัดส่วนโดยมวลของ UT-SF เพิ่มขึ้น ภาพจากกล้องจุลทรรศน์อิเล็กตรอนแบบส่องกราดแสดงให้เห็นว่าอีพอกซีและ UT-SF คอมพอสิต มีพฤติกรรมการแตกหักแบบเปราะ

จากการศึกษาอีพอกซีและ ST-SF คอมพอสิต พบว่า ยังมีมอดูลัส ความทนแรงดึง ค่ามอดูลัสดัดโค้ง และความทนแรงดัดโค้งของอีพอกซีและ ST-SF คอมพอสิต และอีพอกซีและ UT-SF คอมพอสิตไม่ได้แตกต่างกันอย่างมีนัยสำคัญ อุณหภูมิการเกิดโครงสร้างร่างแหของ อีพอกซีและ ST-SF คอมพอสิตมีค่าน้อยกว่าอีพอกซีและ UT-SF คอมพอสิตในขณะที่ค่า T_g ของอีพอกซีและ ST-SF คอมพอสิตที่ได้จากการให้ความร้อนครั้งที่หนึ่ง และค่า T_g หลังการเกิดปฏิกิริยาโครงสร้างร่างแหแบบสมบูรณ์สูงกว่าอีพอกซีและ UT-SF คอมพอสิต นอกจากนี้ภาพจากกล้องจุลทรรศน์อิเล็กตรอนแบบส่องกราดแสดงให้เห็นว่าการยึดติดกันระหว่างพื้นผิวของ ST-SF และอีพอกซีดีกว่าการยึดติดระหว่างอีพอกซีและ UT-SF อย่างไรก็ตามอีพอกซีและ ST-SF คอมพอสิตมีพฤติกรรมแตกหักแบบเปราะ

ยังมีมอดูลัส ความทนแรงดึง ความต้านทานต่อแรงกระแทก มอดูลัสดัดโค้ง และความทนแรงดัดโค้งของวัสดุ อีพอกซีและ ST-SF คอมพอสิต มีค่าต่ำกว่าอีพอกซีและเส้นใยแก้วคอมพอสิต และ อีพอกซีและเส้นใยเคฟลาร์คอมพอสิต อย่างไรก็ตามอุณหภูมิการเกิดโครงสร้างร่างแหของอีพอกซีและ ST-SF คอมพอสิต มีค่าใกล้เคียงกับอีพอกซีและเส้นใยแก้วคอมพอสิตแต่มีค่าสูงกว่าอีพอกซีและเส้นใยเคฟลาร์คอมพอสิตในขณะที่ค่า T_g ของวัสดุ อีพอกซีและ ST-SF คอมพอสิต ที่ได้จากการให้ความร้อนครั้งที่หนึ่งและค่า T_g หลังการเกิดปฏิกิริยาโครงสร้างร่างแหแบบสมบูรณ์มีค่าสูงกว่าของอีพอกซีและเส้นใยแก้วคอมพอสิตและอีพอกซีและเส้นใยเคฟลาร์คอมพอสิต

สาขาวิชา วิศวกรรมพอลิเมอร์

ปีการศึกษา 2555

ลายมือชื่อนักศึกษา _____

ลายมือชื่ออาจารย์ที่ปรึกษา _____

ลายมือชื่ออาจารย์ที่ปรึกษาร่วม _____

NATTIDA CHAISOMKUL: SILK FABRIC AS ALTERNATIVE
REINFORCEMENT FOR EPOXY COMPOSITE. THESIS ADVISOR:
ASST. PROF. WIMONLAK SUTAPUN, Ph.D., 176 PP.

SILK FIBER/EPOXY COMPOSITE/SILK REINFORCED EPOXY COMPOSITE

In this research work, silk fabric was used as a reinforcement for epoxy (diglycidyl ether of bisphenol A, DGEBA) composite. Two types of silk fabric were used, untreated silk fabric (UT-SF) and silane treated silk fabric (ST-SF). Physical properties and surface morphology of UT-SF, ST-SF, glass fabric and Kevlar fabric were comparatively examined. Effect of fabric content and APTES treatment on physical properties of epoxy composites was examined, as well. The UT-SF/epoxy, ST-SF/epoxy, glass fabric/epoxy and Kevlar fabric/epoxy composites were prepared by hand lay-up technique. The UT-SF/epoxy composites were prepared at UT-SF weight fraction of 0, 0.10, 0.15, 0.18, 0.30 and 0.35. The ST-SF/epoxy composites were prepared at ST-SF weight fraction of 0, 0.18, 0.30 and 0.35. Glass fabric/epoxy composite and Kevlar fabric/epoxy composites were prepared at the fabric weight fraction of 0.35. In addition, mechanical properties, thermal properties and fracture surface morphology of UT-SF/epoxy, ST-SF/epoxy, glass fabric/epoxy and Kevlar fabric/epoxy composite were examined.

By the APTES treatment, tensile properties and thermal stability of ST-SF were better than that of UT-SF. SEM micrographs showed that ST-SF surface was rougher than that of UT-SF. It was confirmed by FT-IR and XRF spectroscopy that APTES deposited onto the ST-SF surface.

For UT-SF/epoxy composite, Young's modulus, tensile strength, impact strength, flexural modulus and flexural strength increased as UT-SF weight fraction was higher than 0.18. With increasing UT-SF content, curing temperature (T_{cure}) of UT-SF/epoxy composites increased with increasing UT-SF content whereas glass transition temperature (T_g) from the 1st heating scan and T_g of the fully cured epoxy composite decreased. UT-SF/epoxy composites broke in a brittle manner.

For ST-SF/epoxy composite, Young's modulus, tensile strength, flexural modulus and flexural strength of ST-SF/epoxy composites were insignificantly different from those of UT-SF/epoxy composite. T_{cure} of ST-SF/epoxy composite was lower than that of UT-SF/epoxy composites whereas T_g obtained from the 1st heating and T_g of the fully cured of ST-SF/epoxy composites was higher than those of UT-SF/epoxy composites. In addition, SEM micrographs showed that the interfacial adhesion between silk fabric and epoxy matrix of ST-SF/epoxy composites was better than that of UT-SF/epoxy composites. However, ST-SF/epoxy composites still broke in a brittle manner.

Young's modulus, tensile strength, impact strength, flexural modulus and flexural strength of ST-SF/epoxy composite were lower than those of glass fabric/composite and Kevlar fabric/composite. However, T_{cure} of ST-SF/epoxy composite was similar to that of glass fabric/composite but higher than that of Kevlar fabric/composite. T_g observed from the 1st heating and T_g of fully cured ST-SF/epoxy composite were higher than those of glass fabric/epoxy composite and much higher than that Kevlar/epoxy composite.

School of Polymer Engineering

Student's Signature _____

Academic Year 2012

Advisor's Signature _____

Co-advisor's Signature _____

ACKNOWLEDGEMENTS

The author wishes to acknowledgement the funding support from Suranaree University of Technology and Center of Excellence on Petrochemical, and Materials Technology. The grateful thanks and appreciation are given to the thesis advisor, Asst. Prof. Wimonlak Sutapun, for her consistent supervision, advice, and support throughout this project. Special thanks are also extended to Asst. Prof. Nitinat Suppakarn for her valuable suggestion and guidance given as a thesis coadvisor. The author is also grateful to all the faculty and staff members of the School of Polymer Engineering and the Center for Scientific and Technological Equipment of Suranaree University of Technology for their help and assistance throughout the period of this study. The author wishes to thank Queen Sirikit Sericulture Center (Nakhon Ratchasima) for providing the equipment facility for fiber tensile test.

Finally, I thank my parents and teachers who support and encourage me throughout the course of this study at the Suranaree University of Technology.

Nattida Chaisomkul

TABLE OF CONTENTS

	Page
ABSTRACT (THAI)	I
ABSTRACT (ENGLISH)	III
ACKNOWLEDGEMENTS	V
TABLE OF CONTENTS.....	VI
LIST OF TABLES	XII
LIST OF FIGURES	XVII
SYMBOLS AND ABBREVIATIONS.....	XXV
CHAPTER	
I INTRODUCTION	1
1.1 Background.....	1
1.2 Motivation.....	4
1.3 Research objective	6
1.4 Scope and limitation of the research.....	6
II LITERATURE REVIEW	8
2.1 Epoxy resin	8
2.1.1 Type and chemical structure of epoxy	9
2.1.2 Type of hardener	11
2.1.3 Curing reaction.....	13

TABLE OF CONTENTS (Continued)

	Page
2.1.4 Factor affecting physical properties of cured epoxy resin.....	16
2.1.5 Mechanical properties of DGEBA and TETA system	16
2.1.6 Thermal properties of DGEBA and TETA system	17
2.1.7 Fracture surface of neat epoxy	19
2.1.8 Effect of hardener ratio on tensile properties of neat epoxy and fracture surface morphology	20
2.1.9 Effect of loading rate on mechanical properties and fracture surface morphology	24
2.1.10 Effect of curing condition on mechanical properties.....	25
2.1.11 Effect of temperature on mechanical properties and fracture surface morphology	27
2.2 Bombyx Mori (<i>B. mori</i>) silkworm silk	30
2.2.1 Structure of <i>B. mori</i> fiber	30
2.2.2 Chemical composition of <i>B.mori</i> silk fibroin	31

TABLE OF CONTENTS (Continued)

	Page
2.2.3	Microstructure and conformation of silk fibroin 36
2.2.4	Tensile properties and toughness 39
2.2.5	Thermal properties of silk 44
2.2.6	Silk fiber treatment 48
2.3	Fiber reinforced epoxy composite 54
2.3.1	Kevlar/epoxy composite 54
2.3.2	Glass/epoxy composite 58
2.3.3	Silk/epoxy composite 60
2.3.4	Fracture surface of fiber reinforced epoxy composite 62
III	EXPERIMENTAL 68
3.1	Materials 68
3.2	Experimental 69
3.2.1	Preparation of neat epoxy 69
3.2.2	Preparation of reinforcement fabrics 69
3.2.3	Preparation of epoxy composites 70
3.3	Material characterization 71
3.3.1	Characterization of reinforcement fabrics 71

TABLE OF CONTENTS (Continued)

	Page
3.3.1.1 Mechanical properties	71
3.3.1.2 Thermal properties	72
3.3.1.3 Chemical functional groups	72
3.3.1.4 Elemental composition.....	72
3.3.1.5 Surface morphology.....	73
3.3.2 Characterization of neat epoxy and epoxy composite.....	73
3.3.2.1 Mechanical properties	73
3.3.2.2 Thermal properties	74
3.3.2.3 Fracture surface morphology	75
IV RESULTS AND DISCUSSION	76
4.1 Physical properties of reinforcement fabrics	76
4.1.1 Mechanical properties	76
4.1.2 Chemical function groups and elemental composition of UT-SF and ST-SF	80
4.1.3 Thermal properties of silk fabric, glass fabric and Kevlar fabric	88

TABLE OF CONTENTS (Continued)

	Page
4.1.4 Surface morphology of silk fabric, glass fabric and Kevlar fabric	91
4.2 Effect of UT-SF content on physical properties of epoxy composite	94
4.2.1 Tensile properties	94
4.2.2 Flexural properties	96
4.2.3 Impact property	97
4.2.4 Heat distortion temperature	100
4.2.5 Thermal properties	101
4.2.6 Fracture surface morphology	108
4.3 Effect of silane treatment on physical properties of epoxy composite	112
4.3.1 Tensile properties	112
4.3.2 Impact property	114
4.3.3 Flexural properties	117
4.3.4 Heat distortion temperature	121
4.3.5 Thermal properties	122
4.3.6 Fracture surface morphology	129
4.4 The epoxy composite reinforced with ST-SF, glass fabric and Kevlar fabric	132

TABLE OF CONTENTS (Continued)

	Page
4.4.1 Mechanical properties of epoxy composite	132
4.4.2 Thermal properties of epoxy composite	138
4.4.3 Fracture surface morphology of the composites.....	145
V CONCLUSIONS	148
REFERENCES	151
APPENDICES	
APPENDIX A. STOICHIOMETRIC CALCULATION FOR EPOXY RESIN PREPARATION	163
APPENDIX B. PUBLICATIONS.....	166
BIOGRAPHY	176

LIST OF TABLES

Table	Page
1.1 Tensile properties of silk fiber, Kevlar fiber, glass fiber, carbon fiber and natural fiber.....	2
1.2 Tensile properties of silk and nylon fiber	5
2.1 Chemical structure of some commonly used epoxy	9
2.2 Chemical structure of some commonly used hardener	12
2.3 Tensile properties of epoxy with various hardener ratios.....	21
2.4 Tensile properties of epoxy resin with amine-cured epoxy prepared at curing temperature of 110°C with various curing times	26
2.5 Tensile properties of epoxy resin with anhydride-cured epoxy prepared at curing temperature of 110°C and post cured at 125°C with various post curing times	27
2.6 Composition of <i>B. mori</i> silk.....	31
2.7 Chemical structure of amino acids in <i>B. mori</i> silk fibroin.....	32
2.8 Tensile properties of silk, elastin fiber and Kevlar fiber	40
2.9 Tensile properties of silk thread.....	41
2.10 Tensile properties of silk with different condition of fibers	42
2.11 Tensile properties of silk fibers degummed with different chemical agents ...	43
2.12 Thermal properties of <i>B.mori</i> silk.....	46

LIST OF TABLES (Continued)

Table	Page
2.13	Tensile properties of untreated silk fabric and epoxy resin
	EFTA treated silk fabric.....54
2.14	Some mechanical properties of plain weaving glass/epoxy composite at fiber volume fraction of 0.4
	60
3.1	The number of fabric layers within epoxy composites reinforced with UT-SF, ST-SF, glass fabric and Kevlar fabric.....
	71
4.1	Slope, maximum force and elongation at break obtained from load-extension curve of UT-SF, ST-SF, glass fabric and Kevlar fabric.
	78
4.2	Normalized tensile properties of UT-SF, ST-SF, glass fabric and Kevlar fabric.....
	79
4.3	Assignment of FTIR band for UT-SF
	82
4.4	Summarized data corresponding to silk fibroin conformation
	83
4.5	Elemental compositions of UT-SF ash and ST-SF ash.....
	87
4.6	Summary of tensile properties, flexural properties, and impact strength of neat epoxy and UT-SF/epoxy composites with UT-SF weight fraction of 0.10-0.35.
	99
4.7	Heat distortion temperature of neat epoxy and UT-SF/epoxy composite with UT-SF weight fraction of 0.10-0.35.....
	100

LIST OF TABLES (Continued)

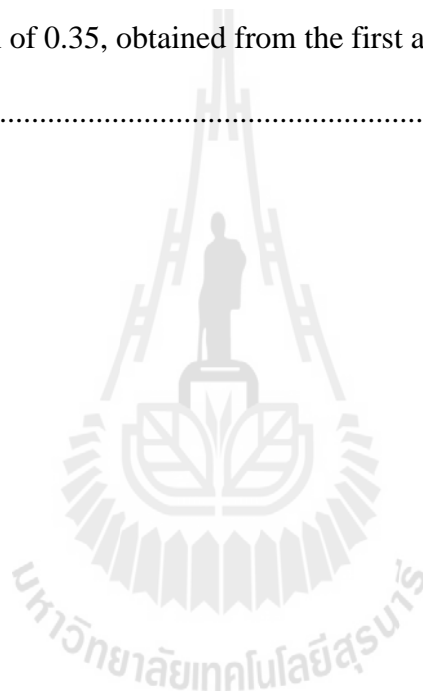
Table	Page
4.8 Thermal decomposition (T_d) of UT-SF, neat epoxy and epoxy composite prepared with various UT-SF weight fraction.....	103
4.9 Glass transition temperature (T_g) and curing temperature (T_{cure}) of neat epoxy before post curing and after post curing.....	104
4.10 Curing temperature (T_{cure}) of neat epoxy and epoxy composite at various UT-SF contents before post curing.....	105
4.11 Glass transition temperature (T_g) of neat epoxy and epoxy composite at various UT-SF contents, obtained from the first and the second heating scan.....	108
4.12 Tensile properties and impact property of UT-SF/epoxy composite and ST-SF/epoxy composite at various contents of silk fabric.	116
4.13 Flexural properties of UT-SF/epoxy composite and ST-SF/epoxy composite at various contents of silk fabric.	120
4.14 Heat distortion temperature of of epoxy composites at various weight fractions of UT-SF and ST-SF	121
4.15 Decomposition temperature of UT-SF/epoxy composite and ST-SF/epoxy composite prepared with fabric weight fraction of 0-0.35.....	125

LIST OF TABLES (Continued)

Table	Page
4.16 Curing temperature (T_{cure}) of UT-SF/epoxy composite and ST-SF/epoxy composite prepared with fabric weight fraction of 0-0.35	126
4.17 Glass transition temperature (T_g) of neat epoxy and epoxy composite at various silk fabric contents, obtained from the first and the second heating scan.....	129
4.18 Tensile properties, flexural properties and impact property of neat epoxy and ST-SF/epoxy composite, glass/epoxy composite and Kevlar/epoxy composite with fabric weight fraction of 0.35.....	136
4.19 Heat distortion temperature (HDT) of neat epoxy and ST-SF/epoxy composite, glass/epoxy composite and Kevlar/epoxy composite prepared at 0.35 reinforcement fabric.....	137
4.20 Thermal decomposition (T_d) of neat epoxy and epoxy composites prepared with ST-SF, glass fabric and Kevlar fabric at fabric fraction of 0.35	141
4.21 Curing temperature (T_{cure}) of neat epoxy and epoxy composites prepared with ST-SF, glass fabric and Kevlar fabric at fabric fraction of 0.35 before post curing	142

LIST OF TABLES (Continued)

Table	Page
4.22 Glass transition temperature (T_g) of ST-SF/epoxy composite, glass/epoxy composite and Kevlar/epoxy composite with the weight fraction of 0.35, obtained from the first and second heating scan.....	145



LIST OF FIGURES

Figure		Page
1.1	The unit cell of nylon fiber (a) and silk fiber (b)	5
2.1	Chemical structure of epoxide group	8
2.2	Synthesis of diglycidyl ether of bisphenol A, DGEBA, n~2	10
2.3	General cure reaction between a curing agent and epoxides	14
2.4	The curing mechanisms of epoxides with several types of curing agents	15
2.5	The curing mechanisms of epoxy/amine system	15
2.6	DSC curve of DGEBA/TETA at various epoxy/hardener ratio.....	18
2.7	DSC curve of epoxy: the first line for non-post cured sample (continuous line), the second line for isothermally at 170 °C for 10 minutes, cooled and afterwards examined by heating up to 220 °C (dashed line), and the third line for repeated measurement by heating up to 220 °C again	19
2.8	General fracture surface of neat epoxy	20
2.9	General topographic aspects of the fracture surface for the epoxy and hardener mixtures with phr \geq 13	23
2.10	Common relative sizes of the mirror zones: (a) phr 11; (b) phr 21	23
2.11	SEM micrographs of fracture surface of epoxy tested under 0.1 mm/min (a), 10 mm/min (b) and 1000 mm/min(c).....	25

LIST OF FIGURES (Continued)

Figure	Page
2.12	Fractographs of epoxy fractured at 300K (a), 77K (b) and 4.2K(c) related to type of crack growth of epoxy 29
2.13	The microstructure of <i>B.mori</i> fiber 30
2.14	Chemical structure of <i>B. mori</i> silk fibroin 32
2.15	SEM micrograph of <i>B.mori</i> silk fiber; Longitudinal section (A), Cross Section (B) 36
2.16	The model of <i>B.mori</i> silk conformation..... 37
2.17	FT-IR spectra of the different forms of silk fiber; <i>B. mori</i> silk with sericin (A) and <i>B. mori</i> silk without sericin (B)..... 39
2.18	The force-displacement curve of silk before and after submerged in water... 42
2.19	TGA curve of <i>B. Mori</i> silk..... 45
2.20	DSC thermograms of <i>B. mori</i> silk fiber with sericin and silk fiber without sericin..... 46
2.21	TMA curves of silk fibers degummed with different chemical agents..... 48
2.22	Chemical structure of silane ; (a) General structure and (b) APTES..... 49
2.23	Interaction between silk fiber and APTES..... 51
2.24	SEM micrograph of silk fabric; untreated (a) and silane treated silk fabric (b) 53
2.25	SEM micrograph of untreated carbon fiber/epoxy composite..... 63

LIST OF FIGURES (Continued)

Figure	Page
2.26	Fracture surfaces of untreated flax/epoxy composite in weft direction (a, b) and warp directions (c, d)..... 64
2.27	SEM micrograph of untreated flax fiber/epoxy composite..... 65
2.28	SEM micrographs of woven silk/epoxy obtained from impact testing specimen 67
4.1	Plot of load-extension curves of UT-SF, ST-SF, glass fabric, and Kevlar fabric obtained in warp and weft direction..... 76
4.2	FT-IR spectrum of UT-SF with wavenumber assignment..... 81
4.3	FT-IR spectra of UT-SF and ST-SF within wavenumber of 1200-600 cm^{-1} 85
4.4	FT-IR spectra of UT-SF and ST-SF corresponding to conformation 86
4.5	TGA (a) and DTGA (b) curves of UT-SF, ST-SF, glass fabric and Kevlar fabric 90
4.6	DSC curves of UT-SF, ST-SF, glass fabric and Kevlar fabric 91
4.7	SEM micrographs of UT-SF (a) and ST-SF (b) at a magnification of x1000 (1) and x5000 (2) and their cross-section at x1500 are (3). 92
4.8	SEM micrographs of glass fabric (a) and Kevlar fabric (b) at magnification of x5000..... 93

LIST OF FIGURES (Continued)

Figure	Page
4.9	Plot of Young's modulus and elongation at break of UT-SF/epoxy composite vs UT-SF weight fraction 94
4.10	Plot of tensile strength of UT-SF/epoxy composite vs UT-SF weight fraction..... 95
4.11	Plot of flexural modulus and flexural strength of UT-SF/epoxy composite vs UT-SF weight fraction 97
4.12	Plot of impact strength of UT-SF/epoxy composite vs UT-SF weight fraction..... 98
4.13	TGA (a) and DTGA (b) curves of neat epoxy and UT-SF epoxy composite with various UT-SF weight fractions 102
4.14	DSC thermograms of neat epoxy before and after post curing..... 104
4.15	DSC curves of neat epoxy and epoxy composite at various UT-SF weight fractions before post curing..... 105
4.16	DSC curves of neat epoxy and epoxy composite at various UT-SF weight fractions from the first heating scan (a) and from the second heating scan (b).. 107
4.17	SEM micrographs of (a) neat epoxy x250 and epoxy composites at (b) 0.10 UT-SF x40, (c) 0.15 UT-SF x50, (d) 0.18 UT-SF x40, (e) 0.30 UT-SF x40, and (f) 0.35 UT-SF x40 110

LIST OF FIGURES (Continued)

Figure	Page
4.18 SEM micrographs of epoxy composites at (a) 0.15 UT-SF, (b) 0.18 UT-SF, (c) 0.30 UT-SF, and (d) 0.35 UT-SF.....	111
4.19 Plot of Young's modulus of epoxy composite at various weight fractions of UT-SF and ST-SF	112
4.20 Plot of elongation at break of epoxy composite at various weight fractions of UT-SF and ST-SF	113
4.21 Plot of Tensile strengths of epoxy composite at various weight fractions of UT-SF and ST-SF	114
4.22 Plot of impact strength of epoxy composite at various weight fractions of UT-SF and ST-SF	115
4.23 Plot of flexural modulus of epoxy composite at various weight fractions of UT-SF and ST-SF	117
4.24 Plot of flexural strain at break of epoxy composite at various weight fractions of UT-SF and ST-SF	118
4.25 Plot of flexural strength of epoxy composite at various weight fractions of UT-SF and ST-SF	119
4.26 TGA (a) and DTGA (b) curves of neat epoxy and ST-SF/epoxy composites	123
4.27 TGA (a) and DTGA (b) curves of neat epoxy and UT-SF/epoxy composites.....	124

LIST OF FIGURES (Continued)

Figure	Page
4.28 DSC curves of neat epoxy and ST-SF/epoxy composite before post curing	126
4.29 DSC curves of neat epoxy and ST-SF/epoxy composites from the first heating scan (a) and from the second heating scan (b).....	128
4.30 SEM micrographs of (a) neat epoxy and ST-SF/epoxy composites at (b) 0.18 ST-SF, (c) 0.30 ST-SF and (d) 0.35 ST-SF.....	130
4.31 SEM micrographs, at fabric weight fraction of 0.18 of UT-SF/epoxy composites at magnification of x500 (a-b) and x1500 (c), and ST-SF/epoxy composites magnification of x500 (d-e) and x1500 (f).	131
4.32 Plot of Young's modulus and elongation at break (%) of neat epoxy and ST-SF/epoxy composite, glass fabric/epoxy composite and Kevlar/epoxy composite at weight fraction of 0.35	133
4.33 Plot of tensile strength and impact strength of neat epoxy and ST-SF/epoxy composite, glass fabric/epoxy composite and Kevlar/epoxy composite at weight fraction of 0.35	133

LIST OF FIGURES (Continued)

Figure	Page
4.34	Plot of flexural modulus of and flexural strain at break of neat epoxy and ST-SF/epoxy composite, glass fabric/ epoxy composite and Kevlar/epoxy composite at weight fraction of 0.35..... 134
4.35	Plot of flexural strength of neat epoxy and ST-SF/epoxy composite, glass fabric/epoxy composite and Kevlar/epoxy composite at weight fraction of 0.35..... 135
4.36	TGA (a) and DTGA (b) curves of neat epoxy and epoxy composites prepared with ST-SF, glass fabric and Kevlar fabric at weight fraction of 0.35..... 140
4.37	DSC curves of neat epoxy and epoxy composites prepared with ST-SF, glass fabric and Kevlar fabric at weight fraction of 0.35 before post curing 142
4.38	DSC curves neat epoxy and epoxy composites prepared with ST-SF, glass fabric and Kevlar fabric at fabric fraction of 0.35 from the first heating scan (a) and from the second heating scan (b). 144
4.39	SEM micrographs of epoxy composites with (a) 0.35 ST-SF, (b) 0.35 glass fabric and (c) 0.35 Kevlar fabric at a magnification of x100. 146

LIST OF FIGURES (Continued)

Figure	Page
4.40 SEM micrographs of epoxy composites with (a) 0.35 ST-SF, (b) 0.35 glass fabric and (c) 0.35 Kevlar fabric at a magnification of x300, x300 and x200, respectively.....	147



SYMBOLS AND ABBREVIATIONS

APTES	=	3-aminopropyltriethoxysilane
DGEBA	=	Diglycidyl ether of bisphenol A
TETA	=	Triethylenetetramine
ST-SF	=	Silane treated silk fabric
UT-SF	=	Untreated silk fabric



CHAPTER I

INTRODUCTION

1.1 Background

Thermosetting polymers are widely used as matrix material in polymer composites (Byung Chul Kim, Sang Wook Park, and Dai Gil Lee, 2008). Epoxy resin is one of the most important thermosets and widely used as a matrix in polymer composites, adhesives in the aerospace industry, binder in coatings, etc. Most of commercially available epoxy resin is oligomers of diglycidyl ether of bisphenol A, DGEBA (Rosu, Cascaval, Mastata, and Ciobanu, 2002). Epoxy are brittle in nature due to high crosslinking densities and they have poor crack resistance in real application (Bernd, Patrick, Frank, and Klaus, 2006; Mohamadreza, Reza, Pooyan, Mohamad, and Kouchakzadeh, 2009). Many reinforcement materials have been used for epoxy composite, both synthetic fibers and natural fibers, in either fabric or mat form. The synthetic fibers are nylon family fiber, glass fiber, polyethylene fiber and carbon fiber. The natural fibers are sisal fiber, flax fiber, plam fiber and waste silk fiber. Normally, the stiffness, strength and price of synthetic fibers are higher than those of natural fibers. For price of silk fiber and conventional fiber, price of *B. mori* silk, glass fiber and Kevlar fiber was 15-40 \$US/kg, 0.1-2.0 \$US/kg and 25-30 \$US/kg, respectively (Cristaldi, Latteri, Recca, and Cicala, 2010). However, silk fiber obtained from spider and silkworm are high in stiffness (Gosline, Guerette,

Ortlepp and Savage, 1999). Some mechanical properties of silkworm silk, Kevlar fiber, glass fiber and natural fiber are comparatively numbered in Table 1.1.

Table 1.1 Tensile properties of silk fiber, Kevlar fiber, glass fiber, carbon fiber and natural fibers (Ku, Wang, Pattarachaiyakoop, and Trada, 2011; Loh and Tan, 2011).

Materials	Density (g/cm ³)	Young's modulus (GPa)	Tensile strength (MPa)	Elongation at break (%)
<i>B.mori</i> silk fiber	1.31-1.38	8.5-8.6	500	15
<i>Araneus</i> spider silk	1.30	6.5	810	22
Kevlar fiber	1.44	130	3600-4100	2.8
glass fiber	2.5	76-79	3100-3800	4.8
Carbon fiber	1.40	235	4000	2
Sisal fiber	1.5	9.4-22	511-635	2.0-2.5
Flax fiber	1.5	27.6	500-1500	2.7-3.2
Hemp fiber	1.47	40	1000	2-4
Jute fiber	1.3	26.5	393-773	1.5-1.8

In addition, those synthetic fibers consumed natural resources as raw material for manufacturing in which if they are continuously consumed, it will be used up in the near future and they take times to regenerate. Silkworm fibers are naturally regenerated, an environmentally compatible and biodegradable material. Actually, it is a biopolymer containing amide linkage between specific fatty acids along the structural chain therefore it is considered to be a member of nylon family, as well. However, silkworm fibers have comparable stiffness and strength to those of nylon family material but higher in toughness.

Nylon is a synthetic polyamide. The widely used nylon fiber is nylon-6 and nylon-6/6. Applications for this fiber largely fall into two classes, woven (such as clothing textiles, carpets, and sails) and non-woven (such as tire reinforcement cord, ropes, fishing line, sports racket and guitar 'strings', and dental floss) (Stephen and David, 2005). Nylons were intended to be a synthetic replacement for silk and substituted for it in many different products after silk became scarce during World War II. It replaced silk in military applications such as parachutes and flak vests, and was used in many types of vehicle tires (Sonwalkar, 1993). However, nylon fiber is not degradable in nature. Besides, with emphasis of environmental awareness, the development of fiber technology needs to grow with the environmental friendly materials.

Silks are naturally occurring protein polymers produced by a wide variety of insects and spiders. The most widely studied silks are cocoon silk from the silkworm (*Bombyx mori*) (Yongzhong, Hyeon, Gordana, and David, 2006). Silk is one of the strongest fiber, only slightly less than steel wires, but concomitantly also one of the light weight fiber (2000 m of silk thread unwound from cocoon weight about 0.250 g) (Sonwalker, 1999). Silk has low density, high toughness, acceptable specific strength, recyclability, biodegradability and also less harmfulness. Moreover, it shows low electrical conductivity compared with the metal alloy and carbon fiber (Fongchan, 2005). Therefore, as a renewable, environmentally comparable and biodegradable along with exceptional stiffness and strength and super toughness, silk is considered to be used as epoxy reinforcement.

Recently, researchers have investigated the potential of silk fibroin as a candidate material for biomedical applications, especially for the care of skin injury

and tissue engineering, because of its distinctive biological properties such as good biocompatibility, good oxygen and water vapor permeability, biodegradability, and minimal inflammatory reaction (Yongzhong, *et al.*, 2006). Moreover, researcher has been used silk fiber as fiber reinforcement for structural material of solar car body due to its low cost, light weight as a potential alternatives to carbon fiber/epoxy composites (Zulkifli, Azhari, Maryam, Ahmad, and Abu, 2009). However, the smooth clean surface of the silk fiber leads to weak interfacial adhesion between silk fiber and epoxy matrix (Zulkifli, *et al.*, 2009). To improve interfacial adhesion between them, silane coupling agents are widely used to modify fiber surface. Silane coupling agent is a chemical substance capable of reacting with both of the fiber surface and the epoxy matrix. The coupling agents act as a bridge at the interfaces of both components.

For silk fiber, 3-aminopropyltriethoxysilane (APTES) is usually used to improve interfacial adhesion between silk fiber and epoxy matrix (Zulkifli, *et al.*, 2009). Zulkifli, *et al.* (2009) have been reported that 3-aminopropyltriethoxysilane treated woven silk fabric improved the interlaminar fracture toughness of woven silk/epoxy composites. In this work, the 3-aminopropyltriethoxysilane was used to modify silk fabric surface.

1.2 Motivation

Silk fiber is natural polyamide which related chemically with nylon fiber. For polyamide, the inter molecular forces are both van der waal's bonds and hydrogen bonds. The latter, entailing the NH and CO moieties, cause the formation of sheet like arrangement adjacent between chains. The stacking of these hydrogen-bonded sheets

control a size and shape of unit cell. As shown in Figure 1.1, the characteristics of size and shape of unit cell control the physical properties of polyamide fiber.

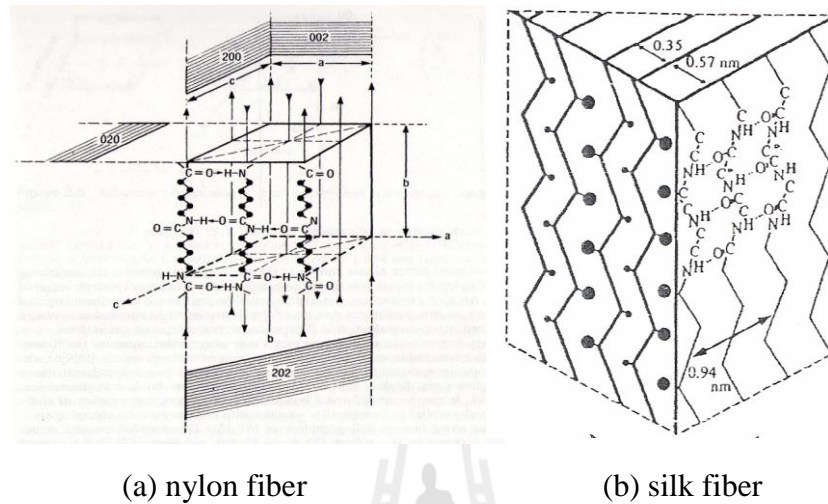


Figure 1.1 The unit cell of nylon fiber (a) and silk fiber (b) (Herbert, 1998).

In comparison, Table 1.2 shows the tensile properties of silk fiber and nylon fiber. The tensile strength and modulus, extensibility, and toughness of the *Bombyx mori* silk fiber (*B. mori* silk, mulberry silkworms) are quite similar to the nylon fiber. (John, Lin and Thomas, 2008).

Table 1.2 Tensile properties of silk and nylon fiber (John, Lin and Thomas, 2008).

Materials	Tensile modulus (GPa)	Tensile Strength, σ_{\max} (GPa)	Extensibility, ϵ_{\max} (%)	Toughness (mJ/m ³)
Silk <i>B.mori</i>	4.8	0.6	18.0	70.0
Nylon	2.7	0.9	18.0	80.0

The advantages of using silk as an reinforcing fiber are its renewable resources, a local product of Thailand, reduction of waste from synthetic fiber (plastics waste 2.5 million ton per year) (Eakkanalaksamee, 2005), disposal costs and reduction of energy consumed for producing synthetic fiber.

1.3 Research objectives

The main purposes of this research are as follows:

- (i) To use silk fabric as a reinforcement for epoxy composite.
- (ii) To study physical properties of reinforcement fabric for epoxy composite.
- (iii) To study the effect of silk content and chemical treatment on the mechanical properties of silk/epoxy composite.

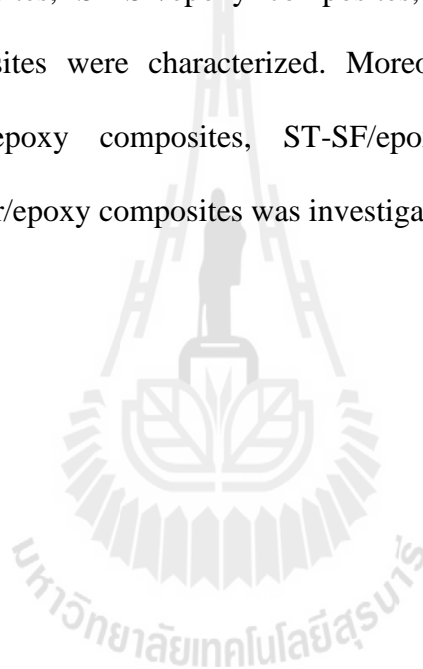
1.4 Scope and limitation of the research

The silk (*Bombyx mori*) fabric was used in a woven form. Two types of silk fabric were used, untreated silk fabric (UT-SF) and silane treated silk fabric (ST-SF). In this work, the 3-aminopropyltriethoxysilane (APTES) was used to modify silk fabric surface.

The neat epoxy was prepared and the deformer was used. The epoxy composite were prepared with various contents of UT-SF within a range of weight fraction 0.10-0.35. The epoxy composite prepared from ST-SF was molded at the fabric weight fraction of 0.18-0.35.

Then, the composites of ST-SF/epoxy composite, glass fabric/epoxy composite and, Kevlar/epoxy composite were prepared with the same fabric content at weight fraction of 0.35.

The thermal properties including DSC and TGA of UT-SF, ST-SF, glass fabric, Kevlar fabric were examined. The tensile properties of silk fabric, glass fabric and Kevlar fabric were also examined. Mechanical properties including tensile, flexural and impact properties of the neat epoxy, UT-SF/epoxy composites, ST-SF/epoxy composites, glass/epoxy composites and Kevlar/epoxy composites were investigated. In addition, thermal properties including DSC and TGA of neat epoxy, UT-SF/epoxy composites, ST-SF/epoxy composites, glass/epoxy composites and Kevlar/epoxy composites were characterized. Moreover, morphology of fracture surface of UT-SF/epoxy composites, ST-SF/epoxy composites, glass/epoxy composites and Kevlar/epoxy composites was investigated.



CHAPTER II

LITERATURE REVIEW

2.1 Epoxy resin

Epoxy resin has been commercialized since 1946 and widely used in industry as protective coatings and for structural applications, such as laminates and composites, tooling, molding, casting, bonding adhesives, etc. (May, 1988). Some of the characteristics of epoxy resin are high chemical and corrosion resistance, good mechanical and thermal properties, outstanding adhesion to various substrates, low shrinkage upon curing, good electrical insulating properties, and the ability to be processed under a variety of conditions. Depending on the specific needs for certain physical and mechanical properties, combinations of choices of epoxy resin and curing agent can usually be formulated to meet the market demands. Epoxy resin is the most important thermosetting polymers widely used as matrices in reinforced composite, as adhesive in aerospace industry, as binder in surface coatings, etc. (Asi, 2009). Epoxy resin is defined as a molecule containing more than one epoxide group. The epoxide group also termed as, oxirane or ethoxyline group, is shown in Figure 2.1.

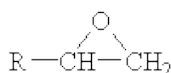


Figure 2.1 Chemical structure of epoxide group (May and Tanaka, 1973)

2.1.1 Type and chemical structure of epoxy

There are two main categories of epoxy resins, namely the glycidyl epoxy resin and non glycidyl epoxy resin. The glycidyl epoxies are further classified as glycidyl-ether, glycidyl-ester and glycidyl-amine. The non-glycidyl epoxies are either aliphatic or cycloaliphatic epoxy resins. Glycidyl epoxies are prepared via a condensation reaction of appropriate dihydroxy compound, dibasic acid or a diamine and epichlorohydrin. While, non-glycidyl epoxies are formed by peroxidation of olefinic double bond. Table 2.1 shows some of the commonly-used epoxy resins and their chemical structures (Lee and Neville, 1967).

Table 2.1 Chemical structure of some commonly used epoxy resins (Lee and Neville, 1967).

Type	Chemical structure
Diglycidyl ether of bisphenol-A (DGEBA)	
4,4 Diglycidyl ether of 3,3', 5,5'-tetramethyl biphenyl	
Tetrafunctional epoxy tetraglycidyl 4,4-diaminodiphenyl methane (TGDDM)	
Liquid crystalline epoxy resins (LCE)	
Ethylene glycol diglycidyl ether (EGDE)	

2.1.2 Types of hardener

Curing agents play an important role in the curing process of epoxy resin because they relate to the curing kinetics, reaction rate, gel time, degree of cure, viscosity, curing cycle, and the final properties of the cured products. Thus, many researchers have been studied the effect of curing agents on the curing process.

Mika and Bauer (1988) gave an overview of the epoxy curing agents and modifiers. They discussed three main types of curing agents. The first type of curing agents includes active hydrogen compounds and their derivatives. Compounds with amine, amides, hydroxyl, acid or acid anhydride groups belong to this type. They usually react with epoxy resin by polyaddition to result in an amine, ether, or ester. Aliphatic and aromatic polyamines, polyamides, and their derivatives are the commonly used amine type curing agents. The aliphatic amines are very reactive and have a short lifetime. Their applications are limited because they are usually volatile, toxic or irritating to eyes and skin and thus cause health problems. Compared to aliphatic amine, aromatic amines are less reactive, less harmful to people, and need higher cure temperature and longer cure time. Hydroxyl and anhydride curing agents are usually less reactive than amines and require a higher cure temperature and more cure time. They have longer lifetimes. Polyphenols are the more frequently used hydroxyl type curing agents. Polybasic acids and acid anhydrides are the acid and anhydride type curing agents that are widely used in the coating field. Table 2.2 gives a list of commonly used curing agents and their chemical structures.

The second type of curing agents includes the anionic and cationic initiators. They are used to catalyze the homopolymerization of epoxy resins. Molecules, which can provide an anion such as tertiary amine, secondary amines, and

metal alkoxides, are the effective anionic initiators for epoxy resins. Molecules that can provide a cation, such as the halides of tin, zinc, iron, and the fluoroborates of these metal, are the effective cationic initiators. The most important types of cationic initiators are the complexes of BF_3 . The third type of curing agents is called reactive cross linkers. They usually have higher equivalent weights and crosslink with the second hydroxyls of the epoxy resins or by self-condensation. Examples of this type of curing agents are melamine, phenol, and urea formaldehyde resins.

Table 2.2 Chemical structure of some commonly used hardener (Mika and Bauer, 1988.)

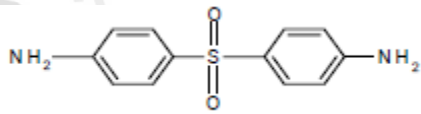
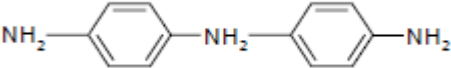
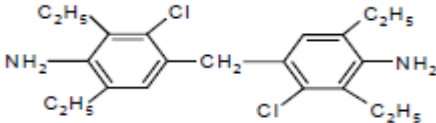
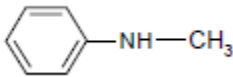
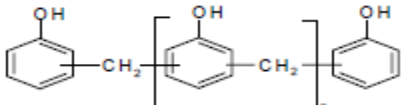
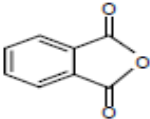
Type	Chemical structure
Diaminodiphenylsulfone (DDS)	
Diamino diphenyl methane (DDM)	
Methylene bis(chloro-diethyl-aniline) (MCDEA)	
Methylaniline	
Triethylenetetramine (TETA)	$\text{NH}_2 \left[\text{CH}_2 - \text{CH}_2 - \text{NH} \right]_2 \text{CH}_2 - \text{CH}_2 - \text{NH}_2$
Phenol novalac	

Table 2.2 Chemical structure of some commonly used hardener (Continued)

Type	Chemical structure
Phthalic anhydride	

Among three types of curing agents, compounds with active hydrogen are the most frequently used curing agents and have gained wide commercial success. Most anionic and cationic initiators have not been used commercially because of their long curing cycles and other poor cured product properties. Cross linkers are mainly used as surface coatings and usually are cured at high temperatures to produce films having good physical and chemical properties (Mika and Bauer, 1988.).

The selection of curing agents is a critical parameter. There are numerous types of chemical reagents that can react with epoxy resins. Besides affecting viscosity and reactivity of the formulation, curing agents determine both the types of chemical bonds formed and the functionality of the cross-link junctions that are formed. Thermal stability is affected by the structure of the hardener (Lee and Neville, 1967).

2.1.3 Curing reaction

Epoxy resins can be cured with a wide variety of curing agents. The choice of curing agents depends on the required physical and chemical properties, processing methods and curing conditions. The majority of curing agents employed in epoxy systems provide a substantial contribution to the properties of the crosslinked products. Thus, the choice of curing agent is very important and needs to be considered very carefully. This is particularly true for modifications of epoxy resins,

where the curing agents can influence the curing chemistry, the curing rate, crosslink density, morphology, thermal stability etc. and eventually affect the fracture toughness of modified epoxy resins (Aziz, 2004).

The epoxide ring can react with chemicals of different structures, especially those that have activated hydrogen atoms such as alcohols, amines, and carboxylic acids, etc. Among them, primary and secondary amines are the most widely used curing agents for epoxy resins (May, 1988).

Many polyfunctional curing agents with active hydrogen atoms such as polyamines, polyamides and polyphenols perform nucleophilic addition reaction with epoxides. Tanaka and Bauer (1988) gave the following general cure reaction as shown in Figure 2.3:

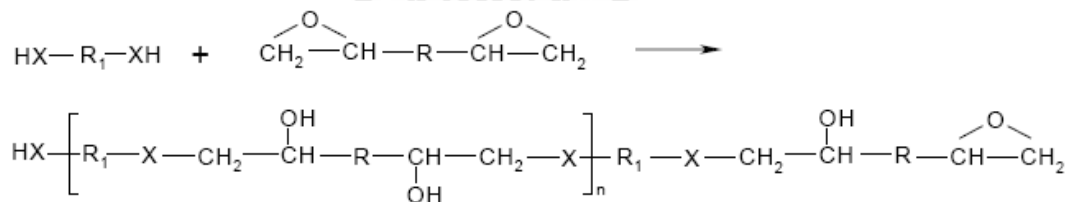


Figure 2.3 General cure reaction between a curing agent and epoxides (Tanaka and Bauer, 1988)

In Figure 2.3, X represents NH, O or S nucleophilic group or element and n is the degree of polymerization, having a value of 0, 1, 2 ...

The curing mechanisms of epoxides with several types of curing agents are shown in Figure 2.4.

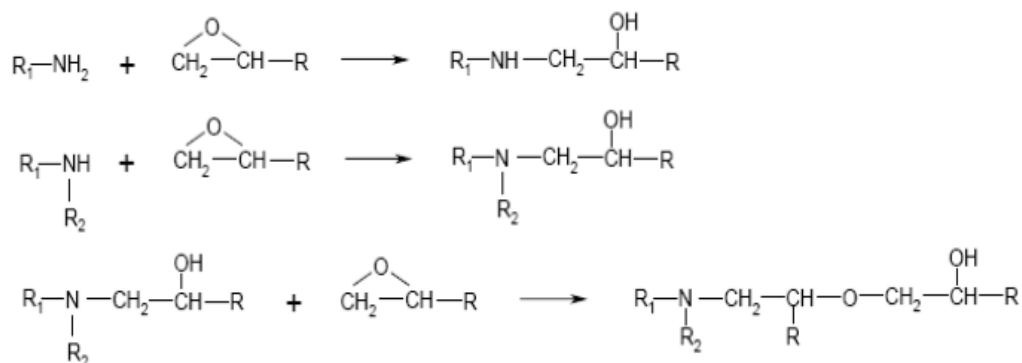


Figure 2.4 The curing mechanisms of epoxides with several types of curing agents (Tanaka and Bauer, 1988)

Xu and Schlup (1998) studied the curing mechanism of epoxy resin/amine system using near-infrared spectroscopy and derived the following equation of curing reaction as shown in Figure 2.5:

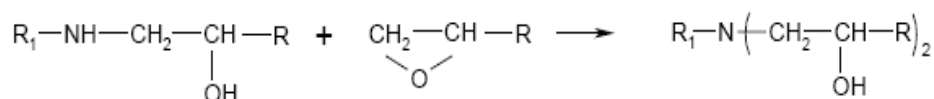


Figure 2.5 The curing mechanisms of epoxy/amine system (Xu and Schlup, 1998)

They pointed out that the etherification during the epoxy resin curing was significant only at certain reaction conditions such as at a high curing temperature and for only some epoxy resin/amine systems (Mika and Bauer, 1988.; Xu and Schlup, 1998).

2.1.4 Factor affecting physical properties of cured epoxy resin

The physical properties of the cured epoxy resin depend on extent of curing, the curing process, and the time and temperature of cure (Zhang and Evans, 2003). All these factors will significantly affect the final molecular network developed. Therefore, a comprehensive picture of the molecular changes that occur as a function of the variation of these variables will be of interest, in order to understand the resulting changes in the final physical and mechanical properties of the epoxy (Plangsangmas, Mecholsky and Brennan, 1999).

Moreover, fracture behavior of epoxy also depend on the type of epoxy resin, the curing agent, the stoichiometry of the mix, the cure profile, and the temperature and rate of testing (Kanchanomai and Rattananon, 2008).

2.1.5 Mechanical properties of DGEBA and TETA system

Mechanical properties of epoxy systems can be varied by variation of processing conditions such as time and temperature of cured (Zhang and Evans, 2003) or by the use of different hardener to monomer ratios (Jose Roberto Moraes D'Almeida, Menezes and Monteiro, 2003). For the particular system made of the triethylene tetramine (TETA) hardener, and the DGEBA monomer the variation of the hardener to monomer ratio promotes strong changes on the mechanical behavior (Jose Roberto Moraes D'Almeida *et al.*, 2003; Jose Roberto Moraes D'Almeida and Monteiro, 1995). The tensile properties of DGEBA/TETA with stoichiometric ratio have been reported around 13 phr (Jose Roberto Moraes D'Almeida *et al.*, 2003). D'Almeida and co-worker were found that Young's modulus, tensile strength and elongation at break of DGEBA/TETA with stoichiometric was 3.84 GPa, 80 MPa and 3.3%, respectively.

In fact, in epoxy resins, a higher degree of cure can be achieved with a higher processing temperature. This results in a polymer structure with greater crosslink density, that is probably stiffer and higher ultimate tensile strength (Jose Roberto Moraes D'Almeida and Monteiro, 1995).

2.1.6 Thermal properties of DGEBA and TETA system

Curing temperature of DGEBA was studied using DSC from 20-300°C with a heating rate 10°C/min. The different of hardener/epoxy ratios were used: 5phr, 13phr (stoichiometric ratio) and 20phr. For non-isothermal scan, it was found that the peak of curing temperature was lower for higher hardener ratio because the reaction was more effective due to the fact that there were more amine groups when the ratio was increased. The DSC curves of DGEBA/TETA at various epoxy/hardener ratio are shown the Figure 2.6 (Costa, Calado and Tavares, 2005).

Moreover, curing temperature of DGEBA/TETA has been studied at various heating rate of 5, 10, and 20°C/min. It was found that the peak of curing temperatures shifted to 72.5°C, 88.7°C, 104.5°C as the heating rates increased (Mustata and Bicu, 2001).

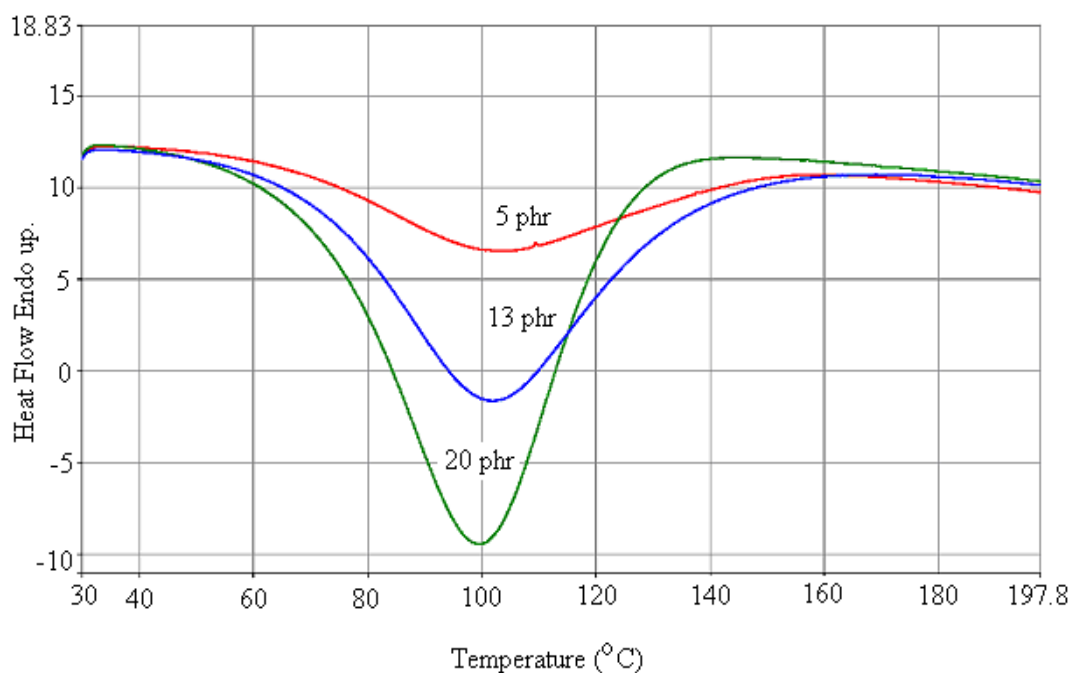


Figure 2.6 DSC curves of DGEBA/TETA at various epoxy/hardener ratios (Costa *et al.*, 2005).

Glass transition temperature (T_g) of epoxy has been often determined by the half of the specific heat (ΔC_p) and the width of the glass transition (ΔT). Other quantities were determined by the position of the overheating peak or so-called stress relaxation peak and its maximum temperature. However, enthalpy relaxation was not no longer observed if the samples were immediately measured again after cooling (Odegard and Yopadhyay, 2011).

The DSC curve of epoxy measured at a heating rate of 20 K/min is shown in Figure 2.7. The first line (continuous line) was non-post cured sample. The second sample was allowed to react by maintaining it isothermally at 170 °C for 10 minutes, cooled and afterwards examined by heating up to 220 °C (dashed line). The third curve (dotted line) was the repeat measurement of this sample. The DSC

measurements led to the complete post curing of the isothermally cured sample. Figure 2.7 represented that enthalpy relaxation peak would no longer be observed if the sample was immediately measured again after cooling (Benzler, 1999).

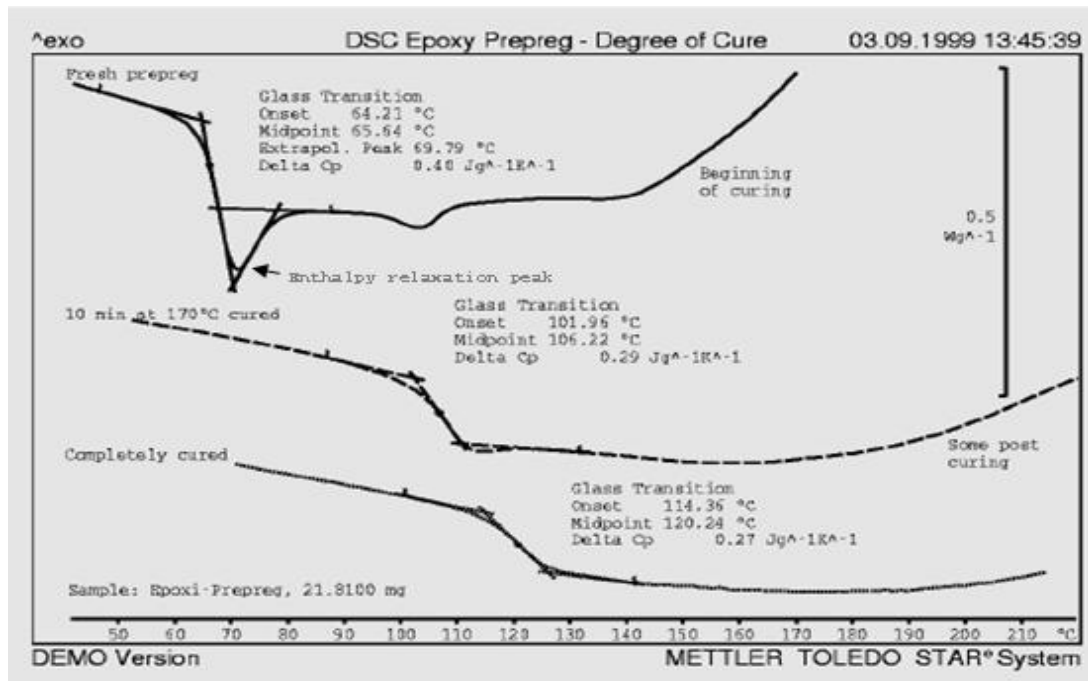


Figure 2.7 DSC curve of epoxy: the first line for non-post cured sample (continuous line), the second line for isothermally at 170 °C for 10 minutes, cooled and afterwards examined by heating up to 220 °C (dashed line), and the third line for repeated measurement by heating up to 220 °C again (dotted line) (Benzler, 1999).

2.1.7 Fracture surface of neat epoxy

The fracture surface morphology analysis is of an important aspect for studying fracture patterns and their corresponding fracture mechanism (Zhao and Luo,

2008). General features of the fracture surfaces of epoxies are shown in Figure 2.8.

They are divided into four regions (Plangsangmas *et al.*, 1999):

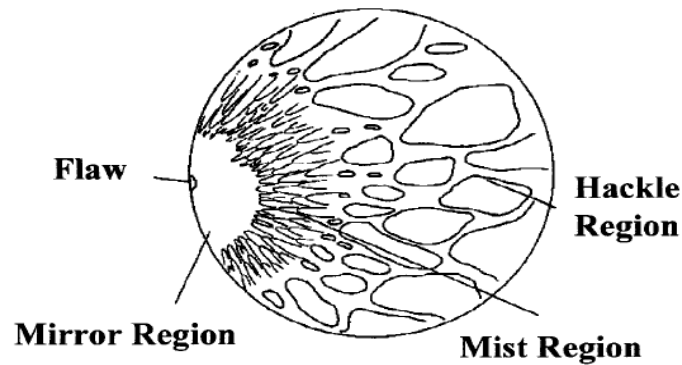


Figure 2.8 General fracture surface of neat epoxy (Plangsangmas *et.al.*, 1998)

The first region is an initiation region or flaw region. This is the region where fracture has started. The fracture origin normally is due to machining, impact, or material defects such as pores or inclusions. The material defects can be inherent defects that exist naturally in a material or as a consequence of processing. The second region is a mirror region. This is an area with a smooth and glossy appearance that surrounds the initiation region. The crack velocity is relatively slow in the mirror region. The third region is a mist region. This is an area that appears to be substantially rougher than the mirror region. The crack velocity, which is higher than in the mirror region, creates parabolic or hyperbolic markings in the mist region. Final region is the hackle region: The hackle region appears to be the roughest area due to highest crack velocity. Macroscopic crack branching initiates at the end of the hackle region (Plangsangmas *et al.*, 1999).

2.1.8 Effect of hardener ratio on tensile properties of neat epoxy and fracture surface morphology

The tensile properties of epoxy with various hardener ratio are shown in Table 2.3. The strain at fracture steadily increased as a function of the hardener ratio. In other words, within an error of 10%, it can be assumed that the values of the strain at fracture were continuously increased as a function of the hardener ratio. The stress data, on the other hand, had a local maximum around the stoichiometric ratio, at phr of 13. The elastic modulus showed only an abrupt transition. The epoxy-rich formulations showed more stiff and the amine-rich formulations showed more compliant (D'Almeida José R. M. and Monteiro, 1998).

Table 2.3 Tensile properties of epoxy at various hardener ratios (D'Almeida José R. M. and Monteiro, 1998).

phr	Elastic modulus (GPa)	Tensile stress (MPa)	Elongation at break (%)
7	3.67	22.20	0.80
9	3.63	29.10	1.00
11	3.74	57.00	1.60
13	3.84	80.00	3.30
15	2.40	73.00	4.60
17	2.46	66.80	5.20
19	2.65	65.70	5.40
21	2.87	86.10	5.70

D'Almeida José R. M. and Monteiro (1998) studied fracture surface of eight resin formulations prepared at various hardener/resin (TETA/ DGEBA) ratios. They varied hardener/resin ratio between 7 and 21 phr. So, the hardener/resin ratio analyzed covered the stoichiometric as well as the epoxy-rich ($\text{phr} < 13$) and amino-rich compositions ($\text{phr} > 13$). Figure 2.9 depicts the overall topographic aspects observed for the hardener ratio of $\text{phr} \geq 13$ formulations. The figure shows the fracture morphology of the mixture with 15 phr. One can identify (a) the mirror zone, (b) the transition zone and (c) the final propagation zone. The features shown are the common ones observed at the fracture surfaces of thermoset resins. The crack initiation point is surrounded by a flat featureless mirror zone. This is followed by a transition zone, where the surface roughness steadily increases, and continued by a final propagation zone with conical marks. These conical marks are generated by the overlapping of the main propagating crack with secondary cracks nucleated ahead of the main crack front. The size of each zone and the conic mark generated at the fracture surface depends, respectively, on the specific characteristics of the epoxy system being analyzed and on the relative velocities between the main crack and the secondary cracks.

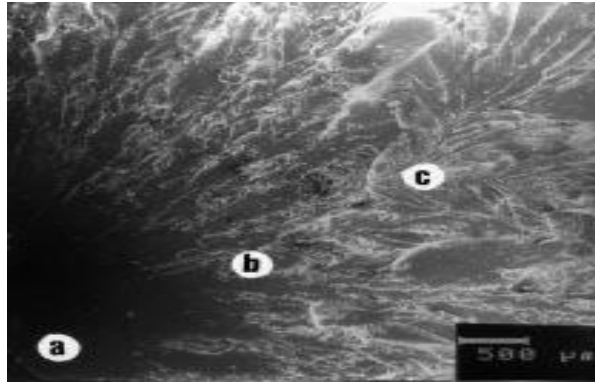


Figure 2.9 General topographic aspects of the fracture surface of the epoxy and hardener mixtures with $\text{phr} \geq 13$ (José R. M. d'Almeida and Monteiro, 1998).

As shown in Figure 2.10, the fracture surface analysis shows that the mirror zone increased with the amount of hardener. The size of the mirror zone for these epoxy-rich formulations ($\text{phr} < 13$) is smaller than that for the amine-rich formulations ($\text{phr} > 13$)

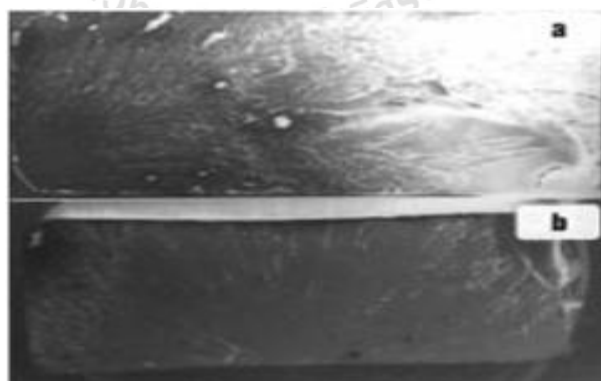


Figure 2.10 Common relative sizes of the mirror zones: (a) $\text{phr} 11$; (b) $\text{phr} 21$ (José R. M. d'Almeida and Monteiro, 1998).

2.1.9 Effect of loading rate on mechanical properties and fracture surface morphology

It is known that the tensile stress and yield stress of polymers are time dependence and the fracture properties of epoxy resin are also expected to be time dependence. Therefore, understanding the fracture behavior and mechanism of epoxy resin under various loading rates is necessary for using this material in engineering applications.

Effects of loading rate on fracture behavior and mechanism of thermoset epoxy resin with polyamine hardener have been studied at various loading rates of 0.1, 10 and 100 mm/min. It was found that The maximum load, critical stress intensity factor (K_{I0}), and critical strain energy release rate (G_{I0}) were high and stable at low loading rates, and became low and stable at high loading rate with the transition of loading rate at approximately 10 mm/min.

SEM micrographs of fracture surfaces of epoxy after 3-point bending test under various loading rates are shown in Figure 2.11. Formation of a stretched zone was clearly seen on the entirely fracture surface of specimen tested at 0.1 mm/min (Figure 2.11a), while a mix between a stretched zone and a smooth surface was seen for the specimens tested at 10 and 1000 mm/min (Figure 2.11 b and c, respectively). The area of the stretched zone decreased with increase loading rate. The stretched zone started from the notch, especially from the intersection between the notch and side surface of specimen.

The formation of a stretched zone, crazing and crack blunting found in the specimens tested under low loading rates was evidence of localized plastic deformation processes. On the other hand, smooth fracture surfaces found in the

specimens tested at high loading rates were evidence of fracture without localized plastic deformation (brittle fracture) (Kanchanomai, Rattananon and Soni, 2005).

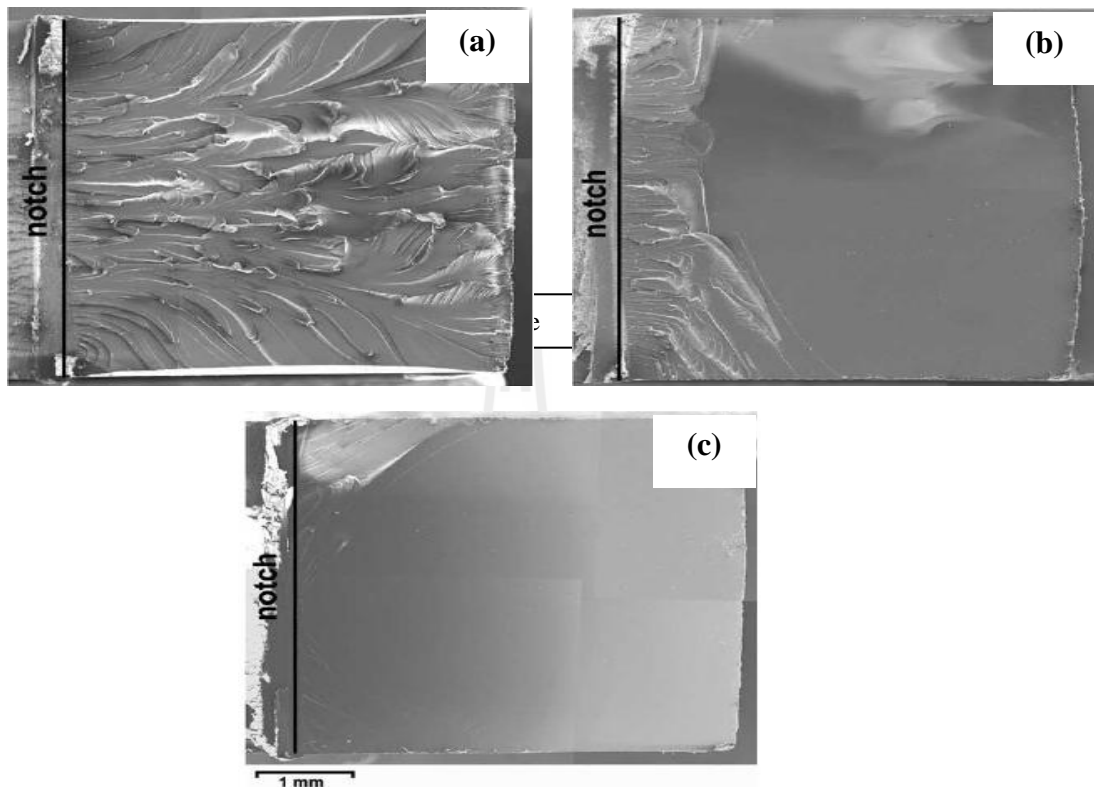


Figure 2.11 SEM micrographs of fracture surface of epoxy tested under 0.1 mm/min (a), 10 mm/min (b) and 1000 mm/min (c) (Kanchanomai *et al.*, 2005).

2.1.10 Effect of curing condition on mechanical properties

Fractured surface behavior of epoxy depends on the type of epoxy resin, the curing agent, the stoichiometry of the mixture, the temperature and rate of testing and curing condition (Robinson, Douglas and Mecholsky, 2002).

Effect of curing time on tensile properties of epoxy resin with amine-cured epoxy has been studied. The samples were prepared with curing temperature of

100°C and varied curing time of 1h, 4h, 24h. The tensile properties of epoxy resin with amine-cured epoxy are shown in Table 2.4.

Table 2.4 Tensile properties of epoxy resin with amine-cured epoxy prepared at curing temperature of 110°C at various curing times (Plangsangmas *et.al.*, 1998).

Curing time (hr)	0.2% Offset yield stress (MPa)	Tensile strength (MPa)	Elongation at break (%)	Elastic modulus (GPa)
1	50.0±3.3	63.2±2.0	3.8±0.4	2.6±0.0
4	43.5±3.2	62.2±1.9	4.4±0.8	2.5±0.0
24	46.0±0.6	59.7±2.0	3.9±2.0	2.8±0.0

Effect of post cured time on tensile properties of epoxy resin with anhydride-cured epoxy has been studied. The samples were prepared by curing at 110°C for 5h and post cure at 125°C by varies post cured time of 8h, 16h and 24h. The tensile properties of epoxy resin with anhydride-cured epoxy are shown in Table 2.5. Anhydride-cured epoxy exhibited brittle behavior and no obvious yielding occurred. On the other hand, amine-cured epoxy exhibited yielding before fracture.

Table 2.5 Tensile properties of epoxy resin with anhydried-cured epoxy prepared at curing temperature of 110°C and post cure at 125°C at various post curing times (Plangsangmas *et al.*, 1999).

Post curing time (h)	Tensile strength (MPa)	Elongation at break (%)	Elastic modulus (GPa)
8	62.9±6.0	2.6±0.3	2.7±0.2
16	69.4±10.7	2.9±0.4	2.8±0.1
24	83.2±3.6	3.1±0.2	2.9±0.1

2.1.11 Effect of temperature on mechanical properties and fracture surface morphology

Low viscosity resin, DGEBF (diglycidyl ether of bisphenol F), was modified by the addition of a long chain aliphatic resin, PPGDE (polypropylene glycol diglycidyl ether) and cured with an aromatic amine hardener, DETD (diethyl toluene diamine). The ratio of DGEBF:PPGDE:DETD was 50:50:20. The work of fracture of epoxy has been measured at room temperature, 77K, and 4.2K respectively using a three-point-bending method with deeply notched specimens. It was found that the work of fracture of epoxy decreased as the temperature decreased. The work of fracture at room temperature, 77K, and 4.2K was 2241, 396 and 218 J/m² respectively. The fracture surface of epoxy at various temperatures are shown in Figure 2.12. Types of crack growth obtained from epoxy fracture surface occurred in three behavior including, Type A-controlled but brittle, unstable crack growth, Type B-mixed type of crack growth, and Type C-ductile stable crack growth.

Figure 2.12a illustrates typically ductile, stable crack growth (Type C). A rough, torn-like surface dominates the fractography, even appearing to be fibrous in some regions. Figure 2.12b shows A→B type of crack growth which is combination between brittle and ductile behavior or semi-flexible deformation. Figure 2.12c illustrates typically of brittle, unstable crack growth (Type A) (Zhang and Evans, 2003).



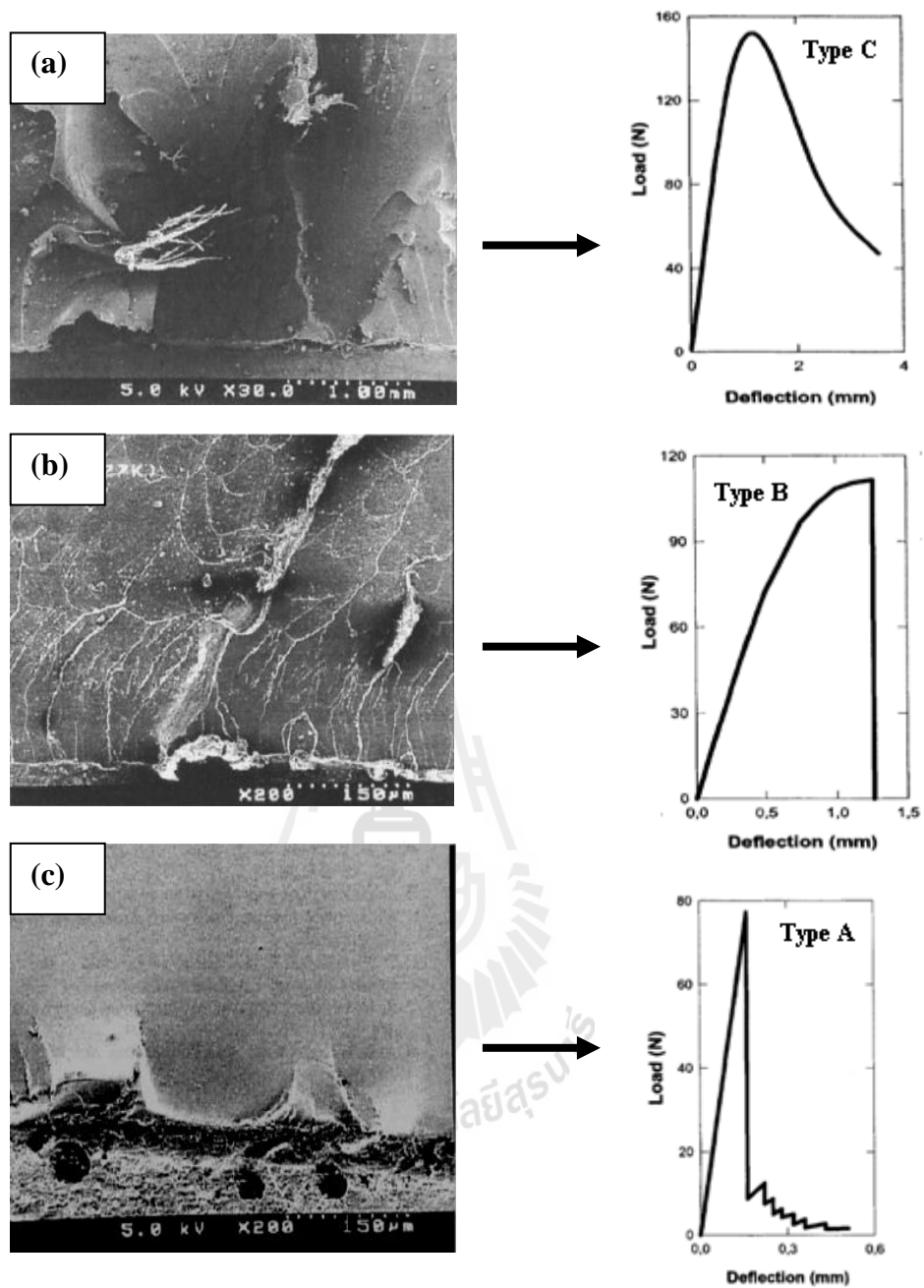


Figure 2.12 Fractographs of epoxy fractured at 300K (a), 77K (b) and 4.2K(c) related to type of crack growth of epoxy (Zhang and Evans, 2003).

2.2 *Bombyx Mori (B. mori)* silkworm silk

Silk is popularly known in the textile industry for its luster and mechanical properties. Silk is produced by cultured silkworms. Silks from silkworms (e.g., *Bombyx mori*) have been explored to the properties for use in various applications (Vepari and Kaplan, 2007).

2.2.1 Structure of *B. mori* fiber

B. mori silk fiber composed of two protein-monofilaments (named brins) embedded in a gluelike sericin coating. A similar structure has been observed in other silkworms silks. The brins comprises fibroin microfilaments made up of bundles of nanofibrils, approximate 5 nm in diameter. The bundle's diameter is around 100 nm (Hakimi, Knight, Knight, Grahn, and Vadgama, 2006). The microstructure of *B. mori* fiber is shown in Figure 2.13.

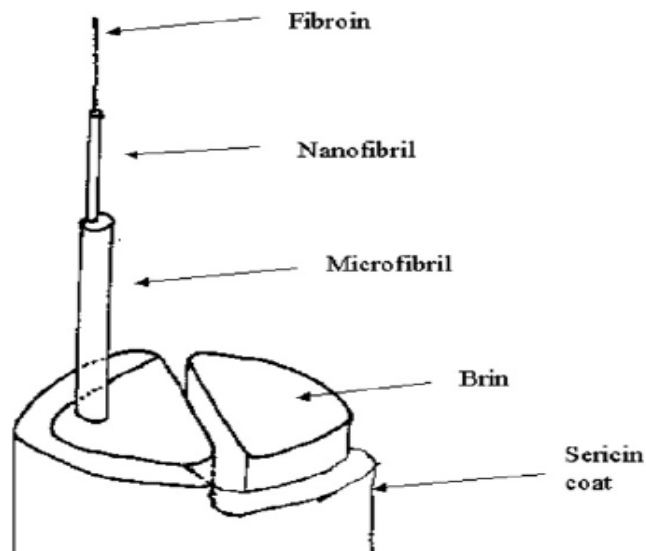


Figure 2.13 The microstructure of *B.mori* fiber (Hakimi, *et al.*, 2006).

2.2.2 Chemical composition of *B.mori* silk fibroin

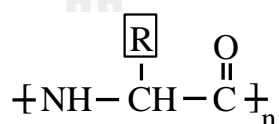
The composition of *B. mori* silk is shown in Table 2.6. The main composition of silk fiber is fibroin, 70-80 wt.%. Another composition composed of carbohydrates, wax matter, inorganic matter and pigment (Mousumi, Kanika, Nirmal, and Vineet, 2007).

Table 2.6 Composition of *B. mori* silk (Mousumi, *et al.*, 2007).

Component	Content (wt.%)
Fibroin	70-80
Sericin	20-30
Carbohydrates	1.2-1.6
Wax matter	0.4-0.8
Inorganic matter	0.7
Pigment	0.2
Total	100

The amino acid sequence of polypeptides plays a very important role in the solubility and crystallization of silk fibroins. The silk fibroin is highly periodic containing amino acids with bulkier side chains, as shown in Figure 2.14. The majority of amino acid composition of silk fibroin are glycine (45%), alanine (30%), and serine (12%) in a roughly 3:2:1 ratio. These three amino acids contain short side chains and permit close packing of crystals through the stacking of hydrogen-bonded α -sheets. The structure is dominated by [Gly-Ala-Gly-Ala-Gly-Ser]_n sequences, with corresponding side groups of H, CH₃, H, CH₃, H, CH₂OH

(Shen, Johnson, and Martin, 1998). Tyrosine with bulky side groups is reported to be in the amorphous region and amino acids of alanine, glycine, and serine are found in the crystalline regions (Reddy and Yang, 2010). The other amino acids of silk fiber are aspartic acid, arginine, glutamic acid, valine, threonine, proline, isoleucine, arginine, lysine, methionine, phenylalanine, cysteine and histidine. Chemical structure and their percent content of amino acids composed in silk fibroin are shown in Table 2.7.



R = side group of amino acid

Figure 2.14 Chemical structure of *B. mori* silk fibroin (Shen, *et al.*, 1998).

Table 2.7 Chemical structure of amino acids in *B. mori* silk fibroin (Meyers, Chen, Lin, and Seki, 2008; Reddy and Yang, 2010).

Amino acids	Chemical structure	Content (wt.%)
Glycine (gly)	$\begin{array}{c} \text{H}_3\text{N}^+ \text{---} \text{CH} \text{---} \text{COO}^- \\ \\ \text{H} \end{array}$	44.6
Alanine (Ala)	$\begin{array}{c} \text{H}_3\text{N}^+ \text{---} \text{CH} \text{---} \text{COO}^- \\ \\ \text{CH}_3 \end{array}$	29.4

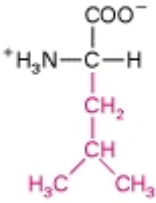
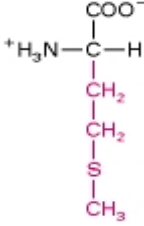
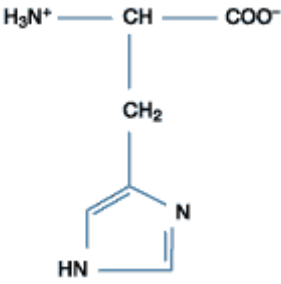
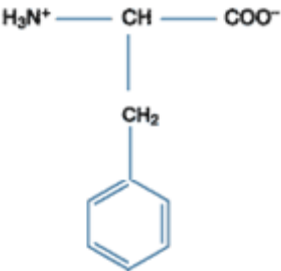
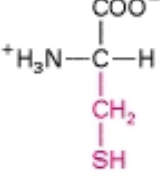
Table 2.7 Chemical structure of amino acids in *B. mori* silk fibroin (Continued)

Amino acids	Chemical structure	Content (wt.%)
Serine (Ser)	$ \begin{array}{c} \text{H}_3\text{N}^+ \text{---} \text{CH} \text{---} \text{COO}^- \\ \\ \text{CH}_2 \\ \\ \text{OH} \end{array} $	12.1
Tyrosine (Tyr)	$ \begin{array}{c} \text{H}_3\text{N}^+ \text{---} \text{CH} \text{---} \text{COO}^- \\ \\ \text{CH}_2 \\ \\ \text{C}_6\text{H}_4 \\ \\ \text{OH} \end{array} $	5.2
Valine (Val)	$ \begin{array}{c} \text{COO}^- \\ \\ \text{H}_3\text{N}^+ \text{---} \text{C} \text{---} \text{H} \\ \\ \text{CH} \\ / \quad \backslash \\ \text{H}_3\text{C} \quad \text{CH}_3 \end{array} $	2.4
Aspartic acid (Asp)	$ \begin{array}{c} \text{H}_3\text{N}^+ \text{---} \text{CH} \text{---} \text{COO}^- \\ \\ \text{CH}_2 \\ \\ \text{COO}^- \end{array} $	1.3
Glumatic acid (Glu)	$ \begin{array}{c} \text{H}_3\text{N}^+ \text{---} \text{CH} \text{---} \text{COO}^- \\ \\ \text{CH}_2 \\ \\ \text{CH}_2 \\ \\ \text{COO}^- \end{array} $	1.0

Table 2.7 Chemical structure of amino acids in *B. mori* silk fibroin (Continued)

Amino acids	Chemical structure	Content (wt.%)
Threonine (Thr)	$ \begin{array}{c} \text{COO}^- \\ \\ {}^+\text{H}_3\text{N}-\text{C}-\text{H} \\ \\ \text{H}-\text{C}-\text{OH} \\ \\ \text{CH}_3 \end{array} $	0.9
Proline (Pro)	$ \begin{array}{c} \text{COO}^- \quad \text{COO}^- \\ \quad \\ \text{H}_1\text{N}-\text{C}-\text{H} \quad \text{C}-\text{H} \\ \quad \quad \quad \\ \text{H}_2\text{C}-\text{CH}_2-\text{CH}_2-\text{CH}_2 \end{array} $	0.8
Isoleucine (Ile)	$ \begin{array}{c} \text{COO}^- \\ \\ {}^+\text{H}_3\text{N}-\text{C}-\text{H} \\ \\ \text{H}-\text{C}-\text{CH}_3 \\ \\ \text{CH}_2 \\ \\ \text{CH}_3 \end{array} $	0.8
Leucine (Leu)	$ \begin{array}{c} \text{COO}^- \\ \\ {}^+\text{H}_3\text{N}-\text{C}-\text{H} \\ \\ \text{CH}_2 \\ \\ \text{CH} \\ / \quad \backslash \\ \text{H}_3\text{C} \quad \text{CH}_3 \end{array} $	0.7
Arginine (Arg)	$ \begin{array}{c} \text{H}_3\text{N}^+ \text{---} \text{CH} \text{---} \text{COO}^- \\ \\ (\text{CH}_2)_3 \\ \\ \text{NH} \\ \\ \text{C} = \text{NH}_2^+ \\ \\ \text{NH}_2 \end{array} $	0.5

Table 2.7 Chemical structure of amino acids in *B. mori* silk fibroin (Continued)

Amino acids	Chemical structure	Content (wt.%)
Lysine (Lys)	 <chem>C[C@@H](C(=O)[O-])[NH3+]</chem>	0.2
Methionine (Met)	 <chem>CSCC[C@@H](C(=O)[O-])[NH3+]</chem>	0.2
Histidine (His)	 <chem>C1=CN=C(N1)CC[C@@H](C(=O)[O-])[NH3+]</chem>	0.1
Phenylalanine (Phe)	 <chem>c1ccc(cc1)CC[C@@H](C(=O)[O-])[NH3+]</chem>	0.1
Cysteine (Cys)	 <chem>SCC[C@@H](C(=O)[O-])[NH3+]</chem>	0.1

2.2.3 Microstructure and conformation of silk fibroin

As a typically natural macromolecule, silk is spun by the silkworm and mainly made up of two different proteins, silk fibroin (the inner core) and sericin (the outer coating) (Bayraktar, Malay, Ozgarip, and Batigun, 2005). The SEM micrographs of silk fiber and their fiber structure are shown in Figure 2.15. Degumming is simply removing the outside layer of sericine. It serves to make the fabric soft and increase its luster. It is performed by extraction with alkali or acids treatments and digestion with enzymes. To extract sericine, the solution is boiled for 30 minutes to 4h. Sericin is almost removed from raw silk fibers by alkaline treatment. After degumming process, the next step is dyeing and weaving (Khan *et al.*, 2010).

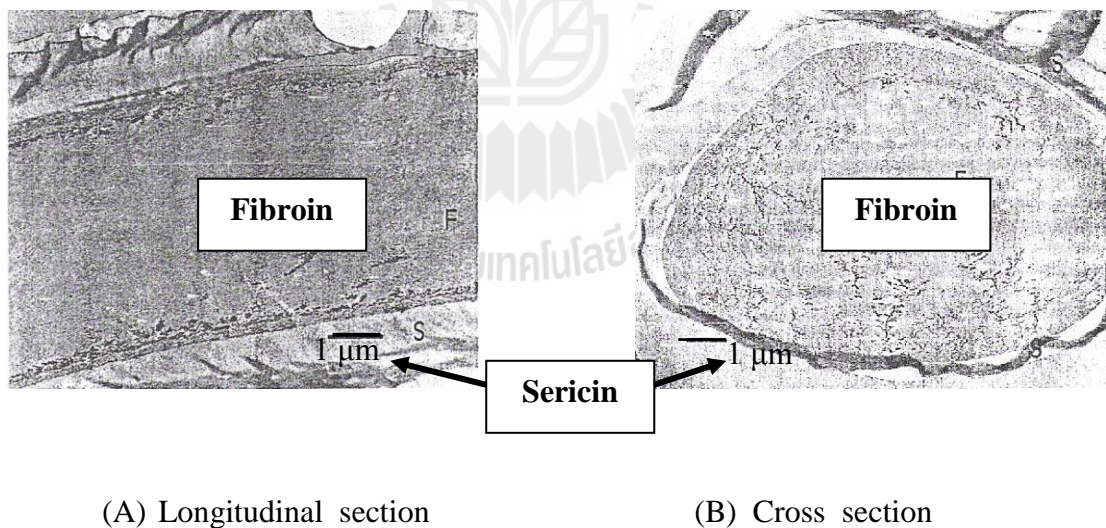


Figure 2.15 SEM micrograph of *B.mori* silk fiber ; Longitudinal section (A), Cross section (B) (Lewin and Pearce, 1998).

The model of *B.mori* silk conformation has been created by Li, H Liu, Li and Wang (2012). They reported that structure of silk fibroin is composed of crystalline phase (β -sheet conformation) and amorphous phase (α -helix/random coil conformations). The model of *B.mori* silk conformation is shown in Figure 2.16.

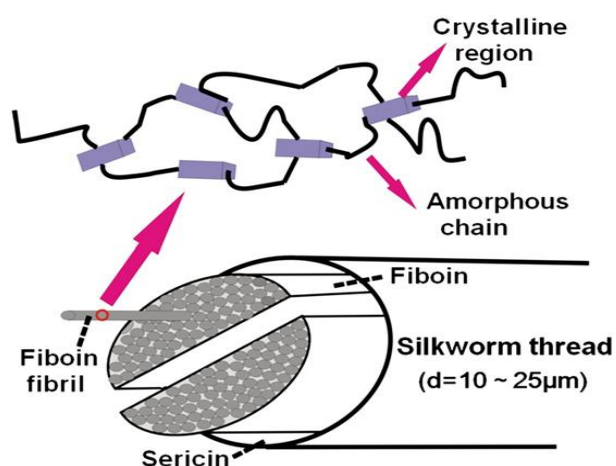


Figure 2.16 The model of *B.mori* silk conformation (Li, Liu, Li, and Wang, 2012).

The silk fibroin comprises three conformations (random coil, α -helix and β -sheet). Each conformation has its own characteristic absorption bands on FTIR spectrum. The bands at 1630, 1530, 1265, and 700 cm^{-1} are assigned to β -sheet conformation while the bands at 1660, 1540, 1265, and 650 cm^{-1} are associated with α -helix/random coil conformations (Kaplan, 1998).

Srihanam, Srisuwan and Simchure (2009) investigated and compared some characteristics of *B. mori* in different forms; with and without sericin. The secondary structures of all kinds of silk were determined by FT-IR. It was found that *B. mori* silk fibers both with and without sericin were very different in absorption bands. The absorption band of *B. mori* silk with sericin appeared at 1649 cm^{-1} (amide

I), 1560, 1523 cm^{-1} (amide II), 1234 cm^{-1} (amide III) and 1021 cm^{-1} (amide IV). The *B. mori* without sericin showed intense absorption bands at 1643 cm^{-1} (amide I), 1509 cm^{-1} (amide II) and 1127 cm^{-1} (amide III). It was found that the absorption band of amide IV was gone. The amide I, II and III have distinct infrared absorption band shapes. Their sensitivity to hydrogen bonding, dipole-dipole interactions, and peptide backbone geometry provides useful indicators of secondary structural changes. The amide I attributed to the stretching motion of the C=O whereas the amide II and III attributed to bending motion of the N-H coupled to C-N stretching (Tomoyuki and Shaul, 2007). Sargunamani and Selvakumar (2006) have reported that the conformation of amide I, amide II, amide III and amide IV were attributed to α -helix (amorphous), β -sheet (crystallinity), β -sheet or α -helix, and α -helix, respectively. With sericin, *B. mori* composed of higher ration of α -helix structure than β -structure. Those of the absorption bands of *B. mori* silk fiber shifted to lower wavenumber after removing sericin as shown in Figure 2.17.

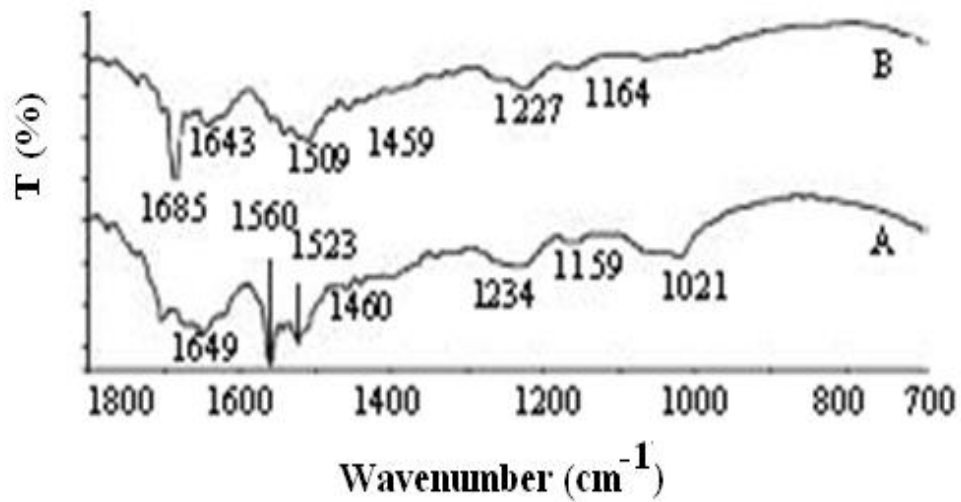


Figure 2.17 FT-IR spectra of the different forms of silk fiber; *B. mori* silk with sericin (A) and *B. mori* silk without sericin (B) (Srihanam, Srisuwan , and Simchure, 2009).

2.2.4 Tensile properties and toughness

The physical properties of silk distinguish them from the other natural fibers. Most importantly, silk are unique for their combined extensibility and high tensile strength (Gosline, Guerette, Ortlepp , and Savage 1999; Sirichaisit, Brookes, Young, and Vollrath, 2003). Gosline *et al.*, (1999) reported that the toughness of *B. mori* silk was higher than Kevlar fiber. Silk proteins have very large average molecular weight (Bini, Knight, and Kaplan, 2004). They were hydrophobic in their solid state, and in some cases their mechanical properties were greatly influenced by water (Plaza *et al.*, 2008). Moreover, silk show variability in their mechanical properties when produced under different conditions (Madsen, Shao, and Vollrath, 1999). Tensile properties of silk and other material are shown in Table 2.8.

Table 2.8 Tensile properties of silk, elastin fiber and Kevlar fiber (Hakimi, Knight, Knight, Grahn, and Vadgama, 2006; Wambua, Ivens, and Verpoest, 2003).

Fiber type	Silk species	Elongation at break (%)	Tensile strength (GPa)	Toughness (MJ/m ³)
Major ampullate	<i>Araenus</i>	27	1.1	160
Viscid	<i>Araenus</i>	270	0.5	150
Cocoon	<i>Bombyx</i>	18	0.6	70
Elastin fiber	-	15	0.002	2
Kevlar 49 fiber	-	2.7	3.6	50
Glass fiber	-	3	2.4	-

Toughness is defined as the ability of a material to deform plastically and dissipate energy before fracture. The toughness of silk has been attributed to its nanofibrillar composition, with strong interactions between nanofibrils in the thread (Poza, Perez-Rigueiro, Elices, and Llorca, 2002), as well as the fine channels in the thread which might be helping to disperse energy (Vollarh *et al.*, 2002).

The tensile properties of *B. mori* silk fiber have been reported. The data is shown in Table 2.9. Tensile strength has also been credited to the presence of β -sheet packed into crystalline regions and hydrophobic interactions between those crystalline regions, which bind molecules together in the fiber (Hayashi and Lewis, 2000).

Table 2.9 Tensile properties of silk thread (Cunniff *et al.*, 1994; Gregory *et al.*, 2003; Lee *et al.*, 2005).

<i>B. mori</i> silk	Young's modulus (GPa)	Tensile strength (MPa)	Elongation at break (%)	References
<i>B. mori</i> silk with sericin ^a	5-12	500	19	Gregory <i>et al.</i>
<i>B. mori</i> silk ^b	15-17	610-690	4-16	Gregory <i>et al.</i>
<i>B. mori</i> silk ^c	10	740	20	Gregory <i>et al.</i>
<i>B. mori</i> silk ^d	12.3-15.7	713.3-786.7	22.2-27	Lee <i>et al.</i>

^aBombyx mori silkworm silk— determined from bave (multithread fibers naturally produced from the silk worm coated in sericin).

^bBombyx mori silkworm silk— determined from single brins (individual fibroin filaments following extraction of sericin).

^cBombyx mori silkworm silk— average calculated from data in Cunniff *et al.*(1994)

^dBombyx mori silkworm silk—The average values are obtained from a single silk fibre thread with seven filaments.

2.2.4.1 Effect of water absorption on mechanical properties of silk

The mechanical properties of silkworm silk after immersion in water for 2 days have been reported. Tensile tests have been performed on silkworm silk fiber after submerged in water. However, only immersion in water leads to a decrease in the mechanical properties of silk, indicating the weakening of hydrogen bonds. These results indicate that water disrupts hydrogen bonds initially present in the amorphous phase. The force-displacement curve of silk after tensile test is shown in Figure 2.18 (Pérez-Rigueiro, Viney, Llorca, and Elices, 2000).

Furthermore, it has also been found that the tensile properties (Young's modulus and, tensile strength) decrease after the silk fiber was submerged in water for 1hr. The data of tensile properties of silk fiber with dry and wet by water were compared in Table 2.10 (Plaza, *et al.*, 2008).

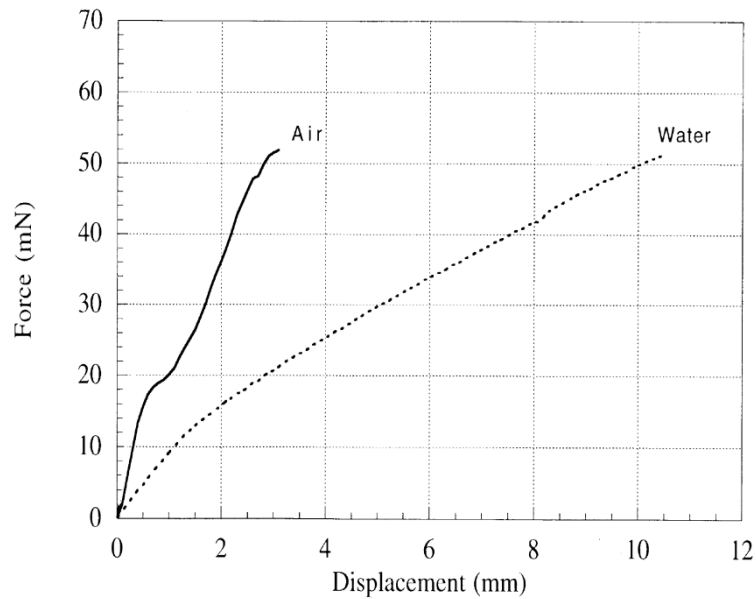


Figure 2.18 The force-displacement curve of silk before and after submerged in water (Pérez-Rigueiro, *et al.*, 2000).

Table 2.10 Tensile properties of silk with different condition of fibers (Plaza *et al.*, 2008).

<i>B. mori</i> Silk	Young's modulus (GPa)	Tensile strength (MPa)	Elongation at break (%)
Dry	14 ± 0.1	570 ± 70	20 ± 3
Wet with water	3.8 ± 0.3	450 ± 20	27 ± 3

2.2.4.2 Effect of degumming process on mechanical properties of silk

Silk fibers from *Bombyx mori* silkworm is degummed with different chemical agents. Tensile properties are the most important factors for evaluating the performance of fibers for proper applications. The tensile strength,

Young's modulus and elongation at break of silk fibers degummed with different chemical agents are presented in Table 2.11. The tensile strength and strain at break of control raw silk fiber was 422 MPa and 13.6%, respectively. After soap degumming, the tensile strength was decreased to about 250 MPa, indicating partial harmful damages of silk molecules after soap-alkali degumming. It is interesting to note that 15% citric acid degumming silk increased the tensile strength to 507 MPa. The elongation at break of silk fibers was noticeably increased for both soap and acid degumming method. There was not much influence on strength and elongation in degumming with hot water samples. The Young's modulus of untreated control silk fiber was 8.3 GPa and this value decreased after degumming with citric acid and soap solutions, suggesting the silk fibers become soft and stretchable after degumming treatment (Khan, *et al.*, 2010).

Table 2.11 Tensile properties of silk fibers degummed with different chemical agents (Khan, *et al.*, 2010).

<i>B. mori</i> Silk	Young's modulus (GPa)	Tensile strength (MPa)	Elongation at break (%)
Raw silk	-	422	13.6
Silk degummed with hot water	6.5	394	13
Silk degummed with 15 wt.% soap	25.3	250	18.1
Silk degummed with 15 wt.% citric acid	22	507	20

2.2.4.3 Effect of tensile deformation on the molecular structure

The silk fibroin has three conformations (random coil, α -helix and β -sheet) (Kaplan, 1998). The mechanical properties of the silk fibroin protein can be attributed to the formation of an extended crystalline β -sheet structure that is composed of recurrent sequences of glycine, alanine and serine amino acids, in majority. The extent of β -sheet structure can be controlled through physical or chemical methods, leading to materials with controlled crystallinity and degradation rate (Murphy, John, and Kaplan, 2008).

The effect of mechanical deformation of a silk monofilament of the silkworm *Bombyx mori* has been studied in order to detect tensile stress-induced changes of the fibroin conformation and reorientation up to the breaking point. They also show that the intensity of some FT-IR bands is affected by tensile deformation. In particular, the amide III/amide I intensity ratio decreases as the strain increases and the variation is proportional to the stress applied on the fiber. These variations in intensity suggest that the alignment of the protein chains decreases with strain which might be due to the reorganization of the amorphous phase (Lefevre *et al.*, 2009).

2.2.5 Thermal properties of silk

The TGA data of the initial weight loss at a temperature lower than 100°C, was due to water evaporation (Kweon, Park, Ye, Lee, and Cho, 2001; Reddy and Yang, 2010; Srihanam, *et al.*, 2009). The thermal decomposition (T_d) of *B.mori* silk has been reported to be at 324°C (Reddy and Yang, 2010) and 350°C (Srihanam, *et al.*, 2009). *B. mori* silk with and without sericin showed T_d at 350°C

and 360°C respectively (Srihanam, *et al.*, 2009). The TGA curve of *B. Mori* silk is shown in Figure 2.19.

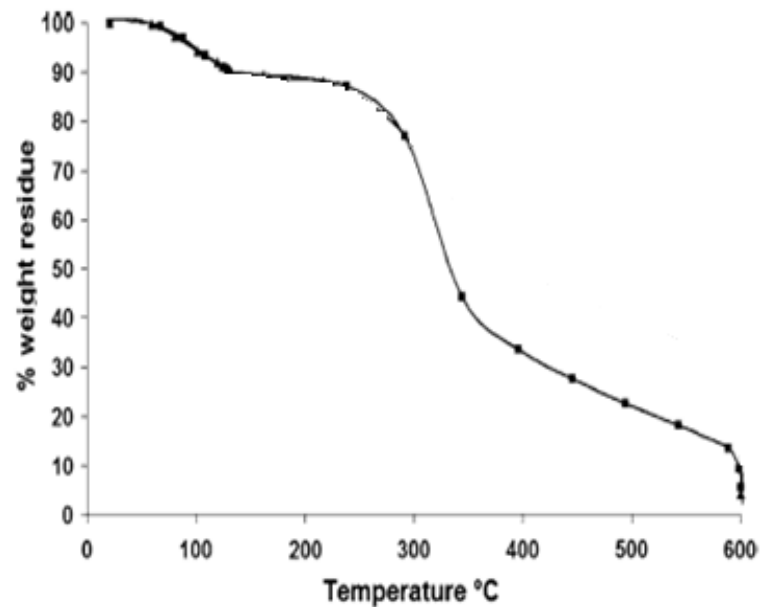


Figure 2.19 TGA curve of *B. Mori* silk (Reddy and Yang, 2010).

From the DSC thermogram, the peak below 100°C attributed to the water evaporation as shown in Figure 2.20 (Tanaka *et al.*, 2002). The DSC curves of silk fiber with sericin and without sericin showed the endothermic peak at 329°C and 334°C respectively attributed to the decomposition of silk fiber (Srihanam, *et al.*, 2009). Some thermal properties of *B.mori* silk are shown in Table 2.12.

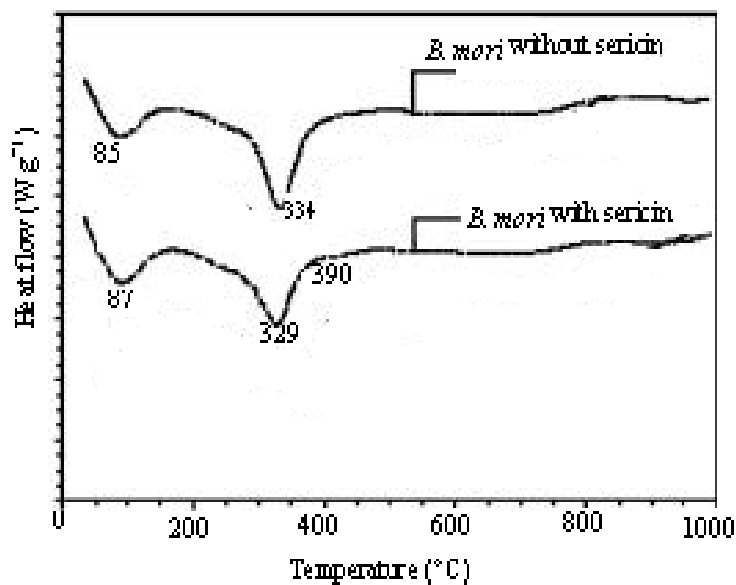


Figure 2.20 DSC thermograms of *B. mori* silk fiber with sericin and silk fiber without sericin (Srihanam, *et al.*, 2009).

Table 2.12 Thermal properties of *B. mori* silk (Srihanam, *et al.*, 2009).

<i>B. mori</i> Silk	DSC		TGA	
	Endo. Peak1 (°C)	Endo. Peak2 (°C)	Water evaporation Temperature (°C)	T _d (°C)
with sericin	81	329	81	350
without sericin	85	334	85	360

2.2.5.1 Effect of silk degumming process on thermal properties of silk fiber

Khan *et al* (2010) studied the thermal behavior of silk fibers degummed with different types of degumming agents. The silk fiber were evaluated on the basis of DSC and thermomechanical analysis (TMA) measurements. Then,

raw silk fibers were degummed with hot water, soap solution (15 wt.%, liquor ratio 1g/30 l) and citric acid solution by 15 wt.% and 30 wt.% concentration with liquor ratio of 1g/20 l. The thermal decomposition temperature were greatly enhanced by soap and citric acid degumming agents.

The influence of citric acid degumming on the expansion and contraction properties of silk fibers was studied by TMA measurements shown in Figure 2.21. The control raw silk fibers demonstrated a little contraction of about 1.0% from room temperature to 200°C, which may be attributed to the evaporation of humidity absorbed by the specimen. Then, the length of the specimen was retained unchanged to 280°C and then started to extend rapidly at a constant rate above 280°C upward. The thermal behaviors of raw silk fiber observed above 280°C are due to the breaking and reforming of the intermolecular hydrogen bonds and to the partial thermal decomposition. The position of the final extension is in accordance with the decomposition temperature of the fiber with β -molecular configuration. The starting onset position of rapid extension of silk fiber at around 280°C corresponds to the initial beginning temperature of endothermic peak.

Silk fiber treated with soap and citric acid of 15 wt.% showed a prominent two-step contraction in the temperature range from 25°C to 180°C. The first step appeared in the range from 25 to about 125°C and could be related to the evaporation of the water absorbed by the fiber. The second step started at above 200°C, accompanied by the abrupt change of slope of the TMA curve, and attained a maximum at 280–300°C. The final abrupt extension for the all silk fibers occurred at about 310°C (Khan, et al., 2010).

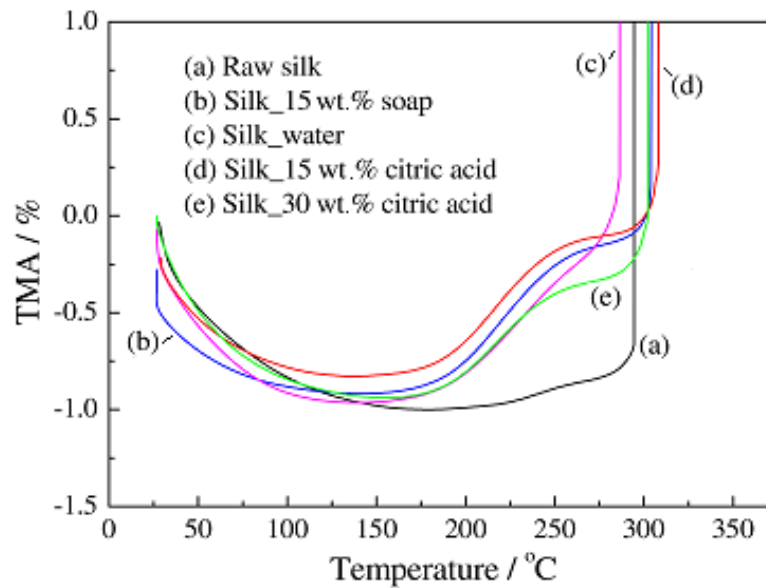


Figure 2.21 TMA curves of silk fibers degummed with different chemical agents (Khan, *et al.*, 2010).

2.2.6 Silk fiber treatment

The properties of composites are critically based on the performance of an interphase between a reinforcing fiber and matrix. The interfacial adhesion between the fiber and matrix plays an important role in binding and transferring the forces to the fiber, thus determining the mechanical and chemical properties of the resulting composites. The surface modification of the fiber was used to improve the interfacial bonding between the fiber and matrix (Tang and Kardos, 1997).

Various methods have been developed to modify the surface of silk fiber. The physical surface treatments widely used for silk fiber include, plasma treatment, corona discharge treatment, UV irradiation treatment. The chemical surface treatment widely used for silk fiber are grafting technique, silane treatment, coating technique.

2.2.6.1 Silane treatment of silk fiber

Silane coupling agents are usually used for fiber contained in polymer matrix to improve the adhesion between fiber and polymer, preferably via chemical bonds. There is extensive literature introduced the influence of silane coupling agents on the physical and mechanical properties of fiber reinforced composites (Xie, Hill, Xiao, Militz, and Mai, 2010). To effectively couple the fibers and polymer matrices, the silane molecule should have bifunctional groups which may respectively react with the two phases thereby forming a bridge between them. Silane coupling agents have a generic chemical structure as shown in Figure 2.22(a) where, R is alkoxy, X represents an organofunctionality, and R' is an alkyl bridge (or alkyl spacer) connecting the silicon atom and the organofunctionality (Xie, *et al.*, 2010).

For silk fiber, the silane coupling agent usually used to improve interfacial adhesion between silk fiber and epoxy matrix is 3-aminopropyltriethoxysilane (APTES) (Zulkifli, Azhari, Maryam, Ahmad, and Abu, 2009). The chemical structure of APTES is shown in Figure 2.22(b).

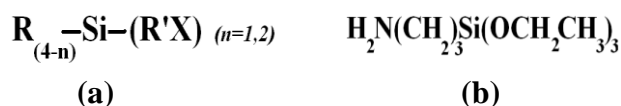


Figure 2.22 Chemical structure of silane ; (a) General structure and (b) APTES.

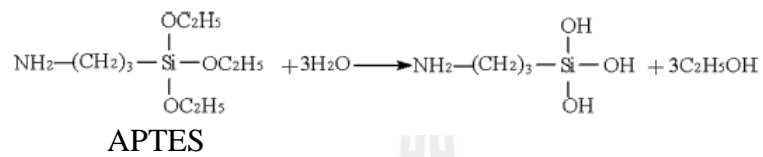
2.2.6.1.1 Interaction between silk fiber and 3-aminopropyltriethoxy silane

In general, interaction of silane coupling agents with natural fibers may mainly proceed through following four steps. The first step is hydrolysis as shown in Figure 2.23(a): The silane monomers are hydrolyzed in the presence of water and catalyst (normally acid or base) liberating alcohol and yielding reactive silanol groups. The second is self-condensation as shown in Figure 2.23 (b). During the hydrolysis process, the concomitant condensation of silanols (aging) also takes place. The condensation should be minimized at this stage to leave the silanols free for being adsorbed to the hydroxyl groups of the silk fibers (Loh and Tan, 2011). For the bulking treatment of fibers, the condensation should also be controlled in order to retain a small molecular size of monomers or oligomers to diffuse into the silk surface. The condensation rate of silanols is controllable by adjusting the pH of the hydrolysis system. An acidic pH environment is usually preferable to accelerate the hydrolysis rate of silanes but slow down the condensation rate of silanols (Xie, *et al.*, 2010).

The next step is adsorption as shown in Figure 2.23(c). The reactive silanol monomers or oligomers are physically adsorbed to hydroxyl groups of fibers by hydrogen bonds on the fiber surfaces which depends on the molecular size of silanol monomers/oligomers formed. The free silanols also adsorb and react with each other thereby forming a rigid polysiloxane structures linked with a stable –Si-O-Si- bond. Final step is grafting as shown in Figure 2.23(d). Under heating conditions, the hydrogen bonds between the silanols and the hydroxyl groups of silk fibers can be converted into the covalent –Si-O-C- bonds and liberating water (Loh and Tan,

2011). The residual silanol groups in the fibers will further condense with each other. The bonds of $-\text{Si}-\text{O}-\text{C}-$ is reversible when the water is removed at a raised temperature (Y. Xie *et al.*, 2010).

(a) Hydrolysis:



(b) Self condensation:

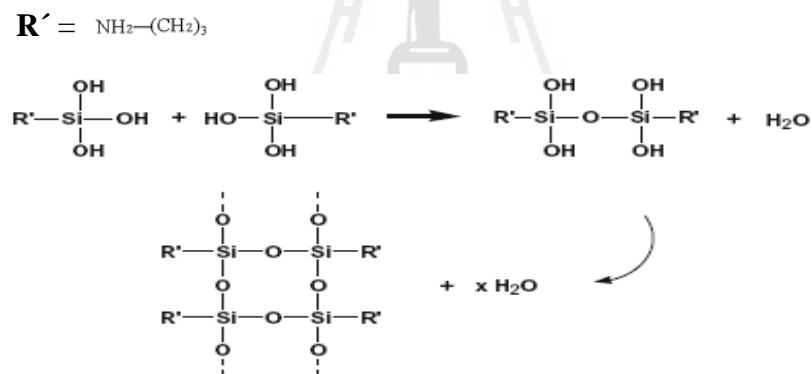
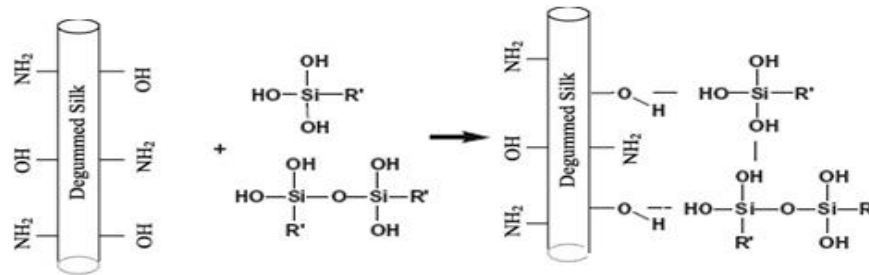


Figure 2.23 Interaction between silk fiber and APTES (Davaranah, Mahmoodi, Arami, Bahrami, and Mazaheri, 2009; Li, *et al.*, 2012; Loh and Tan, 2011; Xie, *et al.*, 2010).

(c) Adsorption:



(d) Chemically grafting:

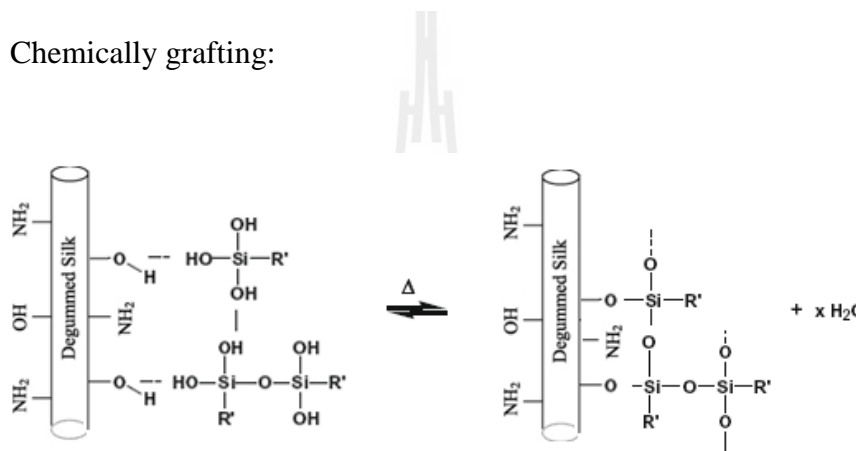


Figure 2.23 Interaction between silk fiber and APTES (Continued).

2.2.6.1.2 Effect of APTES treatment on surface morphology of silk fiber

Surface morphology of silk fabric treated with APTES has been investigated by Zulkifli *et al.* (2009). The smooth clean surface of the fiber of untreated silk fabric is shown in Figure 2.24a. The rough and crude surface of the silane treated silk fabric is shown in Figure 2.24b (Zulkifli, *et al.*, 2009).

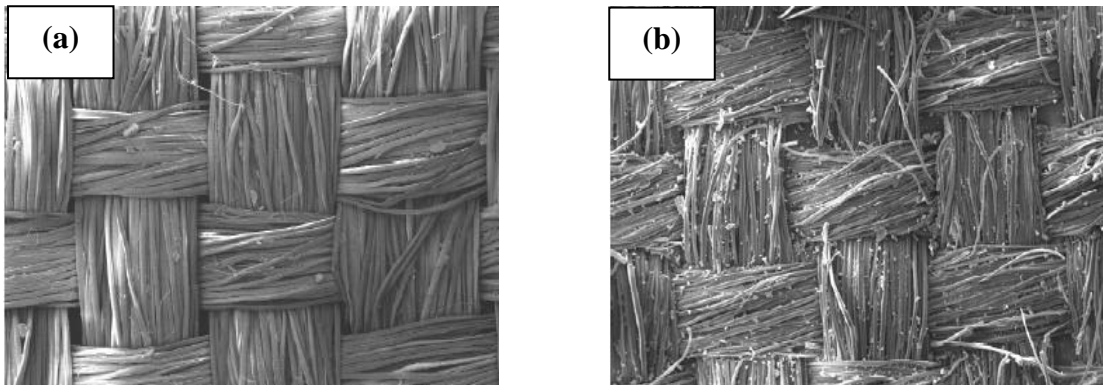


Figure 2.24 SEM micrograph of silk fabric; untreated (a) and silane treated silk fabric (b) (Zulkifli, *et al.*, 2009).

2.2.6.2 Silk treatment with epoxy

Among the chemical modifications, the epoxide treatment for silk seems to be promising with experimental results showing a great effectiveness in improving some intrinsic properties of silk, especially its wet resiliency. The reactivity of monofunctional, functional, bifunctional, multifunctional, and silicone-containing epoxides with silk fibroin and the physical properties of epoxide-treated silk fibers have been extensively studied (He, Jia, Cui, Wang, and Gao, 2010; Hu and Sun, 1998).

Tensile properties of plain weaving silk fabric after treated with epoxy have been reported by Hu and Sun (1998). The multi-functional finishing agent epoxy resin ethanolic phosphotungstic acid (EPTA) was prepared in water solution (solid content 60%). Silk fabric was padded twice with a 100 g/l EPTA at 100% wet pick-up, dried at 40°C for 3 min, then the fabric was treated with 8 g/l sodium carbonate at 75°C for 15 min. Tensile properties of untreated silk fabric and epoxy treated silk fabric are shown in Table 2.13. The result showed that tensile

strength and elongation at break of epoxy treated silk fabric were lower than those of untreated silk fabric (Hu and Sun, 1998).

Table 2.13 Tensile properties of untreated silk fabric and epoxy resin EFTA treated silk fabric (Hu and Sun, 1998).

Sample	Tensile strength (N)	Elongation at break (%)
Untreated silk fabric	396	19.6
Epoxy resin EFTA treated silk fabric	350	19.3

2.3 Fiber reinforced epoxy composite

Epoxy resin represents some of the highest performance resin due to the mechanical properties and resistance to environmental degradation, which leads to their almost exclusive use in aircraft components. In addition, epoxy resin can also be used in both laminating and molding techniques (Chow, 2007). Epoxy resin is also used with reinforcing fibers for advanced composites application. Fiber reinforcements for epoxy resins, such as glass, carbon, Aramid are widely used in advanced composites application. Glass fibers show good performance and play a main function in playground equipment, recreational items, piping for corrosive chemicals, and many other common applications. The cost of the glass fiber is considerably lower than the cost of carbon-based fibers (Mallick, 1997). Fibers such as short Aramid, glass or carbon fibers are used in order to increase creep resistance and compressive strength of polymer matrix system. Fiber-reinforced composites, owing to their superior properties, are usually applied in different fields like defense,

aerospace, engineering applications, sports goods, etc (Jiang, Gyurova, Schlarb, Friedrich and Zhang, 2008).

Nowadays, natural fiber composites have gained increasing interest due to their eco-friendly properties. A lot of work has been done by researchers based on these natural fibers. Natural fibers such as jute, sisal, silk and coir are inexpensive, abundant and renewable, lightweight, with low density, high toughness, and biodegradable (Ku, Wang, Pattarachaiyakooop and Trada, 2011). Silk has the potential to be used as a replacement for traditional reinforcement materials in composites for applications which requires high strength to weight ratio and further weight reduction (Sutapun, Rossapol, Kiaw-on and Kittilertkul, 2007; Zulkifli, Azhari, Maryam, Ahmad and Abu, 2009).

2.3.1 Kevlar/epoxy composite

Kevlar fiber composites are being increasingly used in aircraft, missile and space applications such as rocket motor casings and nozzles. The fiber failure in the longitudinal splitting mode has led to the unique ballistic resistance of Kevlar when used with suitable combination of matrices. Thus the development of Kevlar composites with high strength as well as stiffness, apart from their proven toughness, is highly relevant and significant in the current scenario where the thrust is on good damage tolerance, high strength and stiffness, good hot-wet properties, high fatigue life and low density (Yue and Padmanabhan, 1999). However, the adhesion between Kevlar fibers and most matrices is poor, due to the high crystallinity leading a chemically inactive surface and the relatively smooth surface of the fiber. Fiber-surface modification results in improved wettability, surface energy, surface

roughness, and polar groups on the surface. All these would improve the adhesion between the fiber and matrix (Wu, Sheu and Shyu, 1996).

2.3.1.1 Effect of surface modification of Kevlar fiber on mechanical properties of Kevlar fiber/epoxy composite

Many reports are available on the adhesion related properties of Kevlar fiber. The fiber has also been used as a reinforcement after modifying the surface with chemical treatment or plasma treatment (Guo, Zhang, Liu, Su and Zhang, 2009; Yue and Padmanabhan, 1999). Increasing the Kevlar and matrix adhesion has also resulted in the improvement of the compressive strength of Kevlar composites by retarding the onset of fiber buckling (Day, Hewson and Lovell, 2002; Li *et al.*, 2008).

Wu *et al.* (1996) have been studied effect of plasma treatment of Kevlar fiber on mechanical properties of Kevlar/epoxy composite. Kevlar fibers were surface-modified by NH₃-, O₂-, and H₂O- plasma etching and chlorosulfonation and subsequent reaction with some reagents (glycine, deionized water, ethylenediamine, and 1-butanol) to improve the adhesion to epoxy resin. After these treatments, the interlaminar shear strength (ILSS) between the fiber and epoxy resin, as measured by the short-beam test was remarkably improved by gas plasma and chlorosulfonation.

Ren *et al.* (2007) have been studied influence of Kevlar fiber moisture regain during atmospheric plasma treatment on aging of treatment effects, on surface wettability and bonding strength to epoxy. Immediately after the plasma treatment, the treated fibers have substantially lower water contact angles, higher surface oxygen and nitrogen contents, and larger interfacial shear strength (IFSS) to epoxy than those of the untreated Kevlar fibers. At the end of 30 day aging period,

the fibers treated with 5.5% moisture regain had lower water contact angle and more polar groups on the fiber surface, leading to 75% improvement of IFSS over the untreated fibers while those for the 0.5 and 3.5% moisture regain groups were only 30%.

Recently ultrasound has been applied to improve the interface performance of Kevlar/epoxy composites by forcedly impregnating resin into interbundles of Kevlar fibers. Ultrasound can effectively improve the interface of Kevlar fiber/epoxy composites through activating the surface of fibers and producing the interface interlock. The obvious advantage of ultrasound treatment is that it can be applied easily and directly in the winding process to treat the interface on-line without decreasing the tensile strength of fibers. Kevlar fiber/epoxy composites have been treated by ultrasound during the winding process to enhance the adhesion. According to the ultrasonic treatment ILSS of composites has been greatly improved (Li, *et al.*, 2008).

2.3.1.2 Effect of moisture on mechanical properties of Kevlar fiber/epoxy composite

Since the use of advanced fiber reinforced composites in engineering applications is extended, evaluation of the environmental strength of the composites becomes an extremely important research area. Many researchers have been investigated the influence of environment, especially wet environment, on the fracture characteristics of the Kevlar fiber. The tensile strength of the Kevlar fiber were decreased due to water absorption (Minoshima, Maekawa and Komai, 2000).

Allred and Roylance (1983) have been reported moisture sensitivity of Kevlar 49/epoxy composites on mechanical properties. They were found

that the transverse tensile strength and elongation at break of Kevlar 49/epoxy composites dropped to 35% and 27%, respectively. These were caused by the moisture interrupted hydrogen bonding in fiber filament (Allred and Roylance, 1983).

2.3.1.3 Effect of fiber content on thermal properties of Kevlar

fiber/epoxy composite

Differential scanning calorimetry (DSC) have been used to characterize thermal properties of Kevlar/epoxy composites. DGEBA epoxy matrix have been cured with two systems of hardener (anhydride and diamine). The two systems were varied content of continuous Kevlar fiber. A significant decrease in the glass transition temperature (T_g) was observed as Kevlar content increased when anhydride matrix was used while little change was observed in the reinforced diamine systems.

In a case of the diamine system, the exothermic peak temperature (T_p) slightly increased with the fiber content of 30 wt.%. Above a 30 wt.% fiber content, T_p decreased, was not lower than that of the neat system. For the anhydride system, it was observed that as Kevlar content increased, the heat flow curves were shifted to much lower temperatures, and the exothermic peak temperature T_p decreased to 50°C (Suay Antón, Gómez Ribelles, Monleón Pradas and Arnau Izquierdo, 1999).

2.3.2 Glass/epoxy composite

Glass fiber reinforced composites offer the most reliable engineering materials compared with other composites by virtue of a large technology base and experience in service. Where high Young's modulus values are not required, they

continue to provide one of the best low cost materials for normal applications. Composites containing woven forms of fiber are characterized by high fracture toughness and ease of handling. Their integrated nature provides balanced in-plane properties. The transverse tensile strength of woven-fabric composites is much higher than that of unidirectional composites (Yang, Kozey, Adanur and Kumar, 2000).

The effect of weaving type of glass reinforced epoxy composite on their mechanical properties have been reported (Yang, *et al.*, 2000). For the tensile strength and modulus respectively normalized with respect to the density of each lamina. Bending showed similar results. The lamina reinforced with plain glass woven/epoxy (Tensile strength of $127.64 \text{ MPa.g}^{-1}\text{cm}^3$ and Young's modulus of $8.22 \text{ GPa.g}^{-1}\text{cm}^3$) showed the high performances than glass mat/epoxy composite (Tensile strength of $83.78 \text{ MPa.g}^{-1}\text{cm}^3$ and Young's modulus of $7.26 \text{ GPa.g}^{-1}\text{cm}^3$). This result is the consequence of the presence of long and aligned continuous glass fiber (Cristaldi, Latteri, Recca and Cicala, 2010).

Some mechanical properties of plain weaving glass/epoxy composite with the fiber volume fraction of 0.4 are shown in Table 2.14. The composite material consists of six layers of identically oriented woven fibers (Okutan, Aslan and Karakuzu, 2001).

Table 2.14 Some mechanical properties of plain weaving glass/epoxy composite at fiber volume fraction of 0.4 (Okutan, *et al.*, 2001).

Properties	Value
Young's modulus	20 GPa
Shear modulus	461 MPa
Tensile strength	473 MPa
Shear strength	85 MPa

2.3.3 Silk/epoxy composite

Natural fibers such as silk have the potential to be used as a replacement for traditional reinforcement materials in composites for applications which requires high strength to weight ratio and further weight reduction (Sgriccia, Hawley and Misra, 2008). Silk has been an important fabric in the textiles industry due to its luster and superb mechanical properties. Woven fabric silk reinforced epoxy resin has been used as structural materials for solar car body due to its cost and weight advantages as a potential alternatives to the carbon fiber/epoxy composite (Zulkifli, *et al.*, 2009).

2.3.3.1 Effect of silk content on mechanical properties of silk/epoxy composite

The impact response of woven natural silk (WNS)/epoxy composite has been studied by Ude, Ariffin, Sopian, Arifin and Azhari (2010). The composite specimens were made by hand- lay-up. The composite specimens were prepared in configurations of 10, 15, 20, 25 and 30 ply of WNS. Drop weight impact

test was carried out under various impact energies of 32 J, 48 J and 64 J. The results of absorption of energy showed that more energy was absorbed with an increase in the number of woven natural silk ply. The absorption of energy did not increase with an increase in impact load as it was the case with increase in number of ply. The values suggested that absorption capability of a specimen with increasing load could be affected by the internal structures of the specimen. These includes homogenous distributions of fiber and the matrix, the interface bounding between the fiber and matrix, voids created by trapped air and laminations caused by unlapped woven fabrics (Ude, Ariffin, Sopian, Arifin and Azhari, 2010). The mechanical properties like tensile strength and flexural strength of the composites were determined. These properties were found to increase with silk fabric content (Priya, Ramakrishna, Rai and Rajulu, 2005).

2.3.3.2 Silk/epoxy interfacial properties

The mechanical performance of fiber reinforced composites is sensitive to the interfacial bond between fiber and matrix. The interfacial shear strength (IFSS) is therefore a good measurement of the effectiveness of fiber reinforcement. This is frequently characterized via a single fiber pullout test although other techniques such as fragmentation and micro-compression have also been used. Pullout tests exist in several different geometries. The method developed by Miller *et al.* (1987) named the “Microbond Test”, has been used. This technique has grown in popularity and has been used on glass, Kevlar and carbon fibres. The interaction between silkworm silk fiber and a resin matrix was investigated by means of the Microbond Test. Cured resin droplets were sheared from silk fiber by the knife-edged jaws of a microvice. The mean interfacial shear strength was determined as 15 ± 2

MPa: coupled with the high tensile strength of silk, and its high extensibility relative to that of synthetic polymer or glass fibres, this interfacial shear strength could be exploited in tough composites (Craven, Cripps and Viney, 2000).

2.3.3.3 Interaction between epoxy and APTES treated silk

The reaction of epoxy pre-polymer diglycidyl ethers of bisphenol A (DGEBA) with APTES was systematically studied using differential scanning calorimetry (DSC), FTIR, and size exclusion chromatography (SEC), indicating that the epoxy is highly reactive towards the amine group producing an insoluble fraction after reaction. The insoluble fraction is formed via the gelation of silane ethoxy and methylol groups which are produced by the amine-epoxy reaction. The interfacial interactions of DGEBA and silanes were studied by incorporating the polysiloxane powders formed from condensation of hydrolyzed APTES into DGEBA matrix (Jensen, Palmese and McKnight, 2006; Xie, Hill, Xiao, Militz and Mai, 2010).

2.3.4 Fracture surface of fiber reinforced epoxy composite

The structure and properties of the fiber–matrix interface play a major role in controlling the mechanical and physical properties of composite materials (Guduri, Rajulu and Luyt, 2007). In a view that stress is transferred from one fiber to another through the matrix, the interface between the matrix and fiber plays a major role in the overall mechanical performance of composite materials (Guduri and Luyt, 2006). The nature of the bonding between the matrix and the fiber is dependent on the chemical properties of the fiber and the finish (coupling agent) used (Guduri, *et al.*, 2007).

Several investigators have used scanning electron microscopy (SEM) to study fracture surface of untreated carbon fiber/epoxy composite. The SEM photograph of a composite without a coupling agent is shown in Figure 2.25. It can be seen in Figure 2.27 that the carbon fiber shows very poor interfacial bonding with the epoxy resin; the micrograph shows that some of the carbon fibers were pulled out from the epoxy matrix (Guduri and Luyt, 2006).

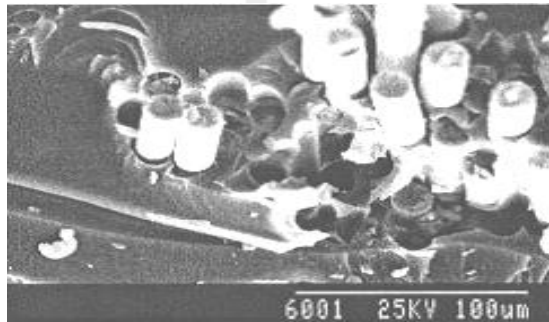


Figure 2.25 SEM micrograph of untreated carbon fiber/epoxy composite (Guduri and Luyt, 2006).

Liu and Hughes (2008) investigated fracture surface of epoxy matrix composites reinforced with untreated woven flax fiber textiles having fiber volume fractions greater than 0.30. Fracture surface obtained from tensile testing both in warp and weft direction were investigated. They found that failure of weft fiber (Figure 2.26b at “B”), debonding of warp fiber from the matrix (Figure 2.26b at “A”) and brittle fracture of matrix were the main fracture mechanisms. In the samples tested in the warp direction, however, the fracture paths were more disordered and it was found that most warp yarns had been pulled out from the matrix (Figure 2.26d at “C”). Good impregnation of the yarns have been occurred by the resin. SEM

micrographs of the fracture surfaces of untreated flax/epoxy composite in both the weft and warp directions are shown in Figure 2.26.

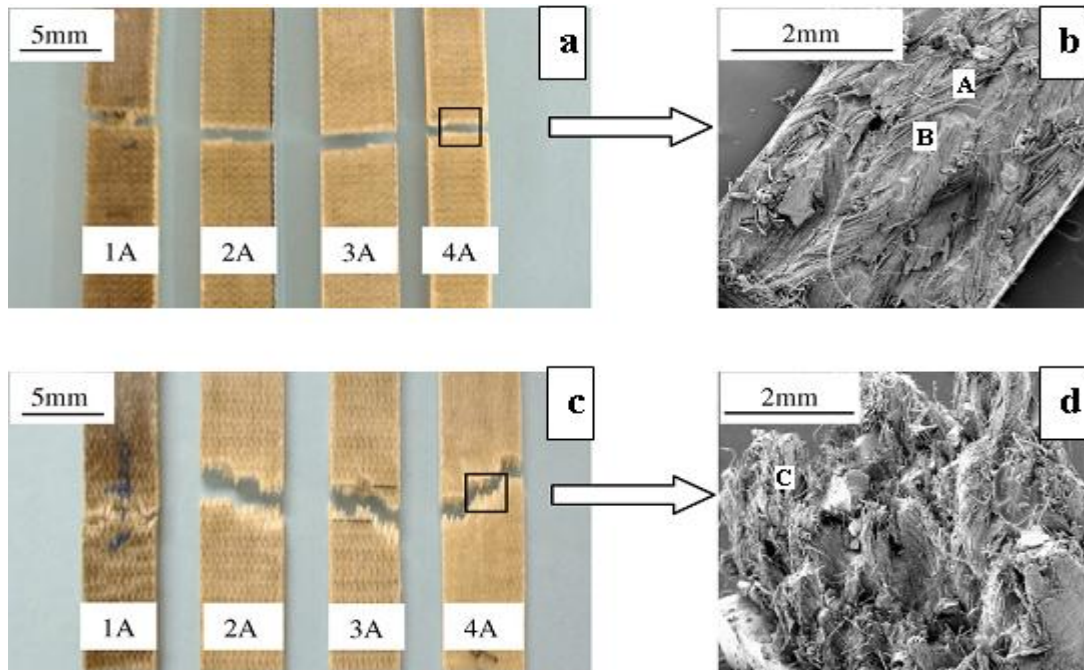


Figure 2.26 Fracture surfaces of untreated flax/epoxy composite in weft direction (a, b) and warp directions (c, d) (Liu and Hughes, 2008).

SEM photographs showing impact fracture surfaces of flax fiber are shown in Figure 2.27. It can be seen that there is a lot of fiber pulled out in untreated fiber composite (George, Ivens and Verpoest, 1999).

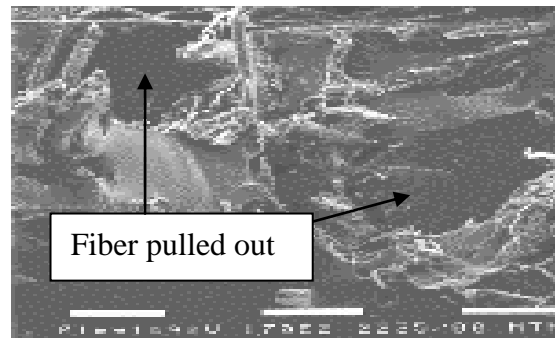
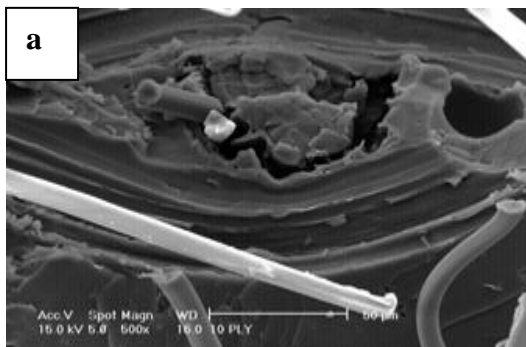


Figure 2.27 SEM micrograph of untreated flax fiber/epoxy composite (George, *et al.*, 1999).

The SEM micrographs *B.mori* woven natural silk (WNS) as a reinforcement for epoxy have been studied by Ude and coworker (2010). They presented the impact response of woven WNS/epoxy composite. The composite specimens were prepared in configurations of 10, 15, 20, 25 and 30 ply of WNS. Drop weight impact test was carried out under varied impact energies of 32J, 48J and 64J. The scanning electronics microscope (SEM) result showed mechanism of failure as a combination of delamination, fiber-matrix debonding, fiber breakage and interlaminar matrix cracking. An impact on composite laminates can cause various types of damages including matrix cracking; delamination; fiber breakage; penetration and perforation of the impacted surface. The important step in studying the impact behaviour of composite materials is to characterise the type and extension of the damage induced in the impacted specimens. SEM photographs of all the impacted specimens under 64 J impact load are shown in Figure 2.28. There is strong evidence from these specimens in Figures 2.28 a – 2.28 e that a combination of matrix cracking, delamination and fiber breakage are the predominant failure modes. These

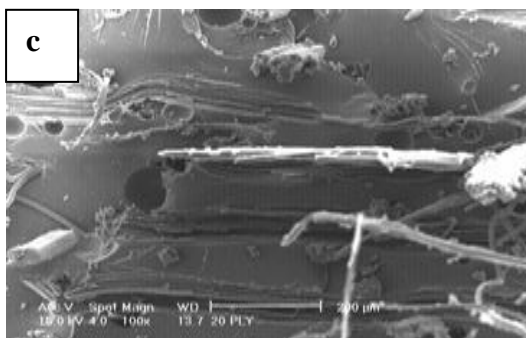
failure mechanisms agree very well with the impact damages reported by Corum *et al.* (2003) for chopped glass fiber composites and carbon fiber reinforced epoxy matrix composites. Further investigations of the specimen photographs in Figures 2.28 a – 2.28 e, proved that their modes of failures are similar irrespective of the number of ply. They all involved a combination of failures. In Figure 2.28 a and 2.28 b, showed matrix cracking, matrix splattering, delaminations, fiber pulled out and fiber breakage. In Figure 2.28 c and 2.28 d, there were voids, fiber pulled out, matrix cracking and fiber breakage. In Figure 2.28 e, a combination of matrix cracks, delaminations, fiber breakage and fiber pulled out were seen. This behaviour seems to be one of the advantages of using woven fabrics other than unwoven. It was reported by Ude *et al.* (2007) that low volume of fiber creates vacant spaces, and there is not enough fiber to restrain matrix; causing resin rich areas present which can lead to highly localised strain. Rong *et al.* (2001) also reported that as the fiber weight fraction increase, the wettability of fiber with resin decreases and weak interfacial bonding potentially occurs. This is not the case in woven natural silk laminates as proved by these micrographs (Ude, *et al.*, 2010).



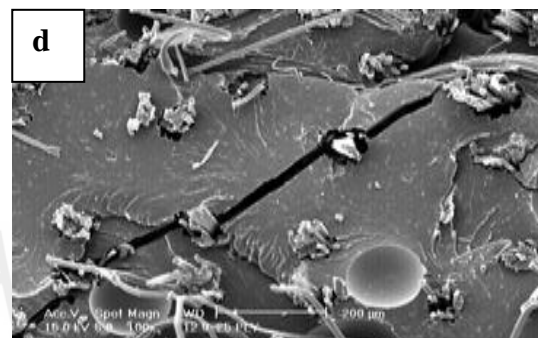
10 ply of woven silk fabric



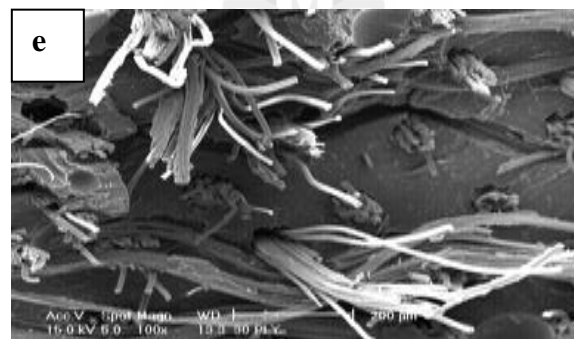
15 ply of woven silk fabric



20 ply of woven silk fabric



25 ply of woven silk fabric



30 ply of woven silk fabric

Figure 2.28 SEM micrographs of woven silk/epoxy obtained from impact testing specimen(Ude, *et al.*, 2010).

CHAPTER III

EXPERIMENTAL

3.1 Materials

The *Bomby mori* silk fabric (plain weaving with 177 ends/10cm x 201 picks/10cm) was purchased from a housewife group of Tumbol Sompoi, Aumphur Rasrisalai, Sisaket, Thailand. The plain weaving of glass fabric with 70 ends/10 cm and 80 picks/10cm and Kevlar fabric with 50 ends/10 cm and 50 picks/10cm were purchased from Concrete Composite Co., Ltd. The fabric density of UT-SF, ST-SF, glass fabric and Kevlar fabric was 125 g/m², 125 g/m², 200 g/m² and 200 g/m², respectively. The diglycidyl ether of bisphenol A, DGEBA (YD127) with epoxy equivalent weight of 180-187 g/eq was purchased from Thai Organics Chemical Co., Ltd. Triethylenetetramine (TETA) curing agent having amine hydrogen equivalent weight of 24.3 g/eq was purchased from Vista Co., Ltd. The BYK-A560 defoamer, for degassing epoxy system, was purchased from Coloshal International Co., Ltd. 3-aminopropyltriethoxysilane (APTES), for modifying silk fabric surface, was purchased from Optimal Tech Co., Ltd.

3.2 Experimental

3.2.1 Preparation of neat epoxy

Neat epoxy was prepared by mixing DGEBA liquid resin and TETA curing agent with a mixture ratio of 100 : 13.2. BYK-A560 of 0.015 cm³ was dropped into DGEBA before mixed with TETA. The DGEBA and BYK-A560 mixture was left at room temperature for 24 h for degassing. When degassed DGEBA and TETA were already mixed, the mixture was stirred by a propeller, poured into a mold (25 cm x 25 cm x 0.6 cm), and then degassed in vacuum for 30 min. The molded epoxy was left at room temperature for 24 h and then cut into test specimens before post cure. They were post cured in an oven at 110°C for 6 h.

3.2.2 Preparation of reinforcement fabrics

Silk fabric was prepared as untreated silk fabric (UT-SF) and silane treated silk fabric (ST-SF). To prepare UT-SF, silk fabric was cut into a square shape of 30 cm x 30 cm and dried in an oven at 110°C for 12 h to remove moisture. To prepare ST-SF, UT-SF was treated with 3-aminopropyltriethoxysilane (APTES) solution. The silane aqueous solution was prepared at a concentration of 2 vol% of APTES in water solvent and the pH of silane solution was adjusted to 3.5 with an acetic acid. UT-SF was then soak in the silane solution with a liquor ratio of 1 g : 10 ml for 2 hr. It was then washed with distilled water and dried in an oven at 70°C for 12 hr to remove moisture. Glass fabric and Kevlar fabric were also cut into a square shape of 30 cm x 30 cm for the composite preparation.

3.2.3 Preparation of epoxy composites

The epoxy composite was prepared with various weight fractions of UT-SF, 0.1, 0.15, 0.18, 0.30 and 0.35. The epoxy composites reinforced with ST-SF were prepared with ST-SF weight fractions of 0.18, 0.30 and 0.35. The epoxy composites reinforced with glass fabric and Kevlar fabric were prepared only at 0.35 weight fraction of those fabrics.

First of all, the reinforcement fabrics (UT-SF, ST-SF, glass fabric and Kevlar fabric) were soaked in degassed DGEBA for 24 h prior to composite preparation. The degassed DGEBA was prepared by mixing DGEBA and BYK-A560 of 0.015 cm³ and the mixture was left at room temperature for 24 h. Epoxy matrix was prepared by mixing DGEBA and TETA curing agent with a mixture ratio of 100 : 13.2. The epoxy composites were molded by hand lay-up technique using a mold size of 25 cm x 25 cm x 0.6 cm. The molded epoxy composites were degassed in vacuum for 30 min and left at room temperature for 24 h and then cut into test specimens before post cure in an oven at 110°C for 6 h. The specimens were further characterized and mechanically tested.

The number of fabric layers within epoxy composites prepared with UT-SF, ST-SF, glass fabric and Kevlar fabric at various fabric weight fractions was numbered in Table 3.1.

Table 3.1 The number of fabric layers within epoxy composites reinforced with UT-SF, ST-SF, glass fabric and Kevlar fabric.

Weight fraction	Number of fabric layers			
	UT-SF/epoxy composite	ST-SF/epoxy composite	glass/epoxy composite	Kevlar/epoxy composite
0.10	3	-	-	-
0.15	5	-	-	-
0.18	6	6	-	-
0.30	12	12	-	-
0.35	18	18	6	6

3.3 Material Characterization

3.3.1 Characterization of reinforcement fabrics

3.3.1.1 Mechanical properties

Tensile properties (tensile modulus, tensile strength and elongation at break) of silk fabrics, glass fabric and Kevlar fabric were determined in accordance with ASTM D5034. The tensile testing was performed using a universal testing machine (UTM, Instron 5565), with a load cell of 5 kN in a uniaxial tension at a crosshead speed of 300 mm/min with a fixed gauge length of 75 mm. The dimension of reinforcement fabrics was 10 cm x 15 cm. UT-SF and ST-SF were tested in both warp and weft direction. Glass and Kevlar fabric were tested in weft direction. Young's modulus, tensile strength and toughness of reinforcement fabrics were normalized with fabric density following equation (3.1)-(3.3), respectively.

$$\text{Normalized modulus} = \frac{\Delta \text{Force}}{\Delta \text{Extension} \times \text{Fabric density}} \dots\dots\dots (3.1)$$

$$\text{Tensile strength} = \frac{\text{Tensile force at break}}{\text{Fabric density}} \dots\dots\dots (3.2)$$

$$\text{Toughness} = \frac{\text{Area under load-extension curve}}{\text{Fabric density}} \dots\dots\dots (3.3)$$

3.3.1.2 Thermal properties

Thermal decomposition temperature and weight loss of UT-SF, ST-SF, glass fabric and Kevlar fabric were monitored by a thermogravimetric analyzer (TA Instrument, SDT 2960) with a heating rate of 20°C/min under a nitrogen atmosphere. Thermal properties of UT-SF, ST-SF, glass fabric and Kevlar fabric were also analyzed by a differential scanning calorimeter (PYRIS Dimond, DSC7) with a heating rate of 20°C/min under a nitrogen atmosphere.

3.3.1.3 Chemical functional groups

Chemical functional groups of UT-SF and ST-SF were determined by a FT-IR spectrometer (Bruker, VERTEX 70) with 32 co-added scans and a resolution of 4 cm⁻¹ in the ATR mode within wavenumber of 4000 cm⁻¹ – 600 cm⁻¹. MIRacle-single reflection ATR equipped with platinum diamond (Type A225/QL) was used.

3.3.1.4 Elemental composition

Elemental composition of UT-SF ash and ST-SF ash was determined by a X-ray fluorometer (XRF, Oxford X-ray Fluorometer ED 2000). The measurement was done using K_α radiation under an accelerating voltage of 80-100 kV

and a current of 24-30 mA. The UT-SF and ST-SF ash were prepared by heating UT-SF and ST-SF at 750°C for 8 h in a chamber furnace (Carbolite, CWF).

3.3.1.5 Surface morphology

Surface morphology of UT-SF, ST-SF, glass fabric and Kevlar fabric was investigated by a scanning electron microscope, (SEM, JSM 6400), with an accelerating voltage of 20 kV. The fabrics were coated with gold to avoid charging under an electron beam.

3.3.2 Characterization of neat epoxy and epoxy composites

3.3.2.1 Mechanical properties

Tensile properties (tensile modulus, tensile strength and elongation at break) of neat epoxy, UT-SF/epoxy composite, ST-SF/epoxy composite, glass fabric/epoxy composite and Kevlar fabric/epoxy composite were determined in accordance with ASTM D 5083. The uniaxial tensile test was performed under a universal testing machine (UTM, Instron 5569) with a load cell of 50 kN and a crosshead speed of 5 mm/min. The epoxy composite specimens were tested in weft direction of fabric. At least five specimens were tested for neat epoxy and each composition of epoxy composites.

Flexural properties of neat epoxy, UT-SF/epoxy composite, ST-SF/epoxy composite, glass fabric/epoxy composite and Kevlar fabric/epoxy composite were tested according to ASTM D 790 using a universal testing machine (UTM, Instron 5569) with a load cell of 50 kN. The testing was performed under a three point bending system with a span length of 96 mm and a crosshead speed of 2.65 mm/min. The epoxy composite specimens were tested in weft direction of fabric.

Unnotched Izod impact strength of neat epoxy, UT-SF/epoxy composite and ST-SF/epoxy composite was evaluated using an impact tester (Atlas, BPI) following ASTM D 256. The specimens from epoxy composite were tested in warp direction of fabric. At least five specimens were tested and average impact strength was calculated.

In addition, notched Izod impact strength of the ST-SF/epoxy composite, glass fabric/epoxy composite and Kevlar/epoxy composites at fabric weight fraction of 0.35 was evaluated using an impact tester (Atlas, BPI) following ASTM D 256. The epoxy composite specimens were tested in weft direction of fabric. At least five specimens were tested and average impact strength was calculated.

Heat distortion temperature (HDT) of neat epoxy, UT-SF/epoxy composite, ST-SF/epoxy composite, glass fabric/epoxy composite and Kevlar fabric/epoxy composite was investigated using a heat distortion temperature instrument (HDV 1 Manual DTVL/VICAT). The testing was followed ASTM D648 with a span length of 100 mm and a heating rate of 2°C/min. Three specimens were simultaneously tested.

3.3.2.2 Thermal properties

Thermal decomposition temperature and weight loss of neat epoxy, UT-SF/epoxy composite, ST-SF/epoxy composite, glass fabric/epoxy composite and Kevlar fabric/epoxy composite were investigated using a thermogravimetric analyzer (TA Instrument, SDT 2960) with a heating rate of 20°C/min under a nitrogen atmosphere.

Thermal analysis of neat epoxy and epoxy composites before post curing was performed using a differential scanning calorimeter (PYRIS Dimond, DSC7) with a heating rate of 20°C/min under a nitrogen atmosphere. Thermal analysis of neat epoxy and epoxy composites after post cure was performed using also a differential scanning calorimeter (PYRIS Dimond, DSC7) under a nitrogen atmosphere. These samples were first heated from 30°C to 150°C with a heating rate of 20°C/min, then was kept at 150°C for 5 min, cooled down to 30°C with a cooling rate of 20°C/min, and finally heated up to 150°C with a heating rate of 20°C/min.

3.3.2.3 Fracture surface morphology

The fracture surface of neat epoxy, UT-SF/epoxy composite, ST-SF/epoxy composite, glass fabric/epoxy composite and Kevlar fabric/epoxy composite obtained from impact test was investigated using a scanning electron microscope, (JSM 6400), with an accelerating voltage of 20 kV. The samples were coated with gold to avoid charging under an electron beam.

CHAPTER IV

RESULTS AND DISCUSSION

4.1 Physical Properties of Reinforcement Fabrics

4.1.1 Mechanical properties

Load-extension curves of UT-SF, ST-SF, glass fabric, and Kevlar fabrics are shown in Figure 4.1. From load-extension curves, Kevlar fabric and glass fabric were stiffer than silk fabrics. The area under curve of force - extension of silk fabrics was higher than that of Kevlar fabric and glass fabric. The area under force - extension of curves UT-SF was lower than that of ST-SF.

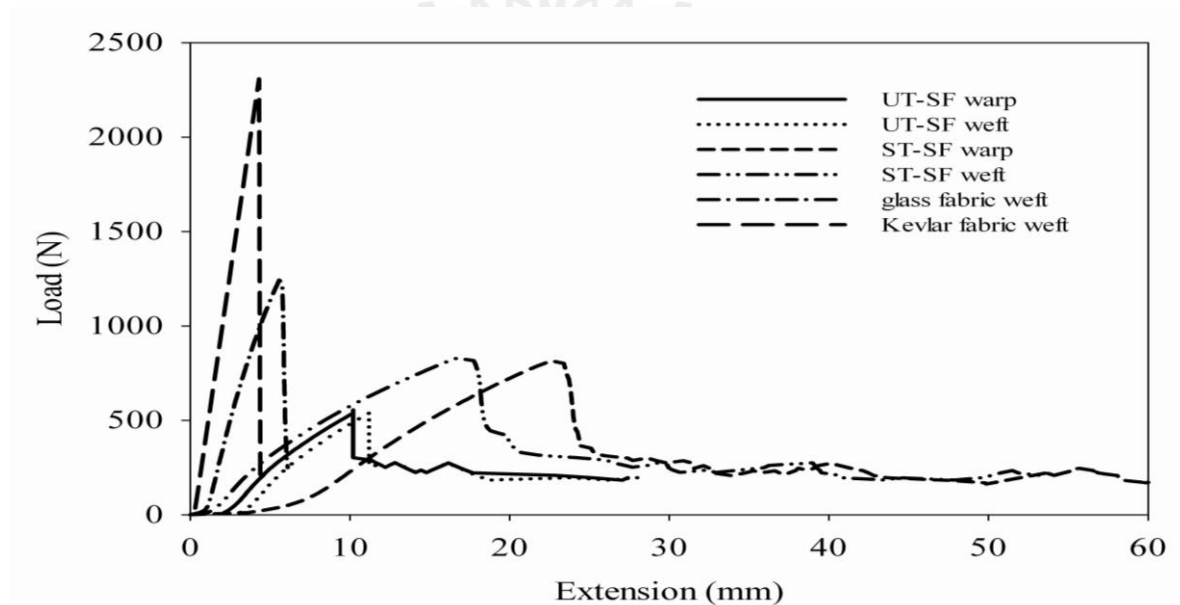


Figure 4.1 Plot of load VS extension of UT-SF and ST-SF obtained in warp and weft direction and glass fabric, and Kevlar fabric obtained in weft direction.

Slope, maximum force and elongation at break of UT-SF, ST-SF, glass fabric and Kevlar fabric are shown in Table 4.1. Slope, maximum force and elongation at break of UT-SF and ST-SF in warp and weft direction were insignificantly different. Slope and maximum force of glass fabric and Kevlar fabric were higher than those of silk fabrics. Whereas, elongation at break of silk fabrics was higher than those of glass fabric and Kevlar fabric.

Normalized modulus, tensile strength and toughness normalized with fabric density of UT-SF, ST-SF, Glass fabric and Kevlar fabric are summarized in Table 4.2. Young's modulus, tensile strength and toughness of UT-SF and ST-SF in warp and weft direction were insignificantly different. It may be due to similar number of yarns in warp and weft direction. Tensile strength of ST-SF was higher than that of UT-SF. This was an indication that silk fiber was strengthened after aminopropyltriethoxysilane (APTES) coupled with some functional groups located at the fiber surface, as schematically shown in Figure 2.24. George, Sreekala and Thomas (2001) were reported that the APTES led to strong covalent bond formation between silk thread and thereby the tensile strength was enhanced. Young's modulus of Kevlar fabric and glass fabric was higher than UT-SF and ST-SF. Tensile strength of Kevlar fabric was higher than that of silk fabric and glass fabric. However, toughness of ST-SF was higher than that of UT-SF, Kevlar fabric and glass fabric. In addition, toughness of UT-SF, Kevlar fabric and glass fabric was insignificantly different. For mechanical testing, epoxy composite specimens were tested in only the weft direction of the fabric. This was because tensile properties of fabric in warp and weft direction were insignificantly different.

Table 4.1 Slope, maximum force and elongation at break obtained from load-extension curves of UT-SF, ST-SF, glass fabric and Kevlar fabric.

Reinforcement fabrics	Slope (N.cm ⁻¹)		Maximum force (N)		Elongation at break (%)	
	warp	weft	warp	weft	warp	weft
UT-SF (177 ends/10 cm and 201 picks/10cm)	674.38 ± 19.67	689.67 ± 29.76	537.00 ± 0.95	555.00 ± 1.26	15.22 ± 0.57	16.08 ± 0.86
ST-SF (177 ends/10 cm and 201 picks/10cm)	536.12 ± 8.55	580.88 ± 11.76	813.41 ± 97.40	827.87 ± 116.62	45.04 ± 1.70	33.80 ± 5.06
Glass fabric (70 ends/10 cm and 80 picks/10cm)	-	2692.00 ± 0.15	-	1211.34 ± 57.82	-	11.26 ± 0.38
Kevlar fabric (50 ends/10 cm and 50 picks/10cm)	-	5824.00 ± 0.10	-	2309.91 ± 108.51	-	8.58 ± 0.54

Table 4.2 Normalized tensile properties of UT-SF, ST-SF, glass fabric and Kevlar fabric.

Reinforcement fabrics	Normalized modulus (N.cm.g ⁻¹)		Tensile strength (N.cm ² .g ⁻¹)		Toughness (J.cm ² .g ⁻¹)	
	warp	weft	warp	weft	warp	weft
UT-SF (177 ends/10 cm and 201picks/10cm)	3.37 ± 0.09	3.44 ± 0.14	4.29 ± 0.01	4.44 ± 0.01	0.02	0.01
ST-SF (177 ends/10 cm and 201picks/10cm)	2.28 ± 0.04	2.90 ± 0.05	6.50 ± 0.78	6.62 ± 0.93	0.05	0.06
Glass fabric (70 ends/10 cm and 80 picks/10cm)	-	13.46	-	6.05 ± 0.28	-	0.01
Kevlar fabric (50 ends/10 cm and 50 picks/10cm)	-	29.12	-	11.55 ± 0.54	-	0.02

4.1.2 Chemical functional groups and elemental composition of UT-SF and ST-SF

4.1.2.1 Chemical functional groups of UT-SF and ST-SF

The FT-IR spectrum of UT-SF is shown in Figure 4.2. The absorbance at 3280 cm^{-1} belonged to the N-H stretching vibration and 3076 cm^{-1} corresponded to C-NH overtone. The peaks at 2970 cm^{-1} and 2932 cm^{-1} were the characteristic band for the CH-stretching antisymmetric in silk fibroin. The absorbance at 1442 cm^{-1} was attributed to CH_2 and CH_3 bending. The absorbance at 1164 cm^{-1} was attributed to C-N stretching in tyrosine. The absorbance at 1045 cm^{-1} belonged to C-O stretching. The peaks at 1101 cm^{-1} and 1004 cm^{-1} were the characteristic band for the skeletal stretching of phenylalanine in silk fibroin. The peaks at 851 cm^{-1} , 826 cm^{-1} and 690 cm^{-1} were characteristic band for =C-H out-of-plane deformations in aromatic rings of tyrosine (Kweon, Park, Ye, Lee and Cho, 2001).

The absorbances at 1619 cm^{-1} , 1516 cm^{-1} and 1230 cm^{-1} were the characteristic band for amide I, amide II and III, respectively. Tomoyuki and Shaul (2007) reported that the amide I originated from the stretching motion of the C=O whereas the amide II and III attributed to bending motion of the N-H coupling with C-N (Tomoyuki and Shaul, 2007). Peak assignment for FT-IR vibration of UT-SF is shown in Table 4.3.

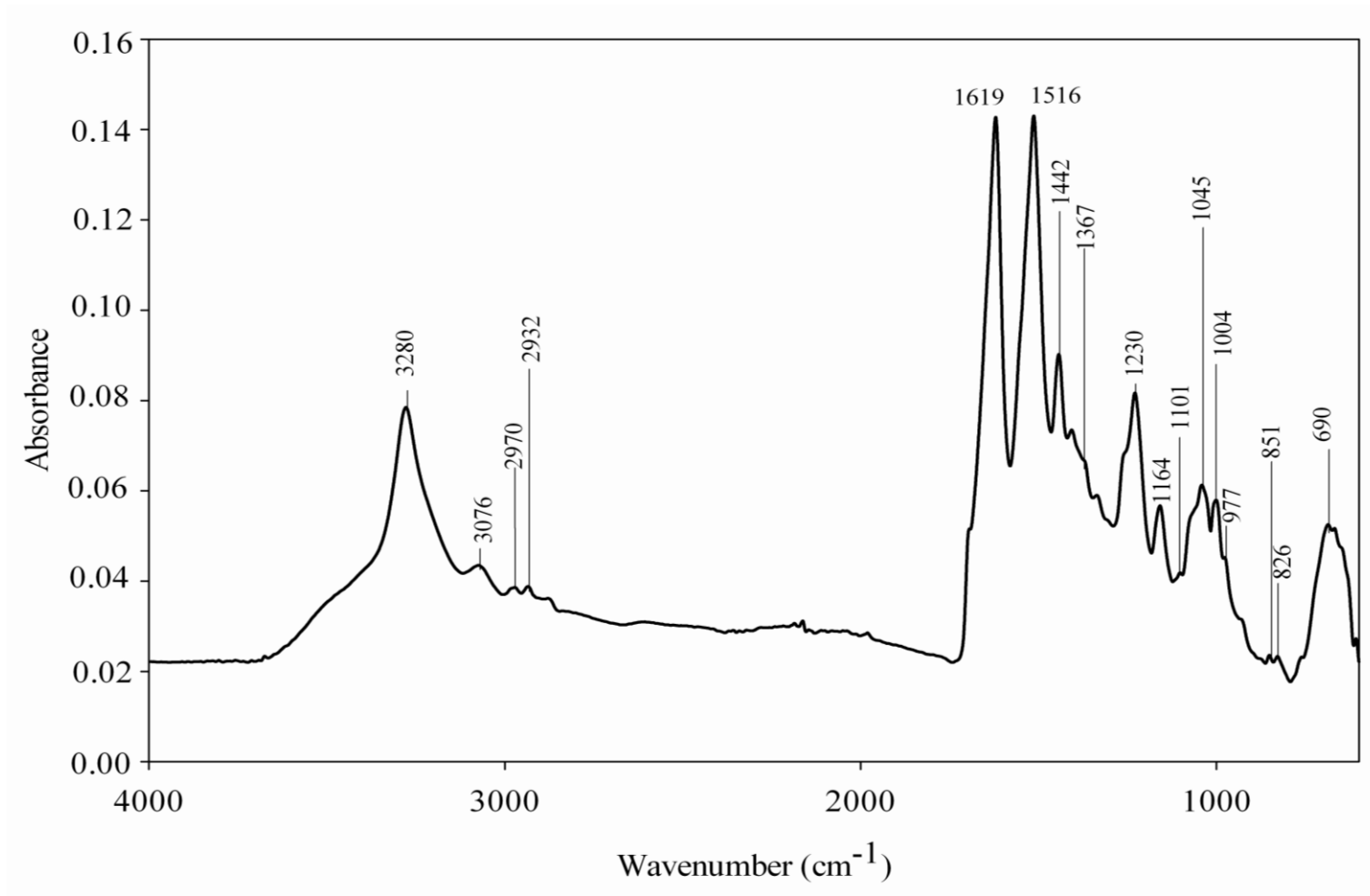


Figure 4.2 FT-IR spectrum of UT-SF with wavenumber assignment.

Table 4.3 Assignment of FT-IR bands for UT-SF (Kweon, Park, Ye, Lee, and Cho, 2001; Lefevre, Paquet-Mercier, Lesage, Rousseau, Bedard, and Pezolet, 2009; Mossotti, Innocenti, Zoccola, Anghileri, and Freddi, 2006).

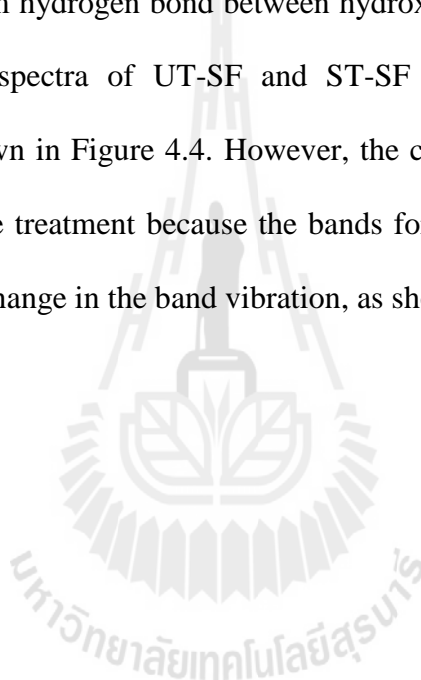
Wavenumber (cm ⁻¹)	UT-SF vibration
3280	N-H stretching
3076	C-N-H overtone
2970	CH-stretching antisymmetric
2932	CH ₃ stretching antisymmetric
1619	amide I stretching motion of the C=O and N-H bond
1516	amide II bending motion of the N-H coupled to C-N
1442	CH ₂ , CH ₃ bending
1367	C-H bending
1230	amide III bending motion of the N-H coupled to C-N
1164	C-N stretching in tyrosine
1101	skeletal stretching of phenylalanine
1045	C-O stretching
1004	skeletal stretching of phenylalanine
977	C-C skeletal stretching
851	=C-H out-of-plane deformations in aromatic rings of tyrosine
826	=C-H out-of-plane deformations in aromatic rings of tyrosine
690	=C-H out-of-plane deformations in aromatic rings of tyrosine

As mentioned previously, the FT-IR spectrum of silk fabric showed vibrations of amide I, amide II amide III at 1619 cm^{-1} , 1516 cm^{-1} , and 1230 cm^{-1} , respectively (Lefevre, *et al.*, 2009). It indicated that silk fibroin comprised of three conformations (random coil, α -helix and β -sheet) (Kaplan, 1998). Sargunamani and Selvakumar (2006) have reported that the conformation of amide I, amide II and amide III attributed to α -helix (amorphous), β -sheet (crystallinity), β -sheet or α -helix, respectively. The absorbance of amide I was the characteristic band for α -helix (amorphous) conformation. The absorbance of amide II was the characteristic band for β -sheet (crystallinity) conformation. The absorbance of amide III was the characteristic band for β -sheet and α -helix conformation. The β -sheet structure with high crystallinity as well as high molecular orientation provided excellent tensile strength to silk fiber (Sargunamani and Selvakumar, 2006). The summarized data corresponding to silk fibroin conformation of UT-SF is shown in Table 4.4.

Table 4.4 Summarized data corresponding to silk fibroin conformation (Sargunamani and Selvakumar, 2006).

(Functional group) wavenumber (cm^{-1})	Conformation
(amide I), 1619	α -helix (amorphous)
(amide II), 1516	β -sheet (crystallinity)
(amide III), 1230	β -sheet and α -helix

After silk fabric was treated with APTES, the new peaks observed from ATR FT-IR spectrum of ST-SF occurred at 1070 cm^{-1} and 1015 cm^{-1} assigned to vibration modes of Si-O-Si stretching and Si-O stretching on ST-SF surface, respectively, as shown in Figure 4.3. Therefore, it was confirmed that APTES deposited onto surface of UT-SF. In addition, the vibration of tyrosine of ST-SF occurred at 1169 cm^{-1} which is 5 cm^{-1} higher than that UT-SF, as shown in Figure 4.3. It may be derived from hydrogen bond between hydroxyl group of tyrosine of ST-SF and APTES. FT-IR spectra of UT-SF and ST-SF corresponded to silk fibroin conformation are shown in Figure 4.4. However, the conformation of ST-SF did not change after the silane treatment because the bands for amide I, amide II and amide III did not show any change in the band vibration, as shown in Figure 4.4.



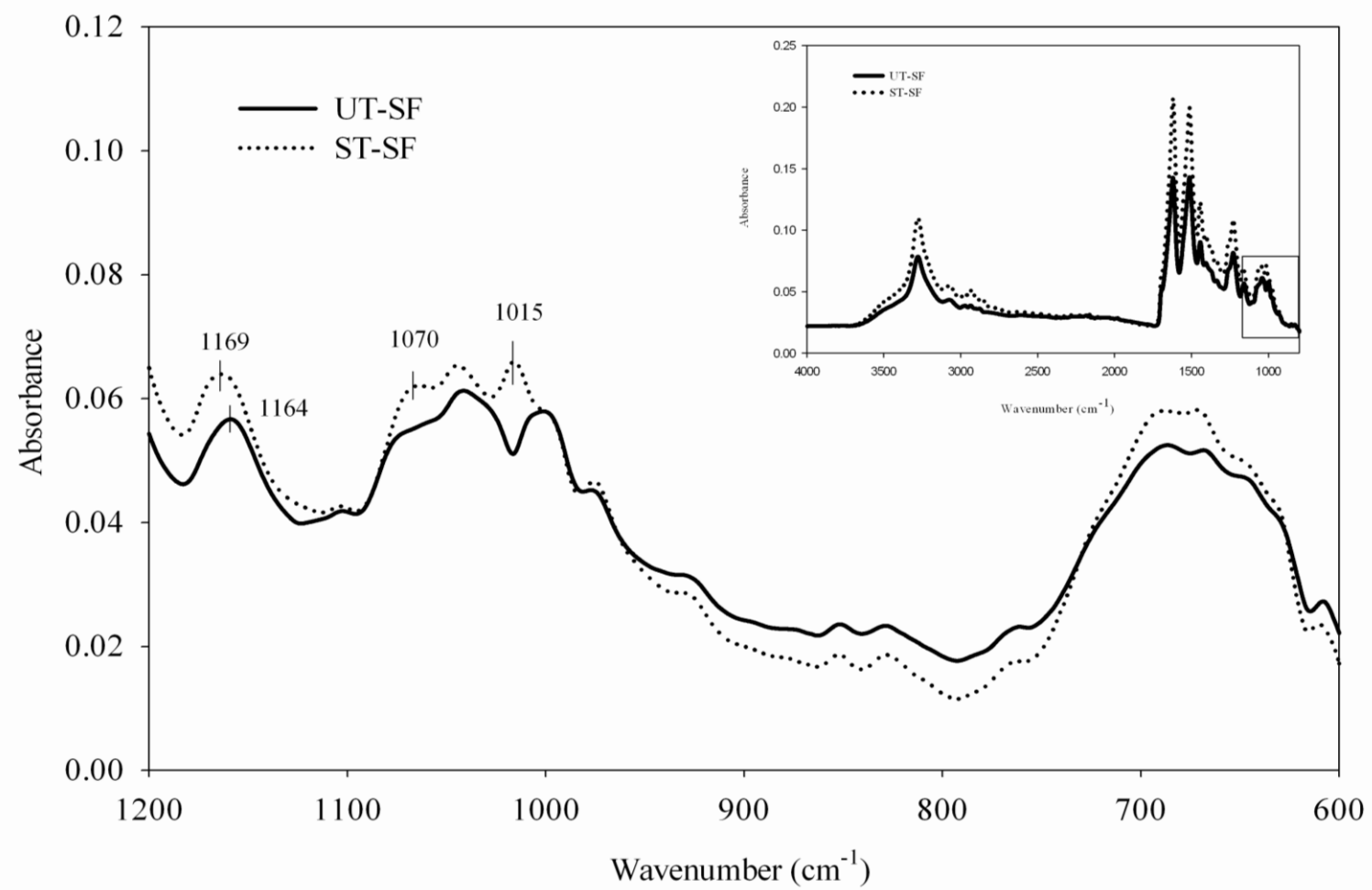


Figure 4.3 FT-IR spectra of UT-SF and ST-SF within a wavenumber range of 1200-600 cm⁻¹.

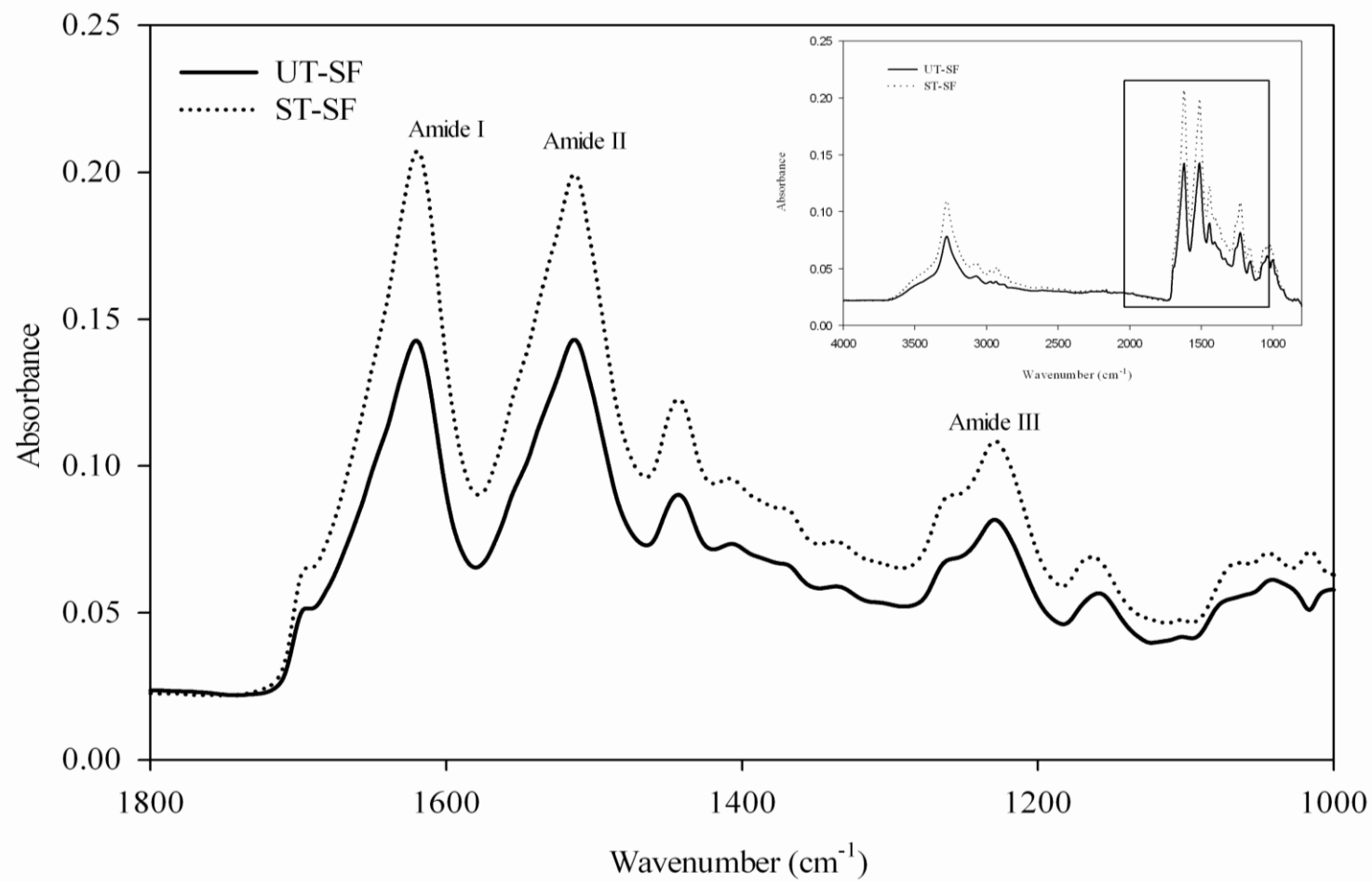


Figure 4.4 FT-IR spectra of UT-SF and ST-SF corresponding to fibroin conformations within a wavenumber range of 1800-100 cm⁻¹.

4.1.2.2 Elemental composition of UT-SF ash and ST-SF ash

Elemental compositions of UT-SF ash and ST-SF ash are shown in Table 4.5. The Si content left in ST-SF was higher than that in UT-SF. It was the evidence that ST-SF gained some more Si by the silane treatment. This indicated that aminopropyltriethoxy silane (APTES) successfully deposited onto the silk fabric. The major element left in UT-SF ash and ST-SF ash were calcium (Ca) and oxygen (O). UT-SF ash and ST-SF ash contained other elements such as Na, Mg, Si, P, K, Fe and Zn. These elements might come from the inorganic residue from larvae (Hacke, 2008). Sulfur (S) was originated from the sulfur bridges connecting fibroin protein chains.

Table 4.5 Elemental compositions of UT-SF ash and ST-SF ash.

Element (%)	Silk fabric ash	
	UT-SF ash	ST-SF ash
O	35.74	41.12
Na	11.04	4.34
Mg	4.81	4.37
Si	9.24	18.6
P	2.5	1.99
K	1.86	1.26
Ca	27.85	20.88
Fe	1.55	2.11
Zn	0.2	0.59
Other (Ag, S, Cl, Mn, Cu)	5.21	4.74
Total	100.00	100.00

4.1.3 Thermal properties of silk fabrics, glass fabric and Kevlar fabric

TGA and DTGA curves of silk fabrics, glass fabric and Kevlar fabric are shown in Figure 4.5. The thermograms of UT-SF and ST-SF showed two transitions in a range of 30-150°C and 200-500°C. The first transition of UT-SF and ST-SF was observed around 66°C and 80°C, respectively. This transition was attributed to evaporation of water. For APTES silane treated silk fiber, it contained H-bonding interaction between water molecules and NH₂ group of amino silane, deposited on silk fiber surface, by which the removal of water molecules from ST-SF was more difficult than that from UT-SF (Joseph, Sreekala and Thomas, 2008). The second transitions was observed at 324°C for UT-SF and 340°C for ST-SF, corresponding to thermal decomposition of silk fibroin structure of silk fiber (Srihanam, Srisuwan and Simchure, 2009). The result showed that thermal stability of ST-SF was higher than that of UT-SF. Similar result has been reported by Sreekala and co-workers that silane treatment increased the thermal stability of flax fiber and sisal fiber (Sreekala, Kumaran, and Thomas, 1997). Gañan and co-workers also reported that the thermal decomposition of untreated sisal fiber and silane treated sisal fiber obtained from DTGA was at 355°C and 390°C, respectively. They explained that the thermal stability of silane treated sisal fiber increased due to the presence of silanol groups on the fiber surface that could introduce restrictions in the segmental mobility. (Gañan, Garbizu, Llano-Ponte, and Mondragon, 2005).

Thermograms of Kevlar fabric in Figure 4.5 showed two transitions in a range of 30-200°C and 450-800°C. The first transition was observed around 130°C and attributed to an evaporation of water. The second transition was observed around 590°C and attributed to thermal decomposition of poly-*p*-paraphenylene

terephthalamide (PPTA) in Kevlar fabric (Iyer and Vijayan, 1999). For glass fabric, there was not any transition observed from 30-800°C. From the results, the thermal degradation of Kevlar and glass fabric was at higher temperature than that of UT-SF and ST-SF.



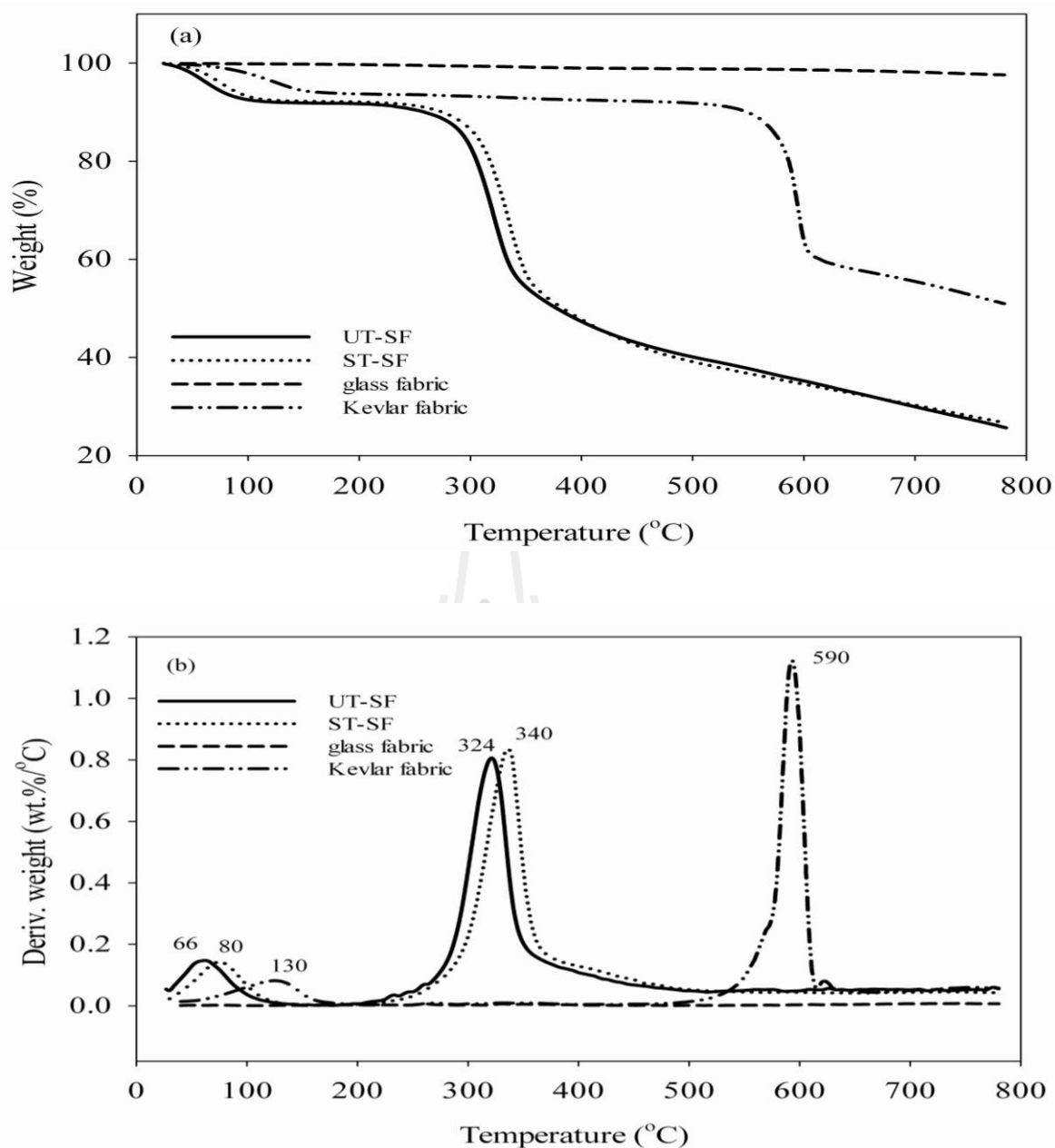


Figure 4.5 TGA (a) and DTGA (b) curves of UT-SF, ST-SF, glass fabric and Kevlar fabric.

DSC curves of silk fabrics, glass fabric and Kevlar fabric are shown in Figure 4.6. The endothermic peaks of ST-SF, UT-SF and Kevlar fabric were observed at 66°C, 80°C and 130°C, respectively attributed to evaporation of water. However, there was no observed endotherm from glass fabric. These result well corresponding to the TGA results of UT-SF, ST-SF, Kevlar fabric and glass fabric analysis.

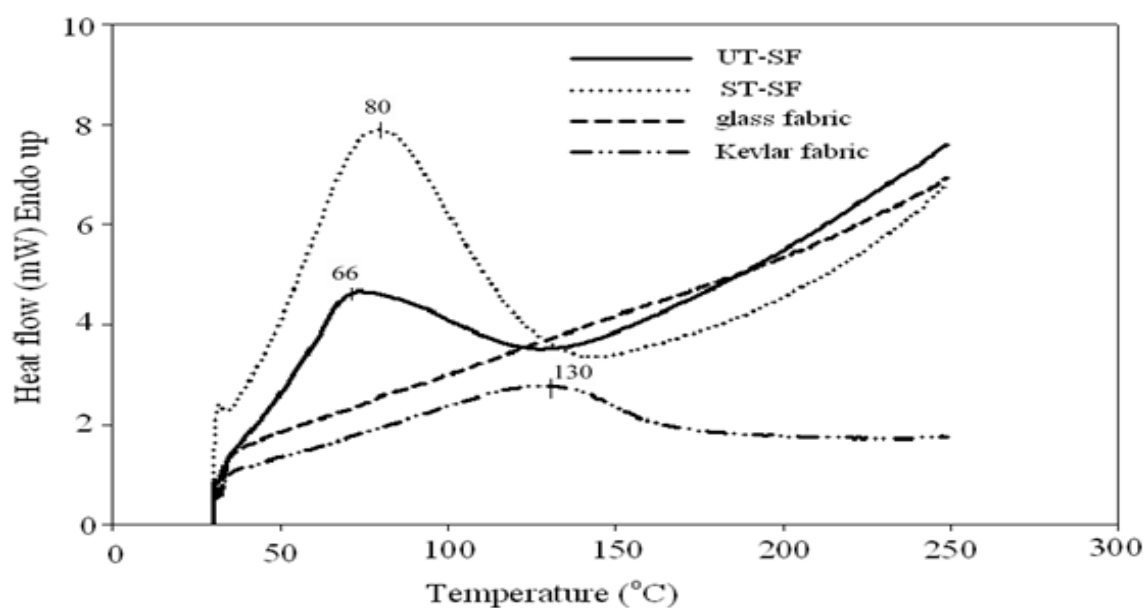


Figure 4.6 DSC curves of UT-SF, ST-SF, glass fabric and Kevlar fabric.

4.1.4 Surface morphology of silk fabrics, glass fabric and Kevlar fabric

SEM micrographs of silk fibers obtained from UT-SF and ST-SF are shown in Figure 4.7. SEM micrographs showed that UT-SF surface was smooth and its cross-section area was in a triangle shape. It has been also reported by Lewin and Pearce that the degummed silk fiber surface was smooth and the cross-section area was in a triangle shape (Lewin and Pearce, 1998). In addition, the SEM micrographs showed that ST-SF surface was rougher than that of UT-SF. This indicated that the

silane coupling agent was coated onto the silk fiber surface. Similar result has been reported by Zulkifli *et al.* that the SEM morphology of silk fabric surface was rougher and cruder after silane treatment (Zulkifli, Azhari, Maryam, Ahmad and Abu, 2009). SEM micrographs of a glass fabric and a Kevlar fabric are shown in Figure 4.8. The glass fabric surface and Kevlar fabric surface were smooth.

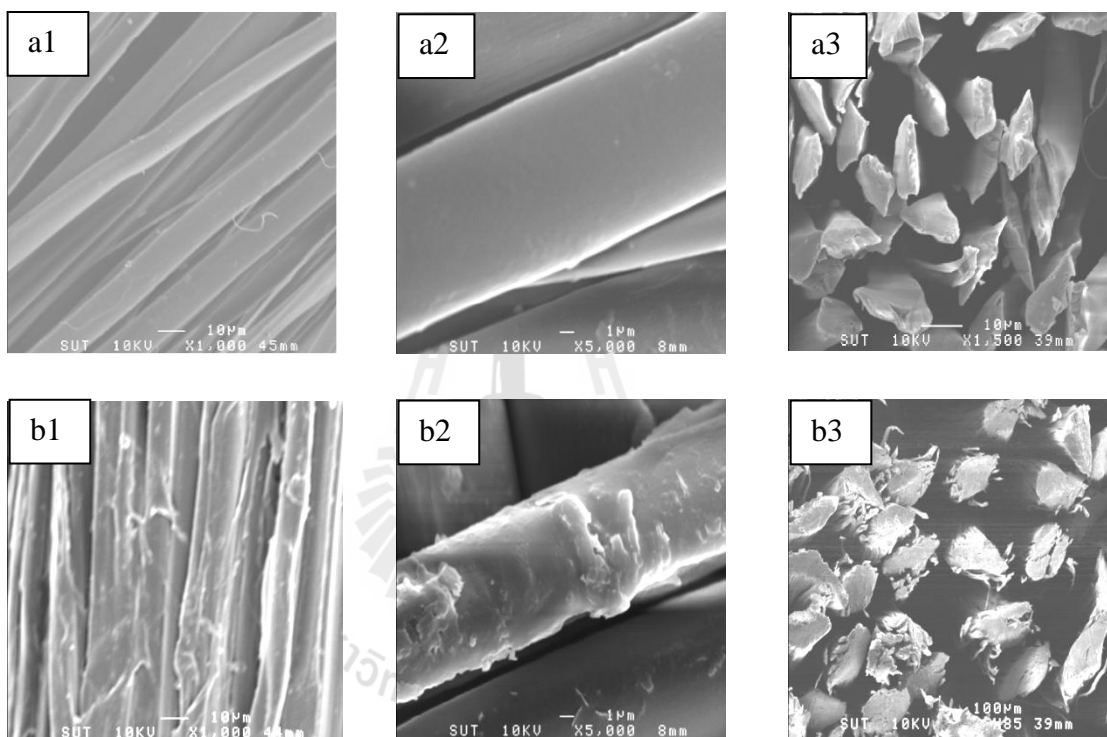


Figure 4.7 SEM micrographs of UT-SF (a) and ST-SF (b) at a magnification of x1000 (1) and x5000 (2) and their cross-section surface at x1500 (3).

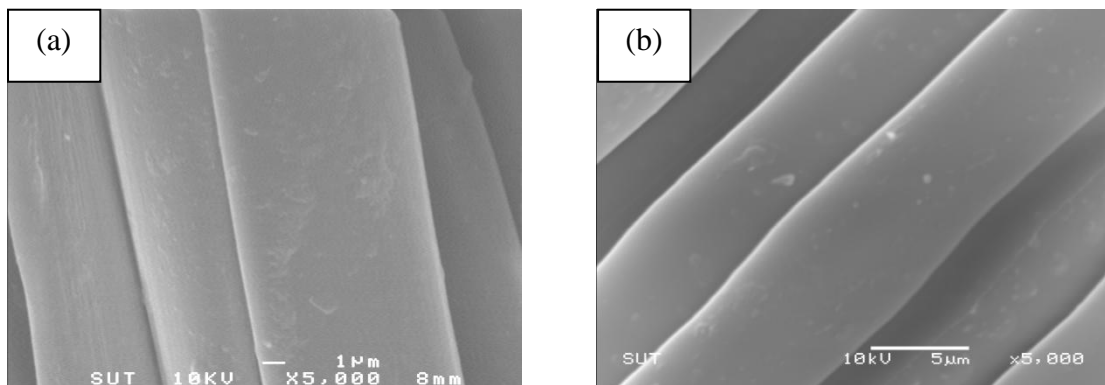


Figure 4.8 SEM micrographs of glass fabric (a) and Kevlar fabric (b) at a magnification of $\times 5000$.



4.2 Effect of UT-SF content on physical properties of epoxy composite

4.2.1 Tensile properties

Young's modulus and elongation at break of neat epoxy and epoxy composites are shown in Figure 4.9. Young's modulus of epoxy composites was higher than that of neat epoxy and slightly changed with increasing weight fraction of UT-SF. This was because the number of layer of fabric within UT-SF/epoxy composite was insignificantly different at weight fraction of 0.10-0.18. Elongation at break of neat epoxy was higher than those of epoxy composites, but elongation at break of epoxy composites at various fabric contents was not significantly different.

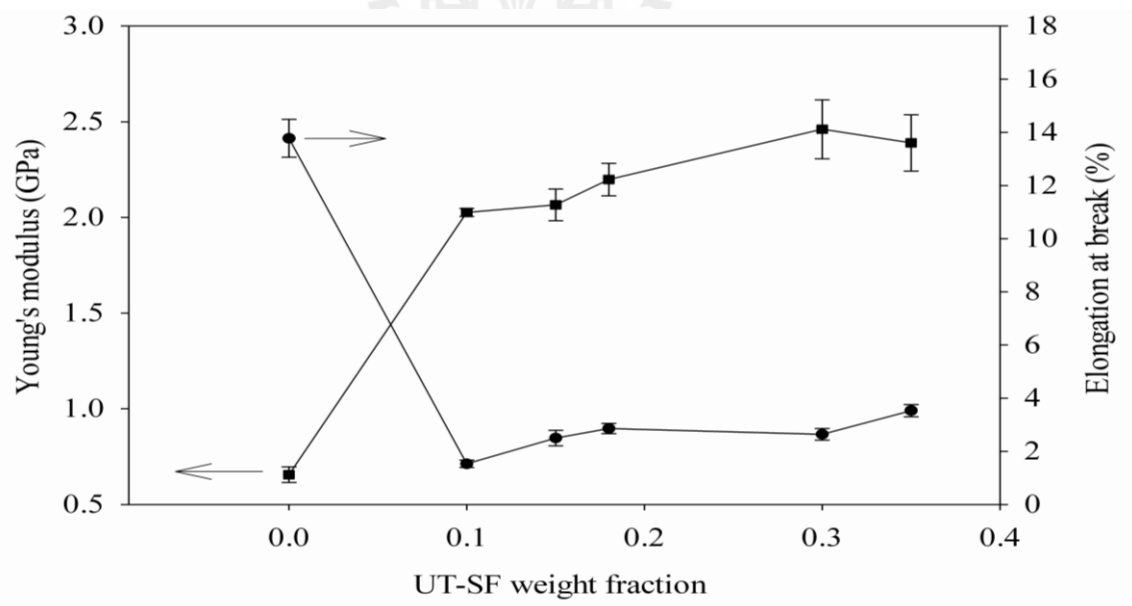


Figure 4.9 Plot of Young's modulus (■) and elongation at break (●) of UT-SF/epoxy composite vs UT-SF weight fraction.

From Figure 4.10, tensile strength of neat epoxy was higher than those of epoxy composites and tensile strength of the composites increased with increasing weight fraction of UT-SF. When UT-SF weight fraction was equal to 0.1, the tensile strength of epoxy composites was much lower than that of neat epoxy. It may be because the distance between layer of fabric to fabric was too far apart. At a fraction of 0.35 UT-SF, tensile strength were increased up to 47.94 MPa close to that of neat epoxy (51.41 MPa). This was because, at higher weight fraction, the fabric–fabric distance decreased and, as a result, the load was easier transmitted between epoxy matrix and the fabric (Rong, Zhang, Liu, Yang and Zeng, 2001). Tensile properties of neat epoxy and UT-SF/epoxy composites were summarized in Table 4.6.

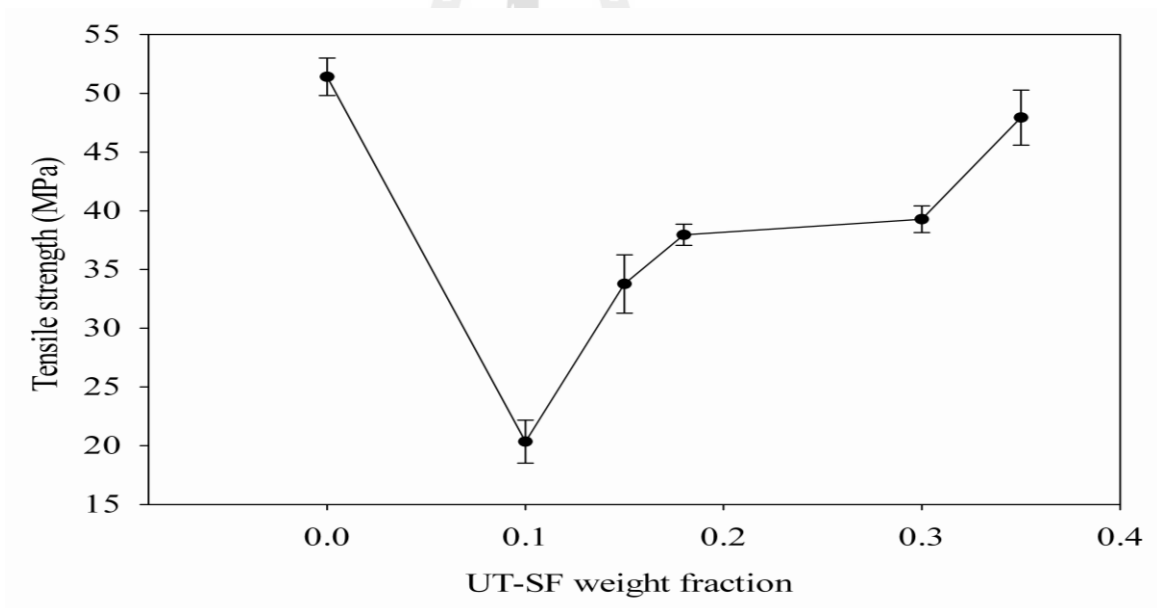


Figure 4.10 Plot of tensile strength of UT-SF/epoxy composite vs UT-SF weight fraction.

4.2.2 Flexural properties

Flexural properties of neat epoxy and epoxy composites are shown in Figure 4.11. The flexural modulus of epoxy composite slightly decreased when UT-SF weight fraction was equal to or lower than 0.18. The flexural strength of neat epoxy and epoxy composite decreased when UT-SF weight fraction was equal and lower than 0.18. However, the flexural modulus and flexural strength tended to increase when the weight fraction of UT-SF was over 0.18. This maybe because, at UT-SF weight fraction higher than 0.18, the fabric–fabric distance decreased as a result the load was easier transmitted between epoxy matrix and the fabric. The data of flexural properties of UT-SF/epoxy composites were also numbered in Table 4.6. From Table 4.6, flexural strain at break of neat epoxy was higher than those of epoxy composites. In addition, UT-SF content did not affect flexural strain at break of the composite. The similar result for natural fiber epoxy composite has been reported by Goud and Rao (2011). They found that flexural strength and flexural modulus of plum fiber/epoxy composite at low fiber content were lower than those of neat epoxy. Flexural strength and flexural modulus of plum fiber/epoxy composite increased with increasing plum fiber content more than 5 wt.% (Goud and Rao, 2011). In addition, Priya *et al.* (2005) has reported that flexural strength of waste silk fabric/epoxy (waste silk of 0.05-0.25 weight fraction) were higher than that of neat epoxy and flexural strength of waste silk fabric/epoxy increased with increasing waste silk fabric content (Priya, Ramakrishna, Rai and Rajulu, 2005).

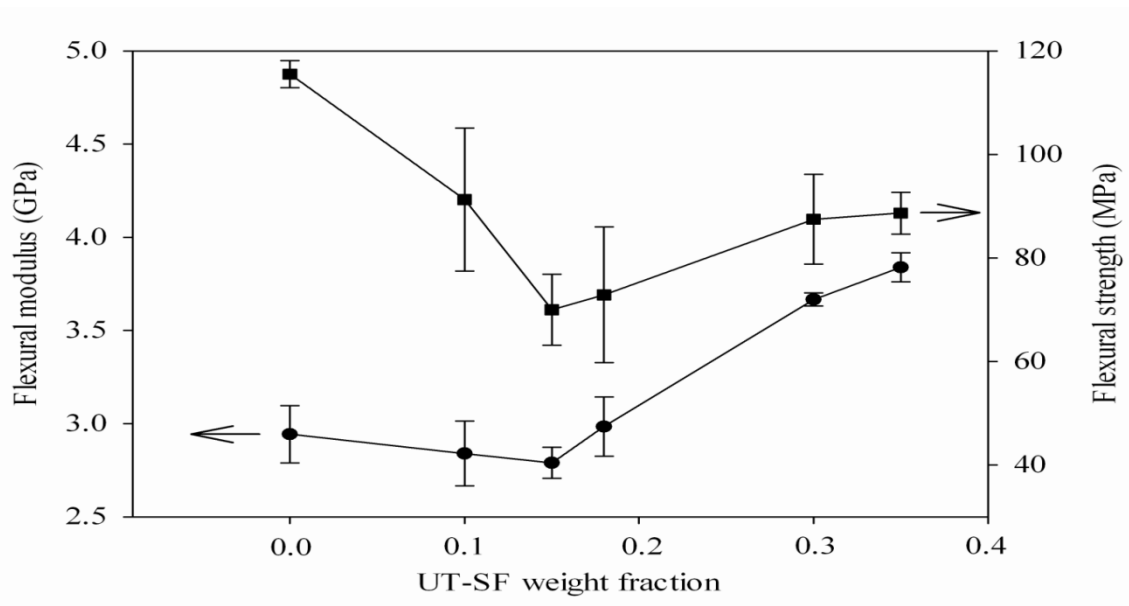


Figure 4.11 Plot of flexural modulus (●) and flexural strength (■) of UT-SF/epoxy composite vs UT-SF weight fraction.

4.2.3 Impact property

Impact property of neat epoxy and epoxy composites is shown in Figure 4.12. The impact strength of neat epoxy was higher than that of UT-SF/epoxy composites. As weight fraction of UT-SF was increased to 0.15, the impact strength of the epoxy composite decreased. However, increasing UT-SF content to the weight fraction of 0.18 to 0.35 led to the improvement of impact strength of the composite upto 13.80 kJ/m^2 . At UT-SF weight fraction lower than 0.18, the specimen breaking under impact stress was possibly initiated by the propagation of voids within the epoxy matrix and at fabric-epoxy interface. Nevertheless, at UT-SF weight fraction of 0.35, the fabrics were closer packed by which this made the fabrics absorbed more impact energy under test. The silk fabric, itself, was able to absorb more impact energy than epoxy resin (Priya and Rai, 2011). As a result, the epoxy composite prepared with UT-SF weight fraction of 0.35 had impact strength higher

than that of epoxy composite prepared with UT-SF weight fraction lower than 0.35. Ude *et al.* (2010) also reported that energy was more absorbed with increase in the number of woven silk ply in the epoxy composite. However, the epoxy composite prepared with 0.35 UT-SF had lower impact strength than that of neat epoxy itself. Impact properties of neat epoxy and UT-SF/epoxy composites were summarized in Table 4.6.

From mechanical properties of UT-SF/epoxy composite, tensile properties, flexural properties and impact property of UT-SF/epoxy composite tended to increase with UT-SF weight fraction was over than 0.18. So, the ST-SF/epoxy composite was prepared with ST-SF weight fraction not lower than 0.18.

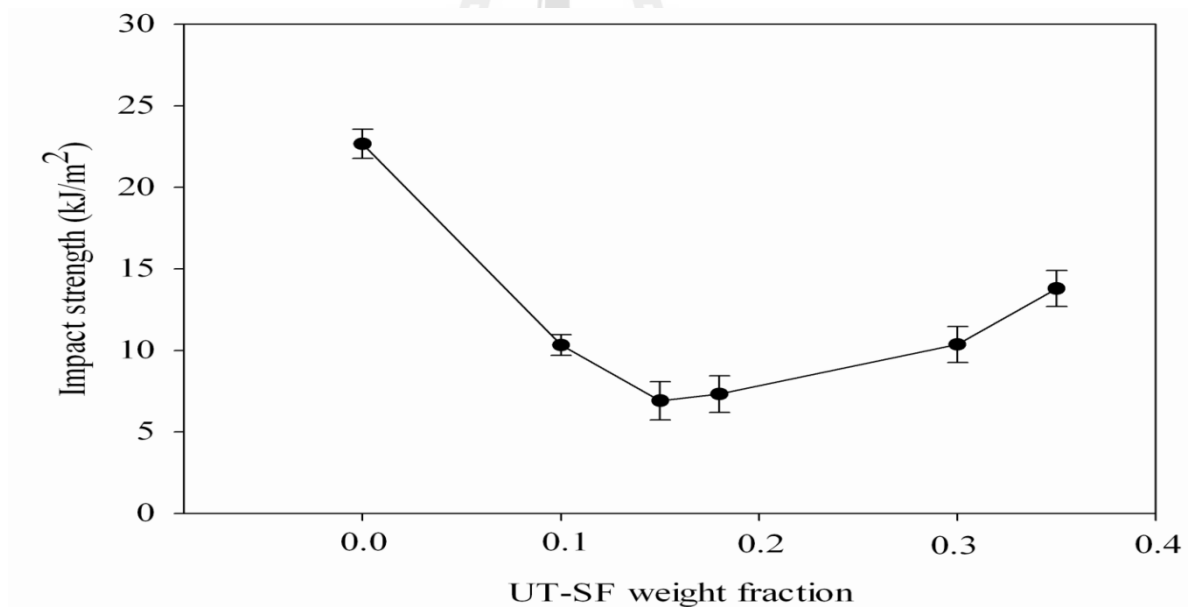


Figure 4.12 Plot of impact strength of UT-SF/epoxy composite vs UT-SF weight fraction.

Table 4.6 Summary of tensile properties, flexural properties, and impact strength of neat epoxy and UT-SF/epoxy composites with UT-SF weight fraction of 0.10-0.35.

Material	Tensile properties			Flexural properties			Impact strength (kJ/m ²)
	Young's modulus (GPa)	Tensile strength (MPa)	Elongation at break (%)	Flexural modulus (GPa)	Flexural strength (MPa)	Flexural strain at break (%)	
Neat epoxy	0.66 ± 0.04	51.41 ± 1.59	13.78 ± 0.71	2.94 ± 0.15	115.53 ± 2.64	9.52 ± 0.15	22.67 ± 0.90
epoxy with 0.10 UT-SF	2.03 ± 0.02	20.35 ± 1.83	1.53 ± 0.14	2.84 ± 0.17	91.31 ± 13.82	3.26 ± 0.13	10.32 ± 0.63
epoxy with 0.15 UT-SF	2.07 ± 0.08	33.77 ± 2.49	2.50 ± 0.29	2.79 ± 0.08	70.00 ± 6.85	5.09 ± 0.29	6.91 ± 1.17
epoxy with 0.18 UT-SF	2.20 ± 0.08	37.96 ± 0.90	2.86 ± 0.19	2.98 ± 0.16	72.90 ± 13.11	2.77 ± 0.22	7.32 ± 1.13
epoxy with 0.30 UT-SF	2.50 ± 0.15	39.29 ± 1.14	2.64 ± 0.22	3.67 ± 0.03	87.51 ± 8.70	3.03 ± 0.11	10.36 ± 1.10
epoxy with 0.35 UT-SF	2.40 ± 0.14	47.94 ± 2.34	3.53 ± 0.23	3.84 ± 0.08	88.68 ± 4.05	2.93 ± 0.25	13.80 ± 1.10

4.2.4 Heat distortion temperature

Heat distortion temperature of neat epoxy was slightly higher than UT-SF weight fraction of 0.10. Heat distortion temperature of epoxy composites increased with increasing fabric content up to UT-SF weight fraction of 0.18. Then, HDT of the UT-SF/epoxy composites started to be decreased at UT-SF weight fraction higher than 0.18, as shown in Table 4.7. Alagar *et al.* (2000) reported that heat distortion temperature of Kevlar fiber/epoxy increased with increasing Kevlar content (Alagar, Ashok Kumar, Mahesh and Dinakaran, 2000).

Table 4.7 Heat distortion temperature of neat epoxy and UT-SF/epoxy composite with UT-SF weight fraction of 0.10-0.35.

Materials	HDT (°C)
Neat epoxy	83.7
epoxy with 0.10 UT-SF	79.3
epoxy with 0.15 UT-SF	91.1
epoxy with 0.18 UT-SF	99.9
epoxy with 0.30 UT-SF	93.3
epoxy with 0.35 UT-SF	92.6

4.2.5 Thermal properties

TGA and DTGA curves of UT-SF, neat epoxy, and UT-SF/epoxy composites are shown in Figure 4.13. TGA and DTGA thermogram of neat epoxy show thermal decomposition of neat epoxy at 381°C. The thermogram of silk fabric show two transitions in a range of 30-150°C and 200-500°C. The first transition around 66°C was attributed to the evaporation of water and the second transition was observed at 324°C corresponding to thermal decomposition of silk fibroin (Srihanam, Srisuwan and Simchure, 2009). Two thermal transitions of UT-SF/epoxy composites were in a range of 220-340°C and 250-550°C. The first transition of UT-SF/epoxy composites in a range of 220°C-340°C was observed as a shoulder peak with an initial approximate at 229-266°C. This was attributed to thermal decomposition of silk fabric existing in the composite (Reddy and Young, 2010). The second transition of UT-SF/epoxy composites in a range of 250°C-550°C corresponded to thermal decomposition of epoxy and the decomposition peaks were approximate at 380-383°C. However, this decomposition peak became boarder with increasing UT-SF fraction of 0.35. This broadening might be derived from interfacial epoxy having higher degree of curing than epoxy matrix far from the fabric surface. The higher in curing degree was caused by excess amino groups located at the fabric surface making the interfacial epoxy decomposed at higher temperature. Thermal decomposition temperature of UT-SF, neat epoxy, and UT-SF/epoxy composites are shown in Table 4.8.

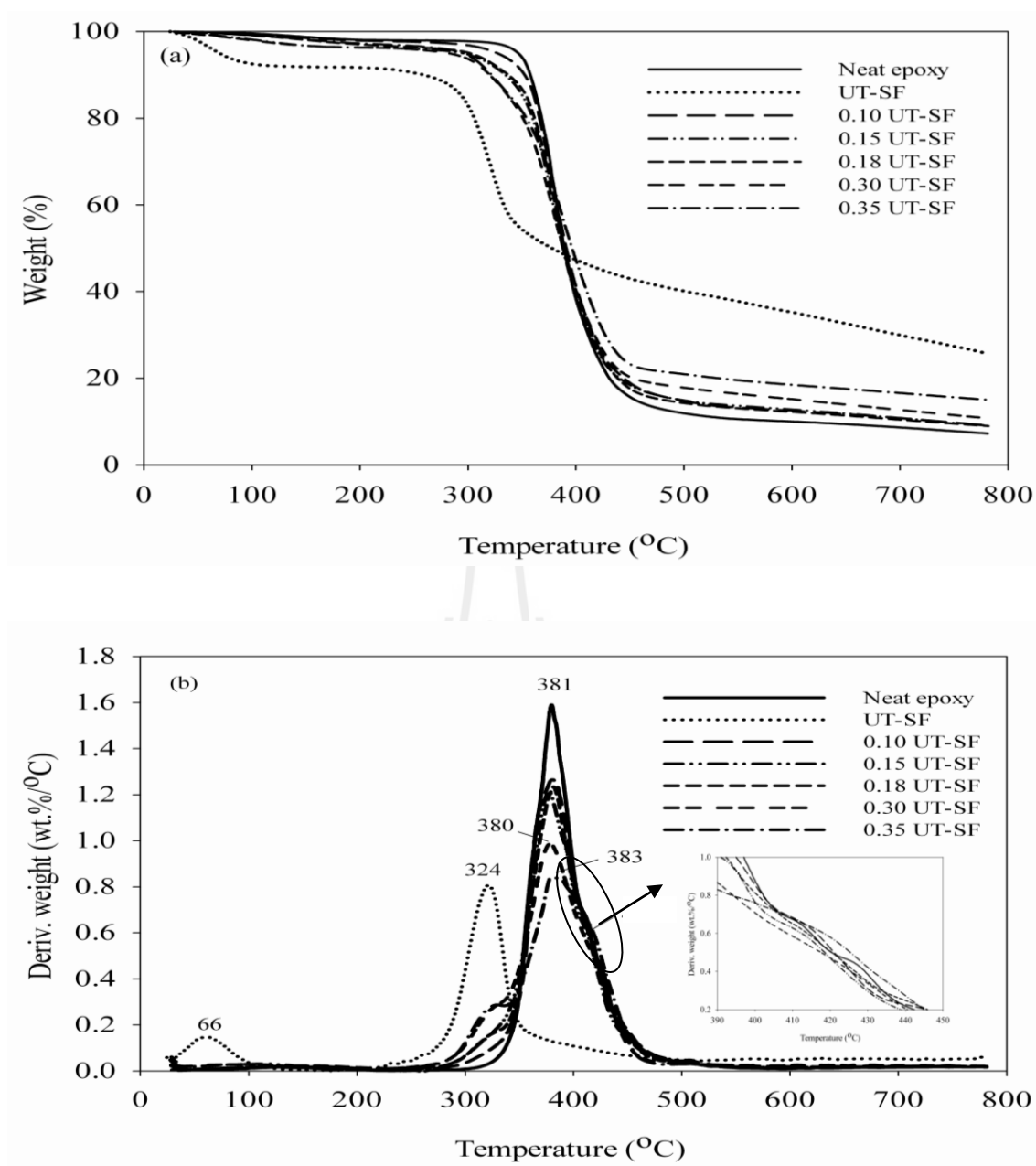


Figure 4.13 TGA (a) and DTGA (b) curves of neat epoxy and UT-SF epoxy composite with various UT-SF weight fractions.

Table 4.8 Thermal decomposition (T_d) of UT-SF, neat epoxy and epoxy composite prepared with various UT-SF weight fractions.

Materials	Temperature ($^{\circ}\text{C}$)		
	Water evaporation	Silk decomposition	Epoxy decomposition
UT-SF	66.0 (peak)	324.0 (peak)	-
Neat epoxy	-	-	381.0 (peak)
epoxy with 0.10 UT-SF	-	266.0 (shoulder initial)	381.0 (peak)
epoxy with 0.15 UT-SF	-	266.0 (shoulder initial)	380.0 (peak)
epoxy with 0.18 UT-SF	-	264.0 (shoulder initial)	380.0 (peak)
epoxy with 0.30 UT-SF	-	229.0 (shoulder initial)	380.0 (peak)
epoxy with 0.35 UT-SF	-	229.0 (shoulder initial)	383.0 (peak)

DSC thermograms of neat epoxy before and after post curing are shown in Figure 4.14. The curing temperature (T_{cure}) of neat epoxy before post curing was observed at 110.5°C . The glass transition endotherm of neat epoxy before post curing was observed as a peak. It was observed as a peak because the glass transition concurrently underwent along with stress relaxation or enthalpy relaxation of epoxy chains (Lettieri and Frigione, 2010). Enthalpy relaxation effect occurred by variation of the internal structure of epoxy as a result of processing temperature, curing time, rate of curing (Calventus, Montserrat and Hutchinson, 2001). The glass transition endotherm of neat epoxy after post curing was also observed as a peak. The glass transition of neat epoxy before and after post curing, determined from the half of specific heat (half C_p), was 58.4°C and 87.6°C , respectively. After post curing, the glass transition of neat epoxy was higher because, by the post curing, neat epoxy

gained more reaction between amide curing agent and epoxide ring. Glass transition temperature and curing temperature of neat epoxy are summarized in Table 4.9.

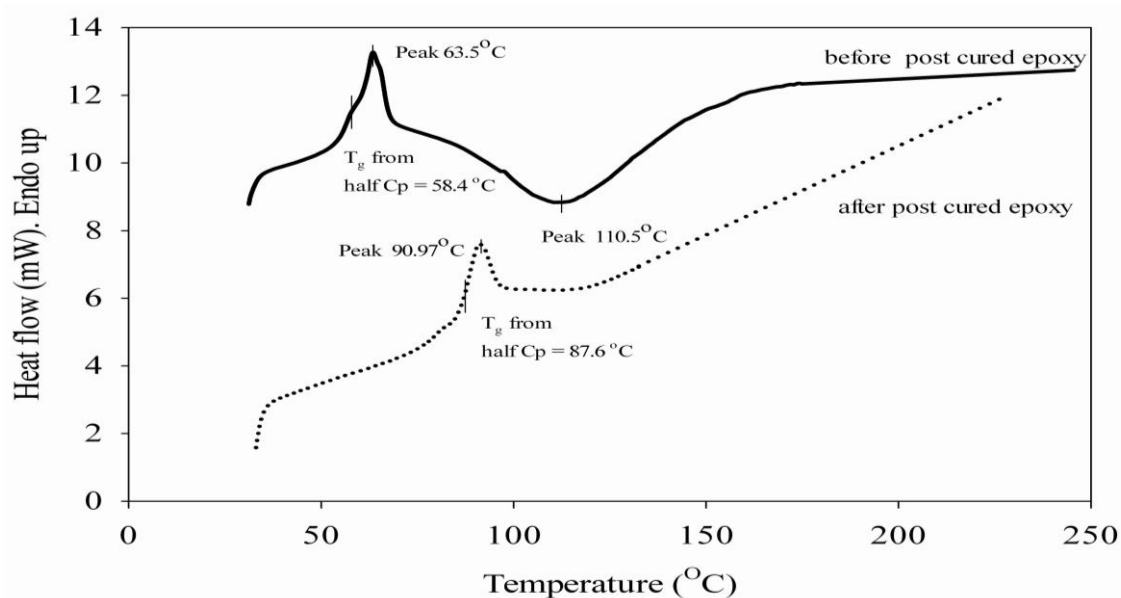


Figure 4.14 DSC thermograms of neat epoxy before and after post curing.

Table 4.9 Glass transition temperature (T_g) and curing temperature (T_{cure}) of neat epoxy before post curing and after post curing.

Materials	T_g (°C)	T_{cure} (°C)
Neat epoxy before post cured	58.4	110.5 (peak)
Neat epoxy after post cured	87.6	-

DSC curves of neat epoxy and epoxy composites before post curing are shown in Figure 4.15. The curing temperature of neat epoxy was lower than those of epoxy composites. The curing exotherm of epoxy composite occurred at higher temperature with increasing of UT-SF content. The same result has been reported by

Suay Ant3n *et al.* (1999). They found that the curing exotherm peak of Kevlar/epoxy composites slightly shifted to higher temperatures with increasing Kevlar content (Suay Ant3n, G3mez Ribelles, Monle3n Pradas and Arnau Izquierdo, 1999).

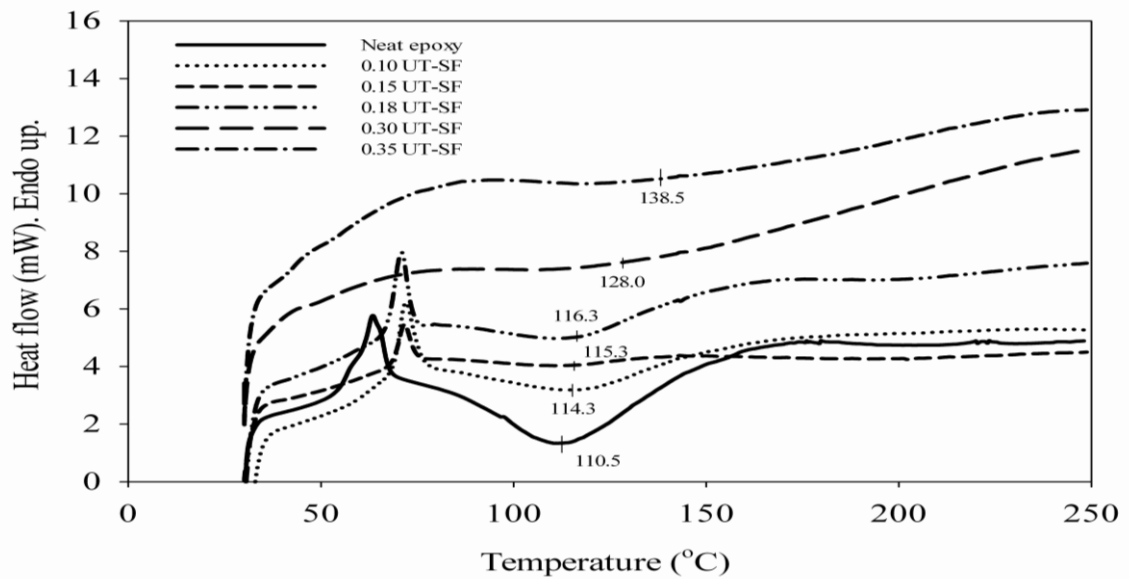


Figure 4.15 DSC curves of neat epoxy and epoxy composite at various UT-SF weight fractions before post curing.

Table 4.10 Curing temperature (T_{cure}) of neat epoxy and epoxy composite at various UT-SF contents before post curing.

Materials	T_{cure} (°C)
neat epoxy	110.5
epoxy with 0.10 UT-SF	114.3
epoxy with 0.15 UT-SF	115.3
epoxy with 0.18 UT-SF	116.3
epoxy with 0.30 UT-SF	128.0
epoxy with 0.35 UT-SF	138.5

For post cured neat epoxy and epoxy composites, their DSC curves from the first heating scan and the second heating scan are shown in Figure 4.16. From the first heating curves, glass transition temperature after post curing of epoxy composites, obtained from the first heating scan, was observed as the shift of the baseline whereas that of neat epoxy was observed as the peak. The glass transition of neat epoxy after post curing determined from half C_p was 87.6°C. Glass transition temperature (T_g) of neat epoxy and epoxy composite at various UT-SF contents, after post curing obtained from the first and the second heating scan are shown in Table 4.11. Glass transition temperature after post curing of epoxy composites, obtained from the first heating scan, at UT-SF content of 0.10, 0.15 and 0.18 was higher than that of neat epoxy. With increasing UT-SF fraction, glass transition temperature after post curing of the composite decreased. As UT-SF content increased to weight fraction of 0.30 and 0.35, the glass transition temperature after post curing of epoxy composites was close to that of neat epoxy, as shown in Table 4.11.

Glass transition temperature from the second heating scan of epoxy composites was higher than that of neat epoxy. With increasing UT-SF fraction, glass transition temperature from the second heating of the composite decreased. As UT-SF content increased to weight fraction of 0.30 and 0.35, the glass transition temperature from the second heating of epoxy composites was close to that of neat epoxy. However, glass transition temperature from the second heating of neat epoxy and epoxy composite was higher than those glass transition temperature obtained from the first heating scan. This was because epoxy gained more reaction between amide curing agent and epoxide ring. The fully curing was obtained in the second heating scan.

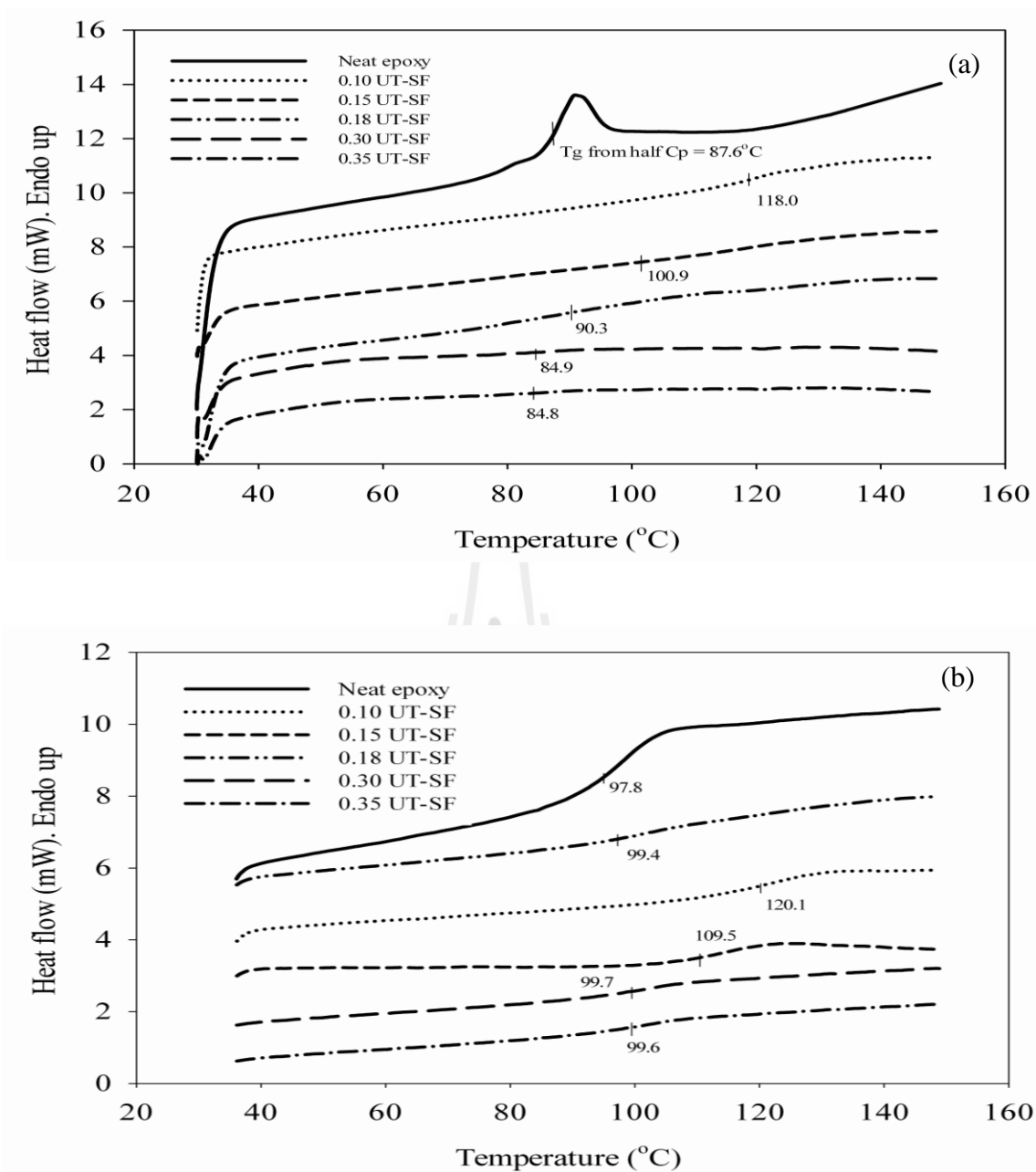


Figure 4.16 DSC curves of neat epoxy and epoxy composite at various UT-SF weight fractions from the first heating scan (a) and from the second heating scan (b).

Table 4.11 Glass transition temperature (T_g) of neat epoxy and epoxy composite at various UT-SF contents, obtained from the first and the second heating scan.

Material	T_g (°C) 1st heating scan	T_g (°C) 2nd heating scan
neat epoxy	87.6	97.8
epoxy with 0.10 UT-SF	118.0	120.1
epoxy with 0.15 UT-SF	100.9	109.5
epoxy with 0.18 UT-SF	90.3	99.4
epoxy with 0.30 UT-SF	84.9	99.7
epoxy with 0.35 UT-SF	84.8	99.6

4.2.6 Fracture surface morphology

SEM micrograph of neat epoxy in the Figure 4.17 (a) shows that the epoxy was broken in a brittle manner under impact load. The fracture surface consist of three regions including, smooth mirror region, mist region and hackle region or so-called radial striation zone. Plangsangmas *et al.* (1999) have reported that mirror region was the area where smooth and glossy appearance and the crack velocity was relatively slow in the mirror region. The mist region was the area that appeared to be substantially rougher than the mirror region. The crack velocity in the mist region was higher than that in the mirror region. The striation zone appeared to be the roughest area due to the highest crack velocity (Plangsangmas, Mecholsky and Brennan, 1999).

SEM micrographs of UT-SF/epoxy composites in the Figure 4.17 (b-d) show that the distance between fabrics was narrower with increasing UT-SF content. At UT-SF weight fraction of 0.35, the silk fabrics were closer packed than other silk fabric weight fractions.

For UT-SF/epoxy composites, radial striations running from one fabric surface to another fabric surface and also smooth mirror zone are observed from the fracture surface, as depicted in Figure 4.18 (b-d). This indicated that the UT-SF/epoxy composites fractured in a brittle manner, as same as neat epoxy. However, the size of a mirror zone was minimized with increasing UT-SF content, as seen in Fig. 4.18 (a-d), resulting in an increase of the impact strength of the composites prepared with 0.30 and 0.35 UT-SF. In addition, the large delamination and crack are observed on fracture surface of a UT-SF/epoxy composites prepared with 0.15 and 0.18 UT-SF, as shown in Figure 4.18 (a,b). The large delamination implied that the interaction between epoxy matrix and the fabric surface was not strong enough to hold the applied stress even though there was some physical and chemical interaction at the fabric-matrix interface (Day, Hewson and Lovell, 2002).

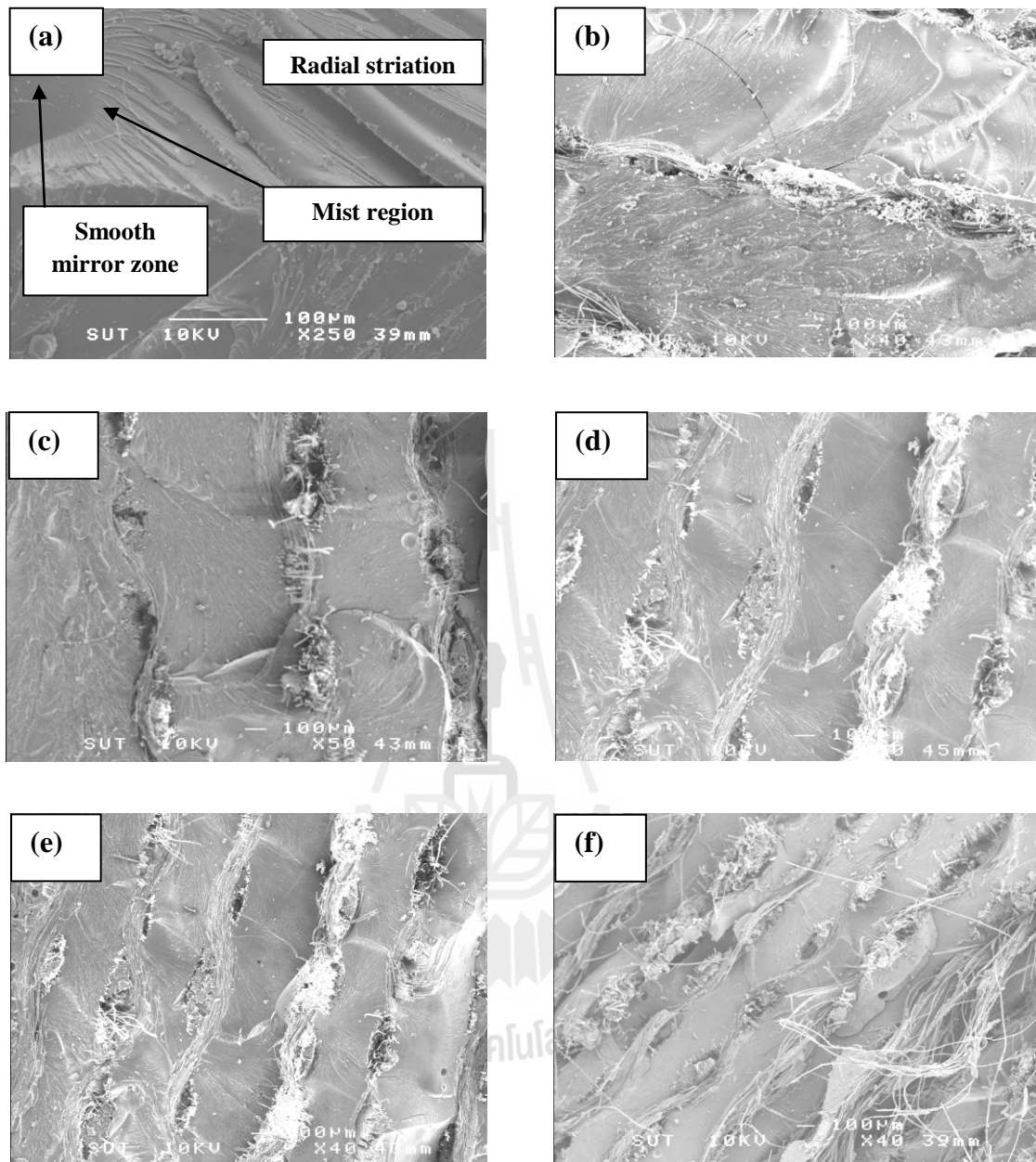


Figure 4.17 SEM micrographs of (a) neat epoxy x250 and epoxy composites at (b) 0.10 UT-SF x40, (c) 0.15 UT-SF x50, (d) 0.18 UT-SF x40, (e) 0.30 UT-SF x40, and (f) 0.35 UT-SF x40.

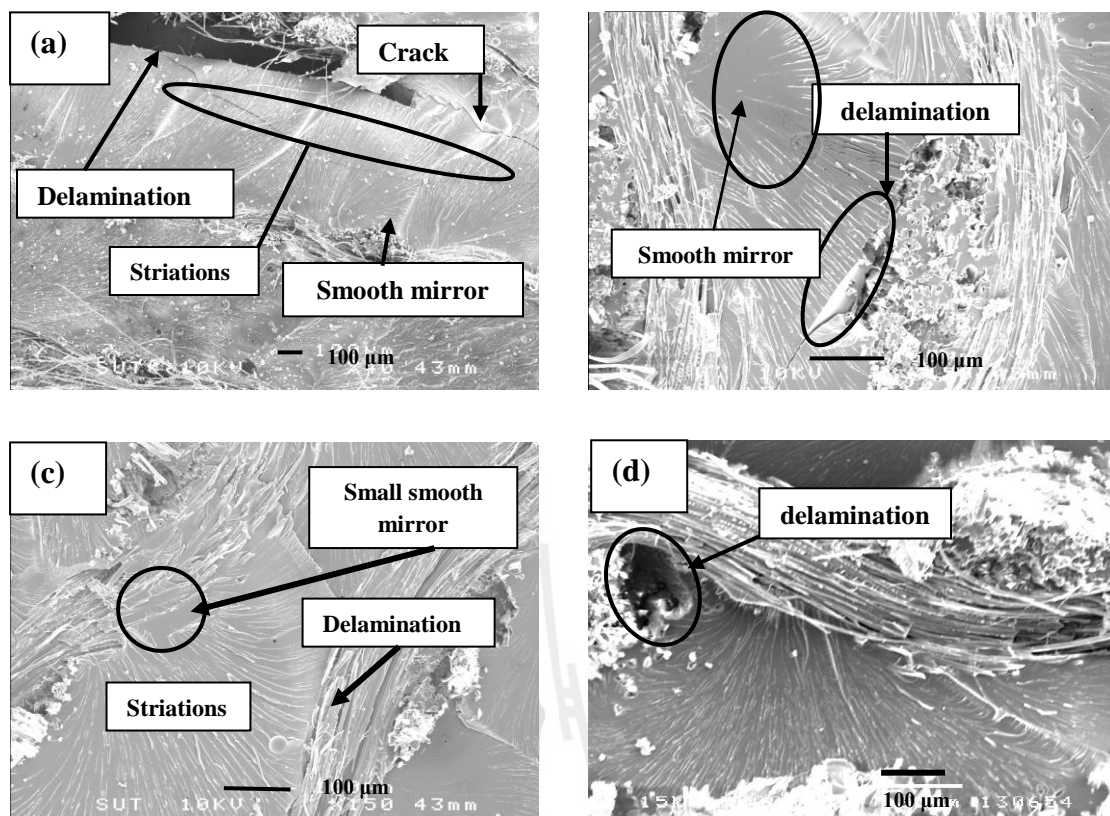


Figure 4.18 SEM micrographs of epoxy composites at (a) 0.15 UT-SF, (b) 0.18 UT-SF, (c) 0.30 UT-SF, and (d) 0.35 UT-SF

4.3 Effect of silane treatment on physical properties of epoxy composite

4.3.1 Tensile properties

From Figure 4.19, the Young's modulus of ST-SF/epoxy composites increased with increasing weight fraction of silk fabric. Young's modulus of ST-SF/epoxy composites was insignificantly different to that of UT-SF/epoxy composites. The similar result has been reported by George and Verpoest (1999) that Young's modulus of flax fiber/epoxy composite insignificantly increased with aminopropyltriethoxysilane treated flax (George and Verpoest, 1999). This result corresponded well with the differences in elongation at break of epoxy composite reinforced with UT-SF and ST-SF.

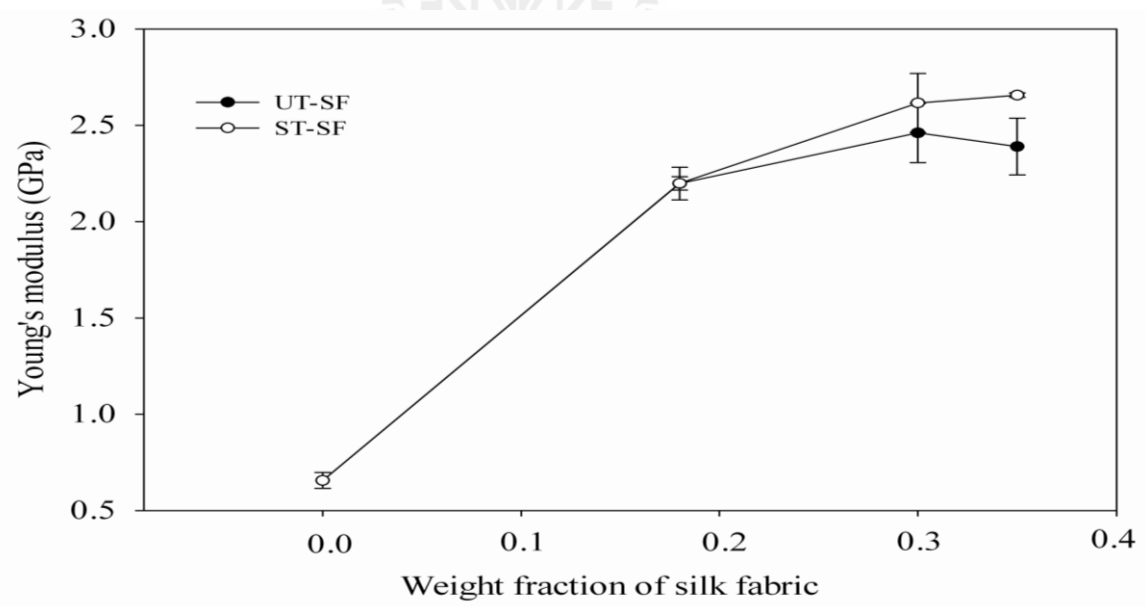


Figure 4.19 Plot of Young's modulus of epoxy composite at various weight fractions of UT-SF and ST-SF.

Elongation at break of neat epoxy and epoxy composites are shown in Figure 4.20. The elongation at break of neat epoxy was higher than that of epoxy composites. The elongation at break of ST-SF/epoxy composite was not different from that of UT-SF/epoxy composite.

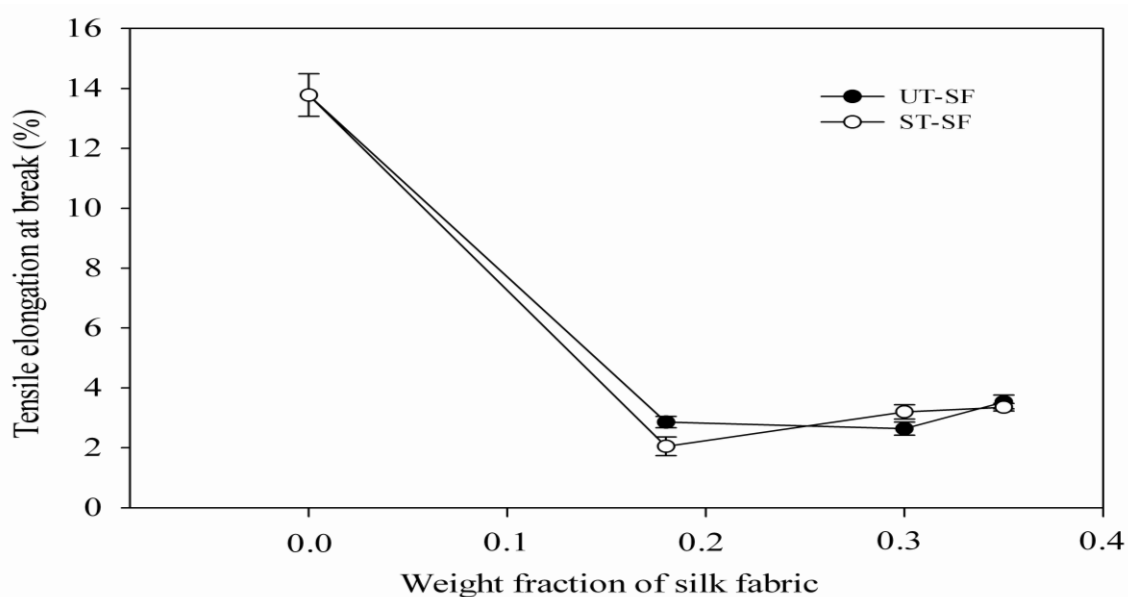


Figure 4.20 Plot of elongation at break of epoxy composite at various weight fractions of UT-SF and ST-SF.

Tensile strength of neat epoxy was higher than those of ST-SF/epoxy and UT-SF/epoxy composite and tensile strength of the ST-SF/composite increased with increasing weight fraction of silk fabric, as shown in Figure 4.21. At weight fraction of 0.18 silk fabric, tensile strength of ST-SF/composite was slightly lower than that of UT-SF/epoxy composite. However, tensile strength of ST-SF/composite was slightly higher than that of UT-SF/epoxy composite when the weight fraction of ST-SF was increased to 0.30, as shown in Figure 4.21. Treating the

silk fabric with APTES did not make significant improvement in tensile strength of epoxy composite.

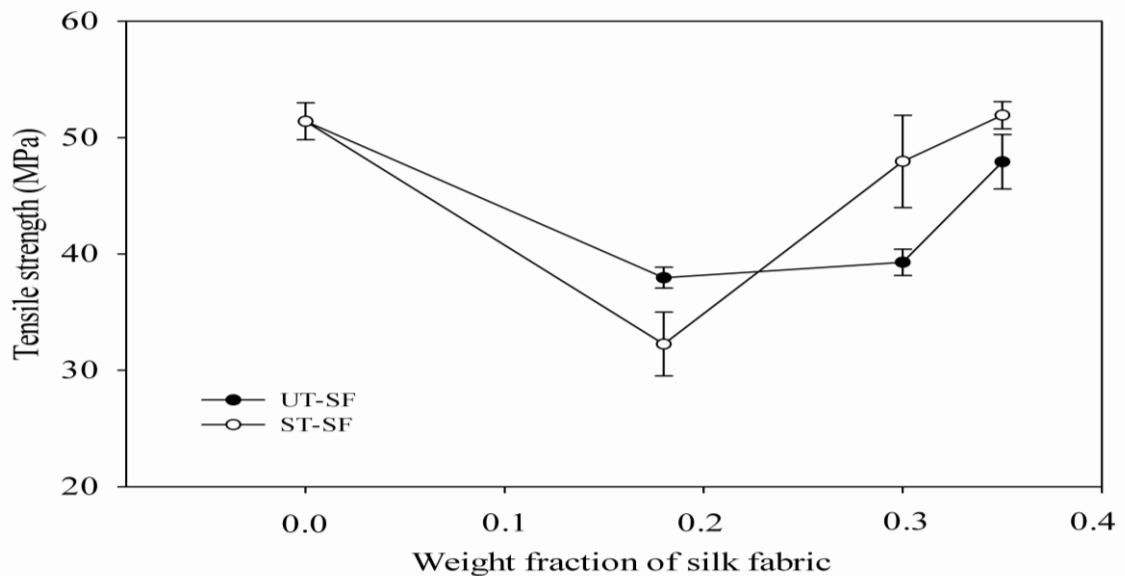


Figure 4.21 Plot of Tensile strength of epoxy composite at various weight fractions of UT-SF and ST-SF.

4.3.2 Impact property

The impact property of neat epoxy and epoxy composites is shown in Figure 4.22. The impact strength of neat epoxy was higher than that of silk fabric/epoxy composite prepared with UT-SF and ST-SF. The impact strength of ST-SF/epoxy composite was higher than that of UT-SF/epoxy composite. This was due to the fact that ST-SF and epoxy matrix had good interfacial adhesion. When interaction between fiber and resin was improved, load transfer under impact load from resin to fiber becomes more efficient (Keusch and Haessler, 1999; Zhao and Takeda, 2000). The tensile properties and impact property of epoxy composites at various weight fractions of UT-SF and ST-SF are summarized in Table 4.12.

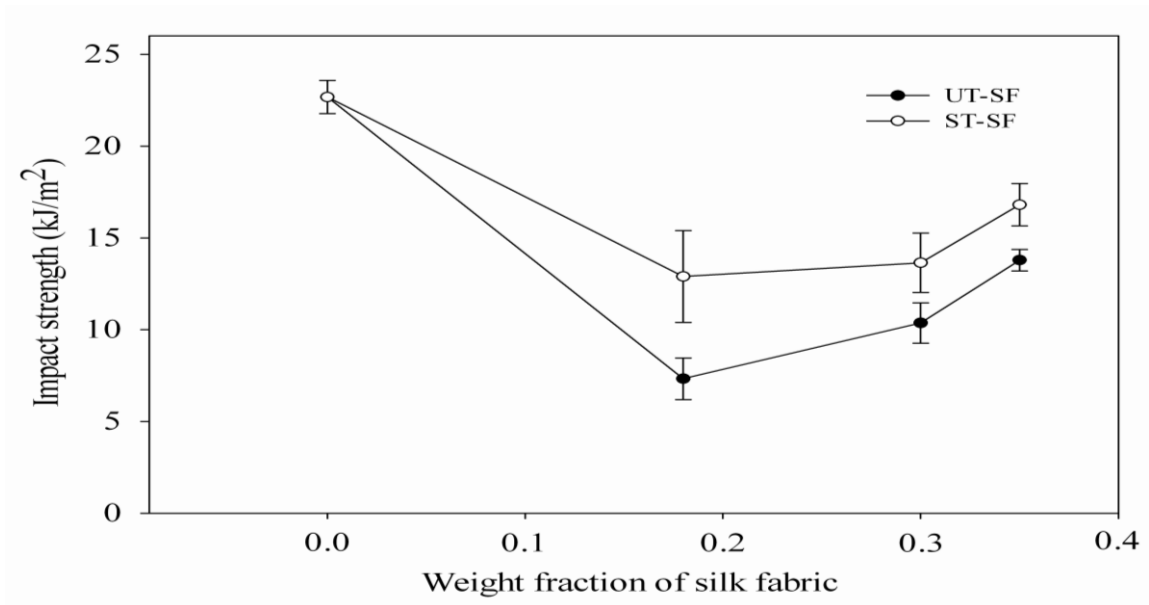


Figure 4.22 Plot of impact strength of epoxy composites at various weight fractions of UT-SF and ST-SF.

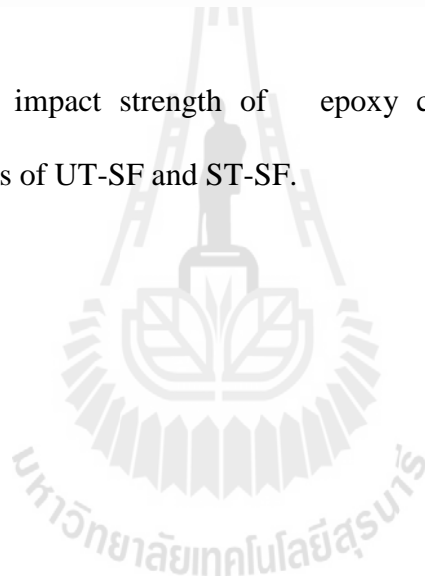


Table 4.12 Tensile properties and impact property of UT-SF/epoxy composite and ST-SF/epoxy composite at various contents of silk fabric.

weight fraction	Young' s modulus (GPa)		Tensile strength (MPa)		Elongation at break (%)		Impact strength (kJ/m ²)	
	UT-SF	ST-SF	UT-SF	ST-SF	UT-SF	ST-SF	UT-SF	ST-SF
0	0.66 ± 0.04	0.66 ± 0.04	51.41 ± 1.59	51.41 ± 1.59	13.78 ± 0.71	13.78 ± 0.71	22.67 ± 0.90	22.67 ± 0.90
0.18	2.20 ± 0.08	2.20 ± 0.03	37.96 ± 0.90	32.26 ± 2.74	2.86 ± 0.19	2.05 ± 0.31	7.32 ± 1.13	12.90 ± 2.50
0.30	2.50 ± 0.15	2.62 ± 0.15	39.29 ± 1.14	47.96 ± 3.96	2.64 ± 0.22	3.20 ± 0.23	10.36 ± 1.10	13.65 ± 1.62
0.35	2.40 ± 0.14	2.66 ± 0.01	47.94 ± 2.34	51.94 ± 1.17	3.53 ± 0.23	3.35 ± 0.12	13.80 ± 1.10	16.81 ± 1.14

4.3.3 Flexural properties

Flexural modulus of neat epoxy was lower than that of silk fabric/epoxy composite, as shown in Figure 4.23. The flexural modulus of ST-SF/epoxy composites increased with increasing weight fraction of ST-SF. Flexural modulus of ST-SF/epoxy composite was almost the same as that of UT-SF/epoxy composites. Similar result has been reported by Li, Mai, and Ye (2000) that the flexural properties (including flexural modulus and flexural strength) of sisal/epoxy composite insignificantly increased after the silane treatment of sisal fiber (Li, Mai and Ye, 2000).

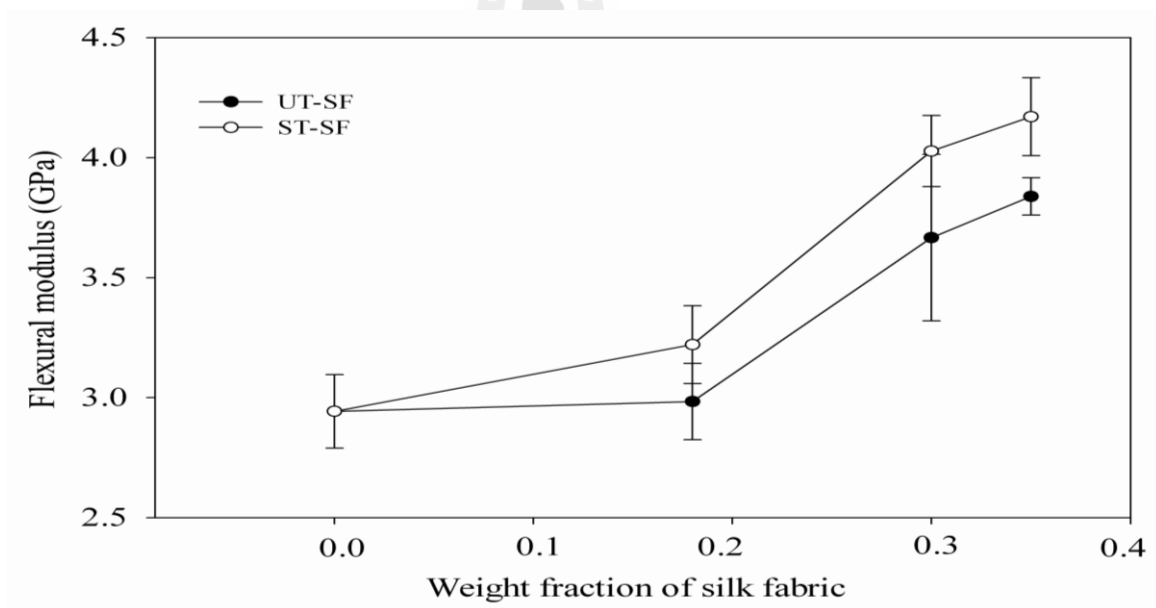


Figure 4.23 Plot of flexural modulus of epoxy composites at various weight fractions of UT-SF and ST-SF.

Flexural strain at break of neat epoxy was higher than that of epoxy ST-SF/composites. Flexural strain at break of ST-SF/epoxy and UT-SF/epoxy composite was not different, as shown in Figure 4.24.

Flexural strength of neat epoxy was higher than that of ST-SF/epoxy composites. Flexural strength of UT-SF/epoxy composite and ST-SF/epoxy composite was not different, as shown in Figure 4.25. Flexural properties of epoxy composites at various weight fractions of UT-SF and ST-SF are summarized in Table 4.13.

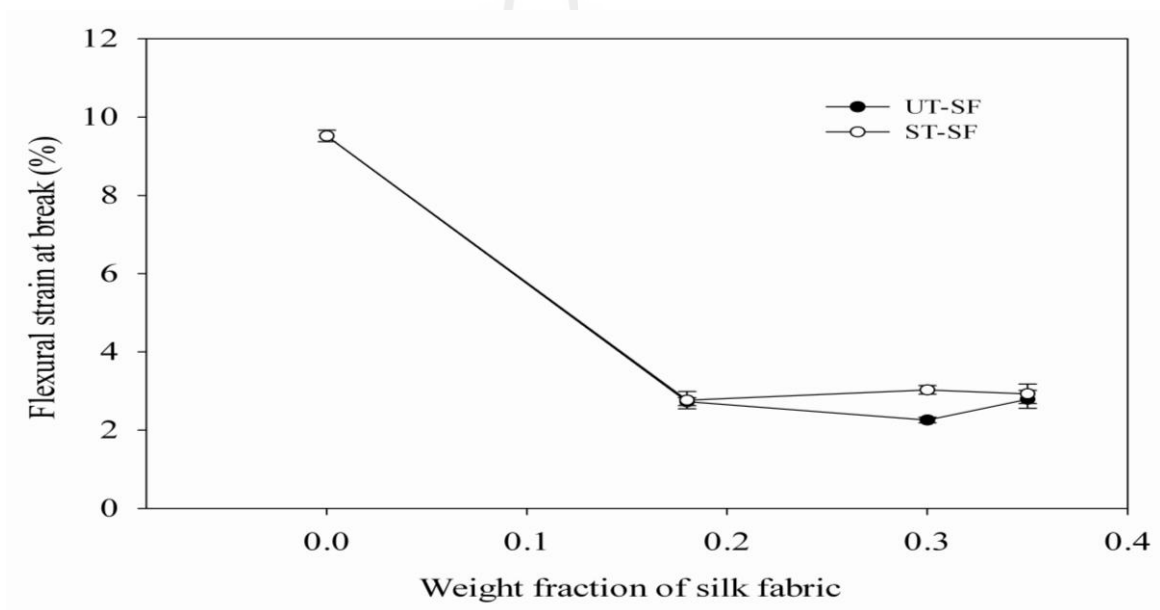


Figure 4.24 Plot of flexural strain at break of epoxy composites at various weight fractions of UT-SF and ST-SF.

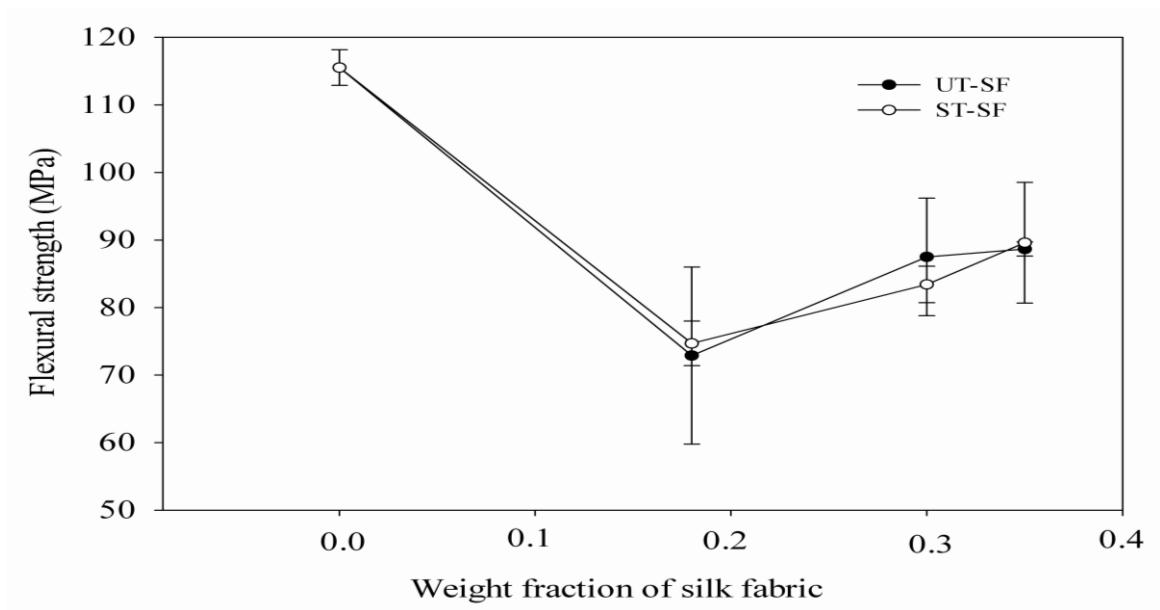


Figure 4.25 Plot of flexural strength of epoxy composites at various weight fractions of UT-SF and ST-SF.

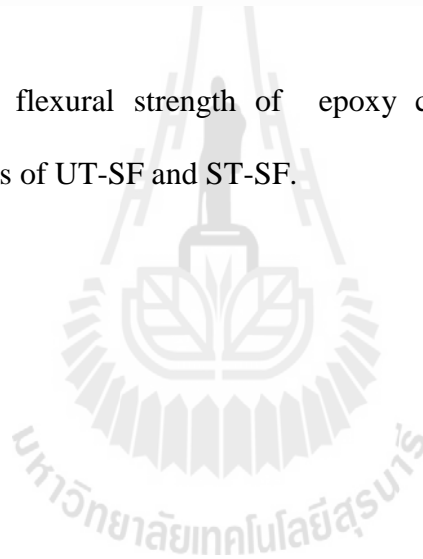


Table 4.13 Flexural properties of UT-SF/epoxy composite and ST-SF/epoxy composite at various contents of silk fabric.

weight fraction	Flexural modulus (GPa)		Flexural strength (MPa)		Flexural strain at break (%)	
	UT-SF	ST-SF	UT-SF	ST-SF	UT-SF	ST-SF
0	2.94±0.15	2.94±0.15	115.53±2.64	115.53±2.64	9.52±0.15	9.52±0.15
0.18	2.98 ± 0.16	3.22±0.16	72.90 ± 13.11	74.7±3.31	2.77 ± 0.22	2.73±0.10
0.30	3.67 ± 0.03	4.03±0.14	87.51 ± 8.70	83.43±2.71	3.03 ± 0.11	2.26±0.07
0.35	3.84 ± 0.08	4.17±0.16	88.68 ± 4.05	89.61±8.94	2.93 ± 0.25	2.79±0.23



4.3.4 Heat distortion temperature

Heat distortion temperature (HDT) of ST-SF/epoxy composite increased with increasing ST-SF content up to ST-SF weight fraction of 0.30. The HDT of ST-SF/epoxy composites was slightly higher than that of UT-SF/epoxy composites, as shown in Table 4.14. The same result has been reported by Lee, Kim, Lee, Kim, and Dorgan (2009). They reported that HDT of 3-glycidoxypropyl trimethoxy silane (GPS) treated kenaf fiber/PLA composite was a slightly higher than that of kenaf fiber/PLA composite. This was attributed to the improved interfacial adhesion (Lee, Kim, Lee, Kim, and Dorgan, 2009).

Table 4.14 Heat distortion temperature of epoxy composites at various weight fractions of UT-SF and ST-SF.

Weight fraction	HDT (°C)	
	UT-SF	ST-SF
0	83.7	83.7
0.18	99.9	103.2
0.30	93.3	105.5
0.35	92.6	103.8

4.3.5 Thermal properties

TGA and DTGA curves of neat epoxy and ST-SF/epoxy composite are shown in Figure 4.26. The TGA and DTGA thermograms of neat epoxy show thermal decomposition at 381°C. The thermograms of ST-SF show two transitions in a range of 30°C-150°C and 200°C-500°C. The first transition around 80°C attributed to the evaporation of water and the second transition observed at 340°C corresponded to silk fibrion decomposition. Two thermal decompositions of ST-SF/epoxy composites were observed in a range of 200-550°C. The first transition was observed as a shoulder peak with an initial temperature at around 237-214°C. This attributed to thermal decomposition of silk fabric existing in the epoxy composites (Srihanam, Srisuwan, and Simchure, 2009). The second transition of ST-SF/epoxy composites in the range of 200-550°C with the decomposition peak were approximate at 378-380°C corresponded to thermal decomposition of epoxy matrix. However, the decomposition peak of epoxy as observed from DTGA thermograms became boarder at half height, especially at higher ST-SF content of 0.30 and 0.35. This was the indication of the difference of microstructure of epoxy within the composite. The initial decomposition temperature and the decomposition temperature of UT-SF/epoxy composite and ST-SF/epoxy composite prepared with fabric weight fraction of 0-0.35 are summarized in Table 4.15. From Table 4.15, the initial of silk fabric decomposition temperature of ST-SF/epoxy composite was lower than that of UT-SF/epoxy composite. However, epoxy decomposition temperature of ST-SF/epoxy composite was not significantly different from that of UT-SF/epoxy composite. TGA and DTGA curves of neat epoxy and UT-SF/epoxy composites at the weight fraction of fabric 0.18- 0.35 are shown in Figure 4.27.

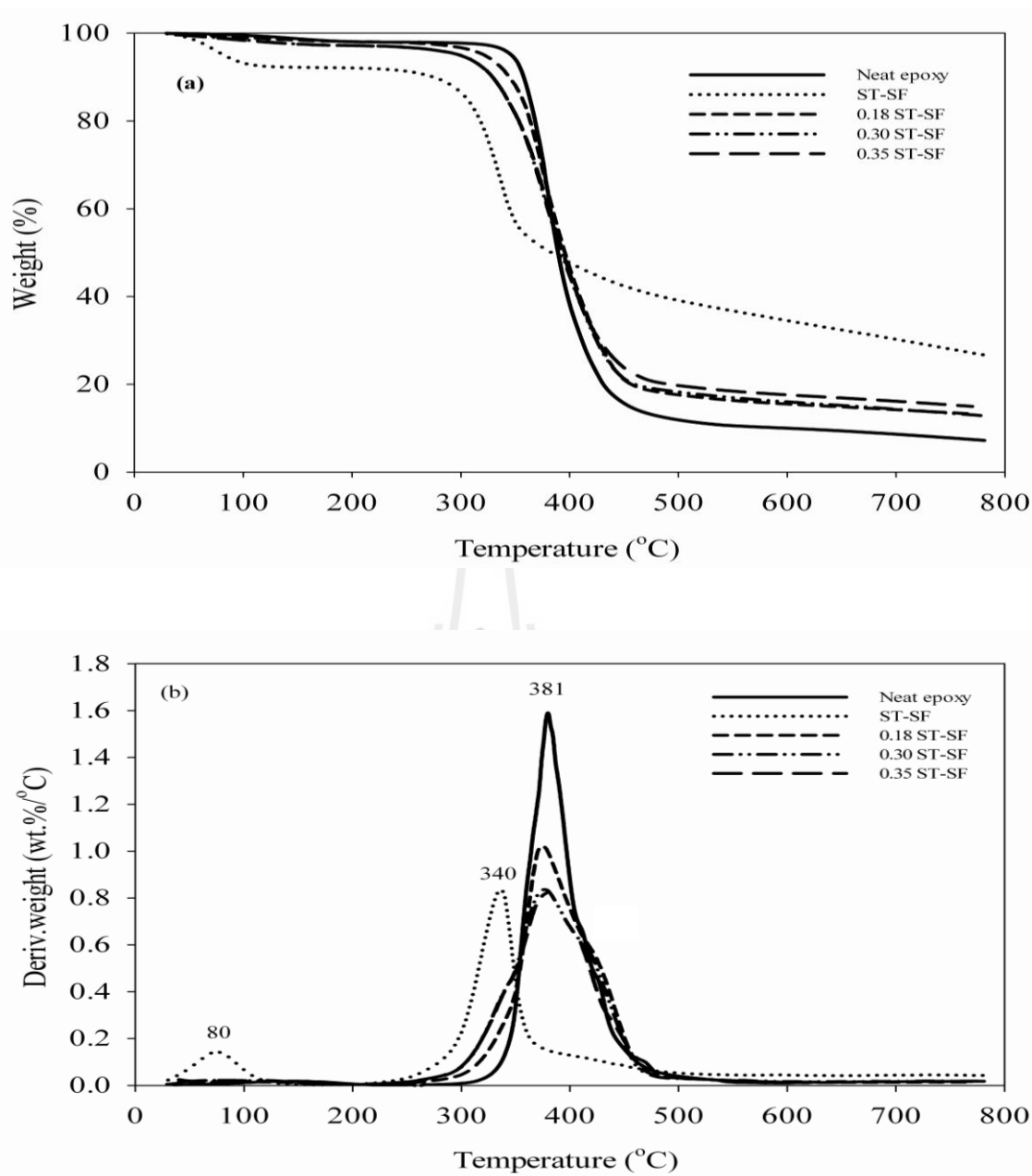


Figure 4.26 TGA (a) and DTGA (b) curves of neat epoxy and ST-SF/epoxy composites.

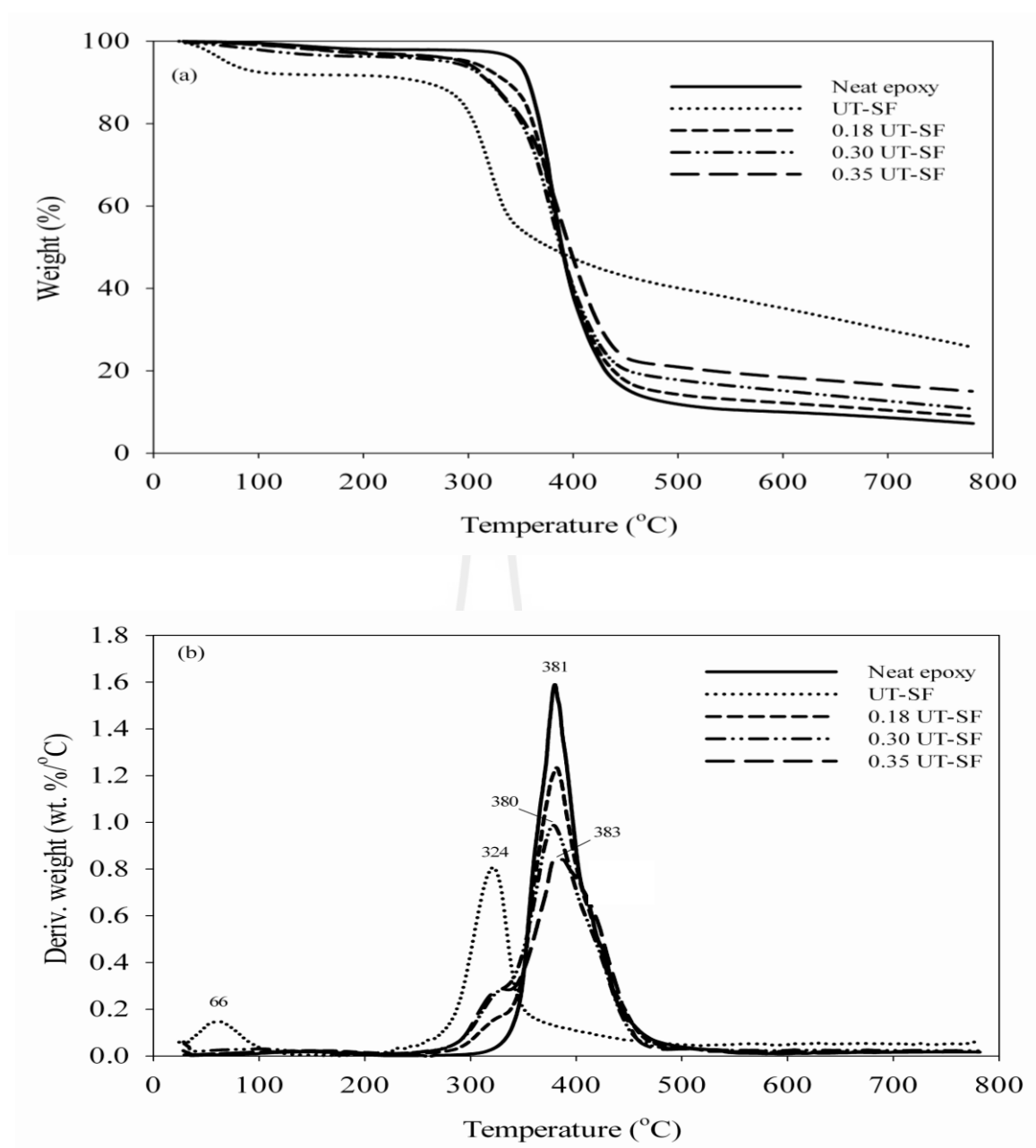


Figure 4.27 TGA (a) and DTGA (b) curves of neat epoxy and UT-SF/epoxy composites.

Table 4.15 Decomposition temperature of UT-SF/epoxy composite and ST-SF/epoxy composite prepared with fabric weight fraction of 0-0.35.

Weight fraction	Initial decomposition temperature of silk		Decomposition peak temperature of epoxy	
	UT-SF	ST-SF	UT-SF	ST-SF
0	-	-	381.0 (peak)	381.0 (peak)
0.18	264.0	237.0	380.0 (peak)	380.0 (peak)
0.30	229.0	208.0	380.0 (peak)	380.0 (peak)
0.35	229.0	214.0	383.0(peak)	378.0 (peak)

DSC curves of neat epoxy and ST-SF/epoxy composite before post curing are shown in Figure 4.28. The curing temperature of ST-SF/epoxy composite was higher than that of neat epoxy and curing temperature of the epoxy composite increased with increasing ST-SF content. The curing temperature of ST-SF/epoxy composite was lower than those of UT-SF/epoxy composite, as observed in Table 4.16. Curing temperature of UT-SF/epoxy composite and ST-SF/epoxy composite prepared with fabric weight fraction of 0-0.35 are summarized in Table 4.16.

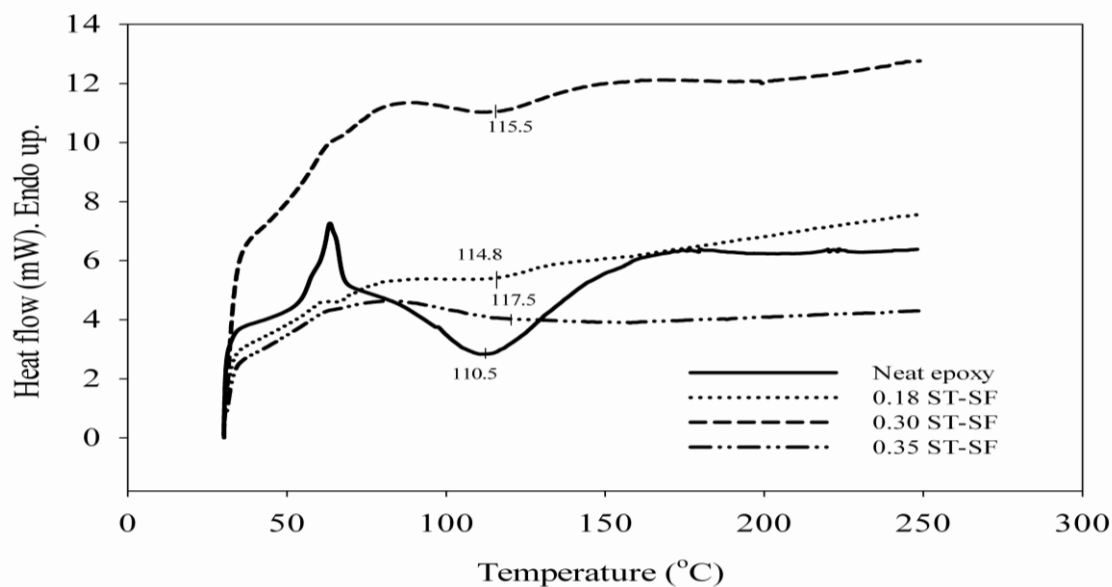


Figure 4.28 DSC curves of neat epoxy and ST-SF/epoxy composite before post curing.

Table 4.16 Curing temperature (T_{cure}) of UT-SF/epoxy composite and ST-SF/epoxy composite prepared with fabric weight fraction of 0-0.35.

Weight fraction	T_{cure} (°C)	
	UT-SF	ST-SF
0	110.5	110.5
0.18	116.3	114.8
0.30	128.0	115.5
0.35	138.5	117.5

For post cured neat epoxy and ST-SF/epoxy composites, their DSC curves from the first heating scan and the second heating scan are shown in Figure 4.29. From the first heating DSC curves, glass transition temperature of epoxy

composites were observed as the shift of the transition whereas that of neat epoxy was observed as the peak. Glass transition temperature (T_g) of neat epoxy and epoxy composite at various silk fabric contents, after post curing from the first and the second heating scan are shown in Table 4.17. Glass transition temperature after post curing of epoxy composites, obtained from the first heating DSC curves, increased with ST-SF weight fraction of 0.18 and then, glass transition temperature after post curing of epoxy composites slightly decreased with ST-SF weight fraction of 0.30 and 0.35. In addition, glass transition temperature after post curing of ST-SF/epoxy composite was higher than those of UT-SF/epoxy composite, as shown in Table 4.17. Similar result has been reported by Lee *et al.* (2009). They found that the glass transition temperature of 3-Glycidoxypropyl trimethoxy silane (GPS) treated kenaf fiber/PLA composite was higher than that of untreated kenaf fiber/PLA composite.

Glass transition temperature from the second heating of epoxy composites increased with ST-SF weight fraction of 0.18 and then, glass transition temperature from the second heating scan of epoxy composites decreased with ST-SF weight fraction of 0.30 and 0.35. In addition, glass transition temperature from the second heating scan of ST-SF/epoxy composite was higher than those of UT-SF/epoxy composite. Moreover, glass transition temperature from the second heating scan of neat epoxy and epoxy composites was higher than that of glass transition temperature obtained from the first heating scan, as shown in Table 4.17. These because epoxy gained more reaction between amide curing agent and epoxide ring. The fully curing was obtained in the second heating scan.

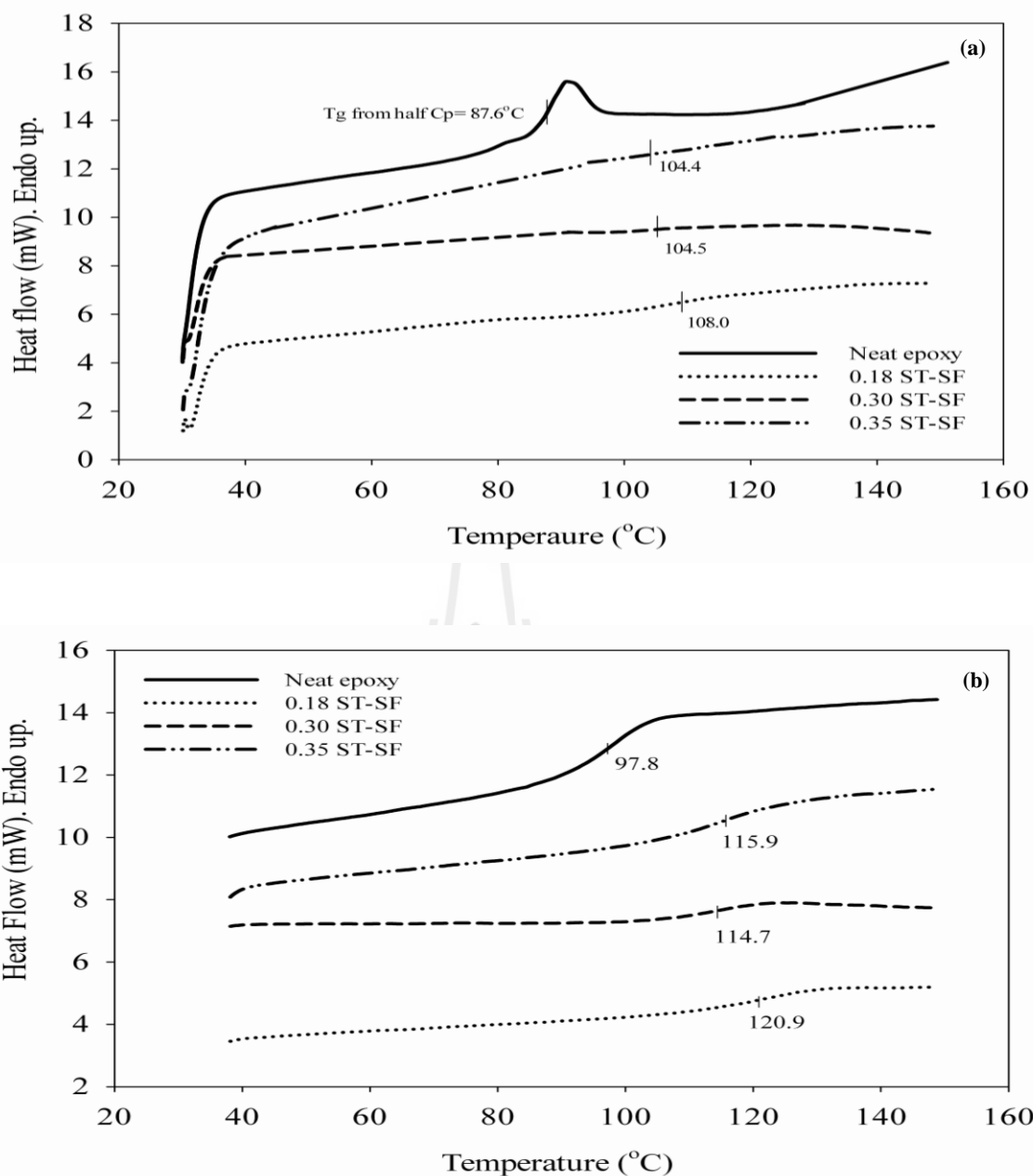


Figure 4.29 DSC curves of neat epoxy and ST-SF/epoxy composites from the first heating scan (a) and from the second heating scan (b).

Table 4.17 Glass transition temperature (T_g) of neat epoxy and epoxy composite at various silk fabric contents, obtained from the first and the second heating scan.

Weight fraction	T_g (°C) 1 st heating scan (°C)		T_g (°C) 2 nd heating scan	
	UT-SF	ST-SF	UT-SF	ST-SF
0	87.6	87.6	97.8	97.8
0.18	90.3	108.0	99.4	120.9
0.30	84.9	104.5	99.7	114.7
0.35	84.8	104.4	99.6	115.9

4.3.6 Fracture surface morphology

The SEM micrographs obtained from impact test specimen of neat epoxy and ST-SF/epoxy composites are shown in Figure 4.30. The SEM micrograph of neat epoxy showed that its fracture surface consisted of three regions including, smooth mirror region, mist region and hackle region or so-called radial striation zone, as shows in Figure 4.30(a). The radial striation of ST-SF/epoxy composite, running from one fabric surface to another fabric surface, was observed in Figure 4.30 (b-d). This indicated that ST-SF/epoxy composite still fractured in a brittle manner. However, the size of mirror zone was minimized with increasing ST-SF content. The increment of fabric layers helped terminate an expansion of mirror zone created in epoxy matrix of the composite.

SEM micrographs of ST-SF/epoxy composites and UT-SF/epoxy composites with the weight fraction of 0.18 are shown in Figure 4.31. From Figure

4.31(a-b), the large delamination, fiber pull-out and crack were observed in UT-SF/epoxy composite. The large delamination, fiber pull-out and crack resulted in the weak interaction between epoxy matrix and silk fiber fabric. SEM micrographs of ST-SF/epoxy composites showed that ST-SF and matrix had better interaction, as seen in Figure 4.31 (c-d). The interfacial adhesion between silk fabric and epoxy matrix of ST-SF/epoxy composite was better than that of UT-SF/epoxy composite. This indicated that the silane treatment improved interfacial adhesion between silk fabric and epoxy matrix. When bonding between fiber and resin improved, load transfer from resin to fiber became more efficient (Zhao and Takeda, 2000). As a result, impact strength of ST-SF/epoxy composites was higher than that of UT-SF/epoxy composites.

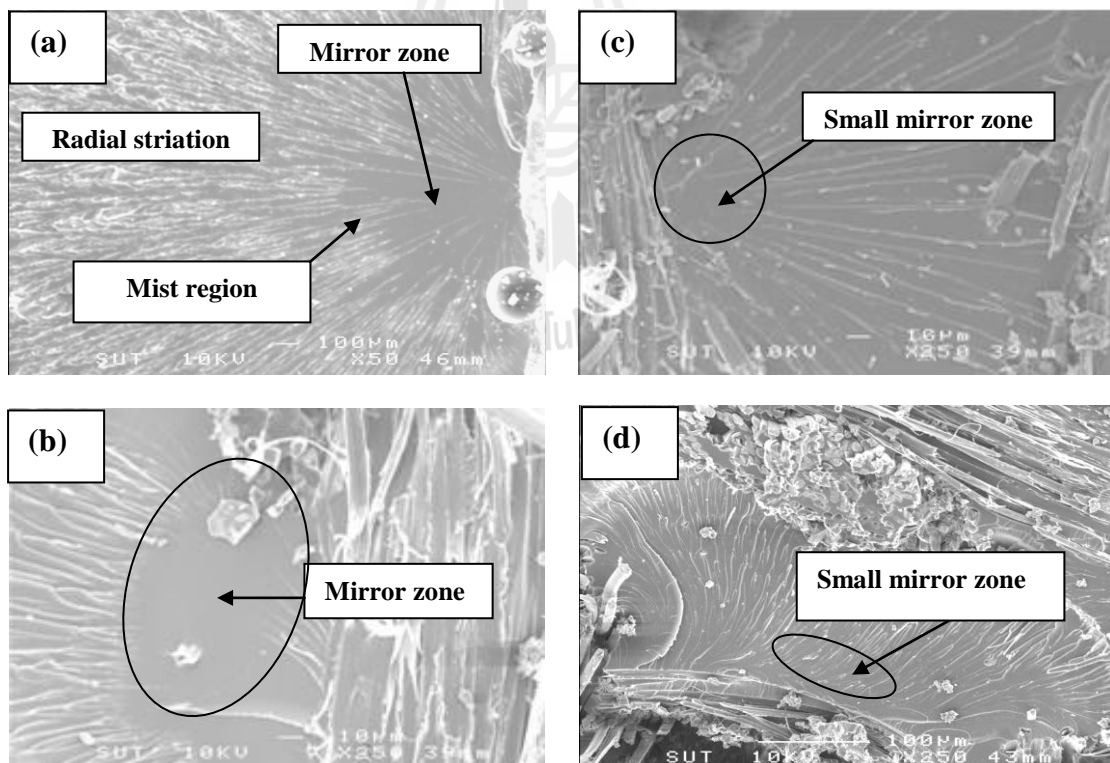


Figure 4.30 SEM micrographs of (a) neat epoxy and ST-SF/epoxy composites at (b) 0.18 ST-SF, (c) 0.30 ST-SF and (d) 0.35 ST-SF.

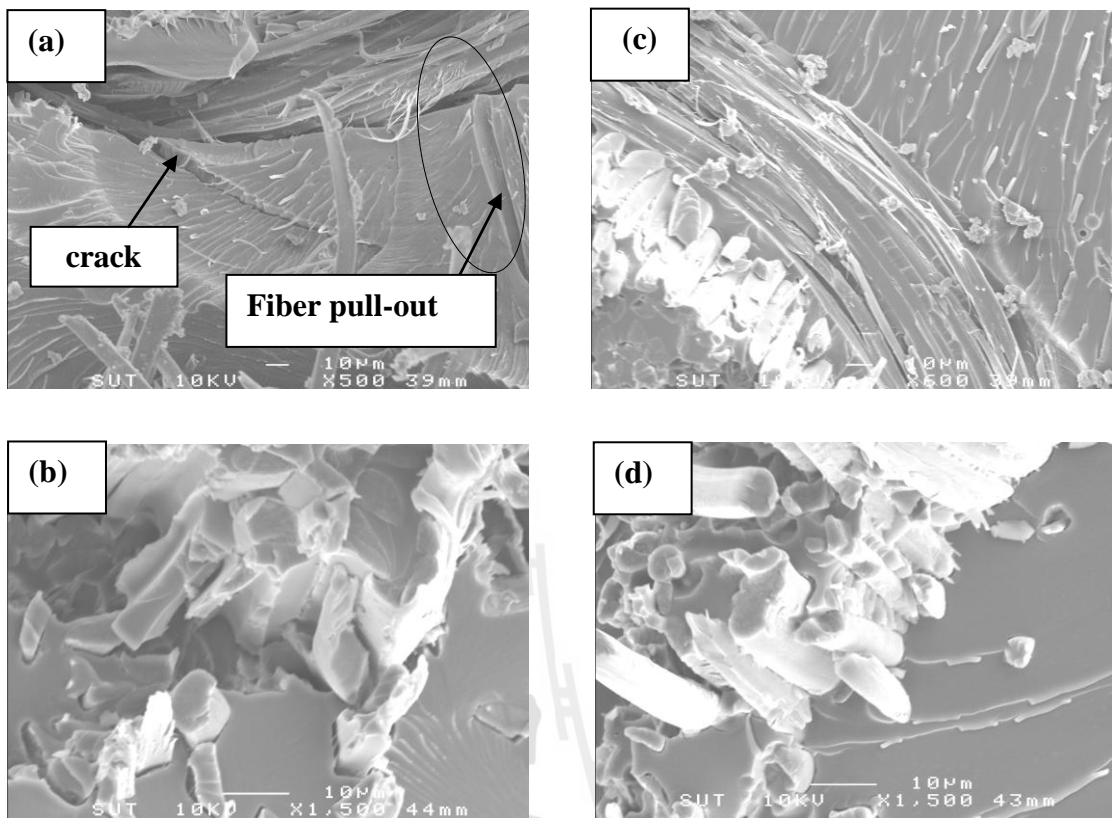


Figure 4.31 SEM micrographs, at fabric weight fraction of 0.18 of UT-SF/epoxy composites at magnification of x500 (a) and x1500 (b), and ST-SF/epoxy composites magnification of x500 (c) and x1500 (d).

4.4 The epoxy composite reinforced with ST-SF, glass fabric and Kevlar fabric

4.4.1 Mechanical properties of epoxy composites

Young's modulus and elongation at break of neat epoxy, ST-SF/epoxy composite, glass fabric/epoxy composite and Kevlar fabric/epoxy composite at weight fraction of 0.35 are shown in Figure 4.32. Young's modulus of neat epoxy was lower than that of epoxy composites. Young's modulus of ST-SF/epoxy composites was lower than that of glass fabric/epoxy composite and Kevlar fabric/epoxy composites. It was because Kevlar fabric and glass fabric have higher Young's modulus than ST-SF. In addition, Young's modulus of Kevlar fabric/epoxy composite was higher than that of glass fabric/epoxy composite. Elongation at break of neat epoxy was higher than that of epoxy composites. Elongation at break of ST-SF/epoxy composites was lower than that of glass fabric/epoxy composite and Kevlar fabric/epoxy composite.

Tensile strength and impact strength of neat epoxy, ST-SF/epoxy composite, glass fabric/epoxy composite and Kevlar fabric/epoxy composite at weight fraction of 0.35 are shown in Figure 4.33. Tensile strength of ST-SF/epoxy composite was comparable to that of neat epoxy. Tensile strength and impact strength of ST-SF/epoxy composite was much lower than those of glass fabric/epoxy composite and Kevlar fabric/epoxy composite. Tensile strength and impact strength of Kevlar fabric/epoxy composite was higher than glass fabric/epoxy composite.

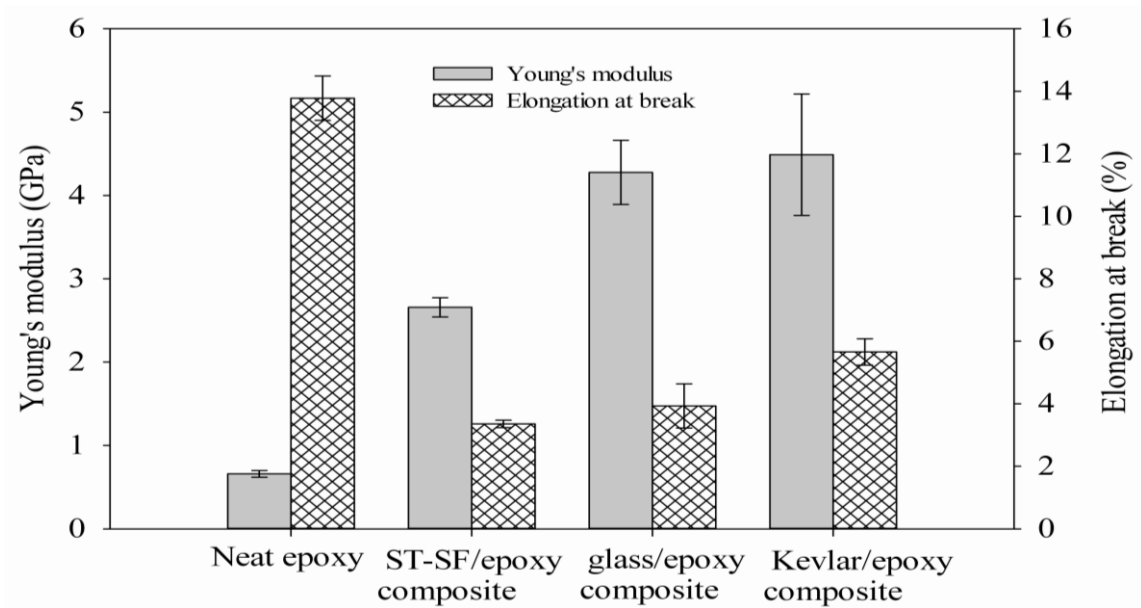


Figure 4.32 Plot of Young's modulus and elongation at break (%) of neat epoxy, ST-SF/epoxy composite, glass fabric/ epoxy composite and Kevlar/epoxy composite at weight fraction of 0.35.

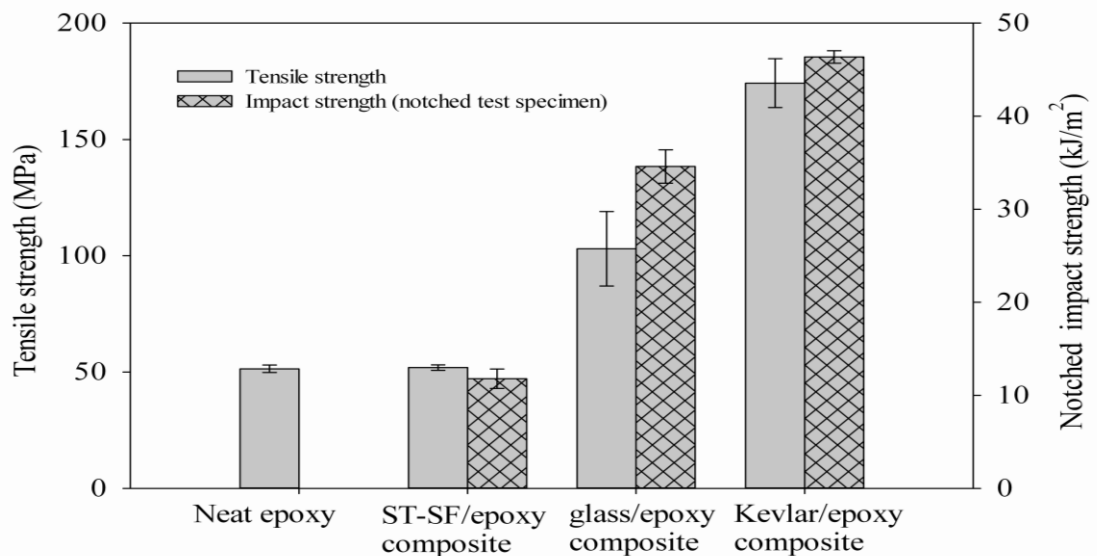


Figure 4.33 Plot of tensile strength and impact strength of neat epoxy, ST-SF/epoxy composite, glass fabric/ epoxy composite and Kevlar/epoxy composite at weight fraction of 0.35.

Flexural modulus of ST-SF/epoxy composite was higher than that of neat epoxy. However, flexural modulus of ST-SF/epoxy composite was lower than glass fabric/epoxy composite and Kevlar fabric/epoxy composite. Flexural modulus of Kevlar fabric/epoxy composite was higher than that of glass fabric/epoxy composite as shown in Figure 4.34. Flexural strain at break of those epoxy composites was lower than that of neat epoxy. Flexural strain at break of ST-SF/epoxy composite, glass fabric composite and Kevlar/epoxy composite was not significantly different.

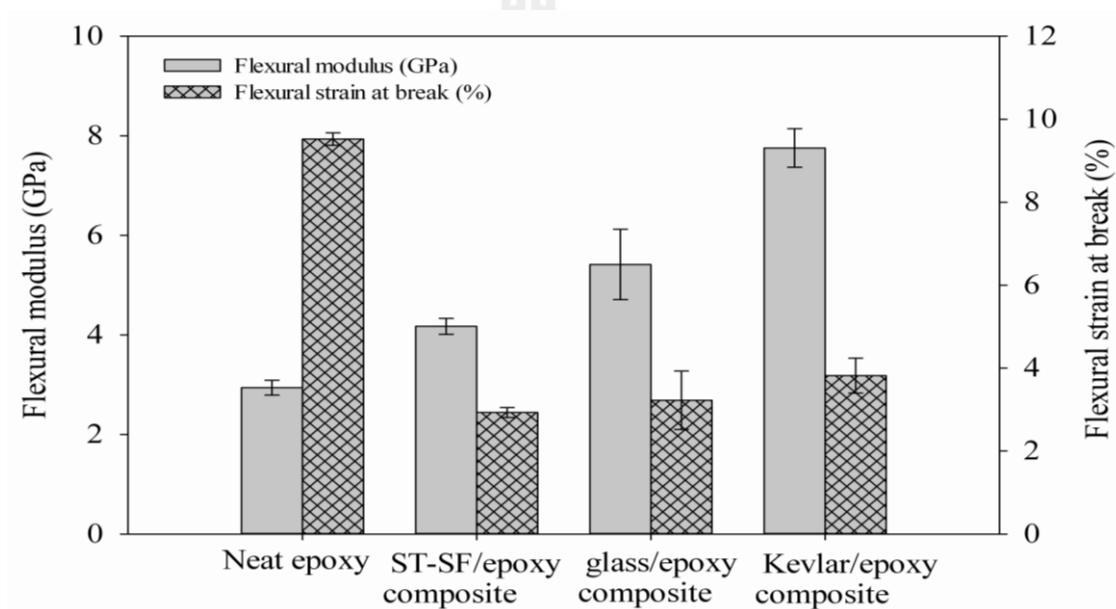


Figure 4.34 Plot of flexural modulus of and flexural strain at break of neat epoxy, ST-SF/epoxy composite, glass fabric/ epoxy composite and Kevlar/epoxy composite at weight fraction of 0.35.

Flexural strength of neat epoxy, ST-SF/epoxy composite, glass fabric composite and Kevlar fabric/epoxy composite at weight fraction of 0.35 is shown in Figure 4.35. Flexural strength of neat epoxy was higher than that of ST-SF/epoxy composite. Flexural strength of ST-SF/epoxy composite was lower than that of glass

fabric/epoxy composite and Kevlar fabric/epoxy composite. Flexural strength of Kevlar fabric/epoxy composite was higher than glass fabric/epoxy composite. The tensile properties, flexural properties and impact property of neat epoxy, ST-SF/epoxy composite, glass fabric/epoxy composite and Kevlar fabric/epoxy composite are summarized in Table 4.18.

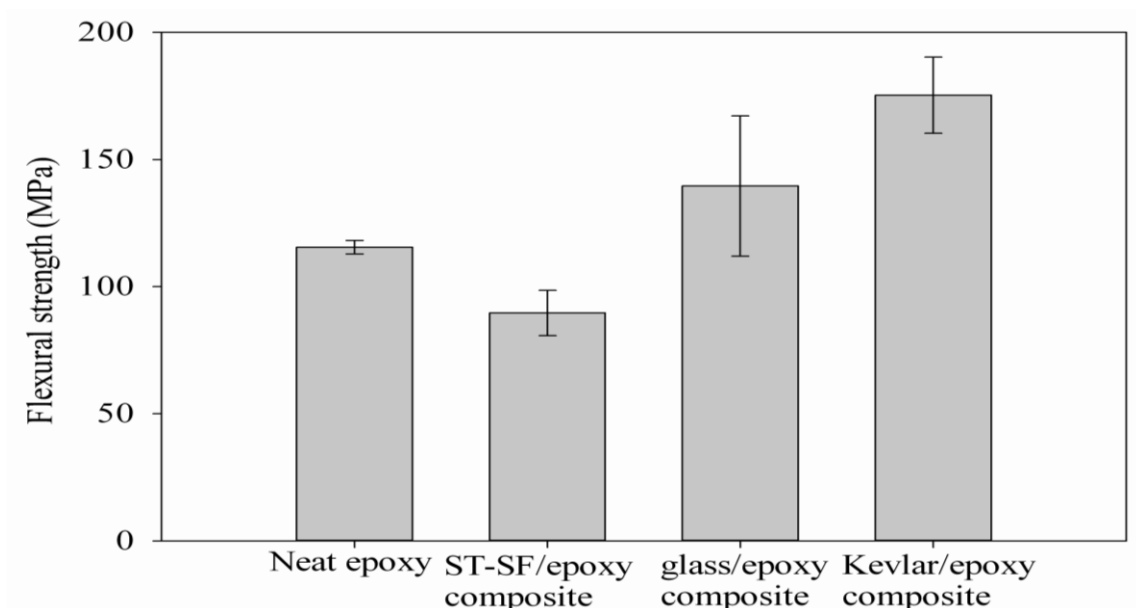


Figure 4.35 Plot of flexural strength of neat epoxy, ST-SF/epoxy composite, glass fabric/ epoxy composite and Kevlar/epoxy composite at weight fraction of 0.35.

Table 4.18 Tensile properties, flexural properties and impact property of neat epoxy and ST-SF/epoxy composite, glass/epoxy composite and Kevlar fabric/epoxy composite with fabric weight fraction of 0.35.

Materials	Tensile properties			Flexural properties			Notched impact strength (kJ/m ²)
	Young's modulus (GPa)	Tensile strength (MPa)	Elongation at break (%)	Flexural modulus (GPa)	Flexural strength (MPa)	Flexural strain at break (%)	
Neat epoxy	0.66 ± 0.04	51.41 ± 1.59	13.78 ± 0.71	2.94 ± 0.15	115.53 ± 2.64	9.52 ± 0.15	-
ST-SF/epoxy composite	2.66 ± 0.01	51.94 ± 1.17	3.35 ± 0.12	4.17 ± 0.16	89.61 ± 8.94	2.79 ± 0.23	16.81 ± 1.14
glass fabric/epoxy composite	4.28 ± 0.38	103.02 ± 16.04	3.39 ± 0.17	5.42 ± 0.70	139.60 ± 27.58	3.22 ± 0.70	34.60 ± 1.79
Kevlar fabric/epoxy composite	4.49 ± 0.73	174.23 ± 10.46	5.67 ± 0.41	7.76 ± 0.39	175.32 ± 14.96	3.81 ± 0.42	46.37 ± 0.37

HDT of neat epoxy was lower than that of epoxy composites. HDT of ST-SF/epoxy composite was comparable to that of glass fabric/epoxy composite but higher than that of Kevlar/epoxy composite, as shown in Table 4.19. This was because glass fabric itself had higher thermal stability than Kevlar fabric.

Table 4.19 Heat distortion temperature (HDT) of neat epoxy and ST-SF/epoxy composite, glass/epoxy composite and Kevlar/epoxy composite prepared at 0.35 reinforcement fabric.

Materials	HDT (°C)
Neat epoxy	83.7
ST-SF/epoxy composite	103.8
glass fabric/epoxy composite	104.8
Kevlar fabric/epoxy composite	99.2

4.4.2 Thermal properties of epoxy composites

TGA and DTGA curves of neat epoxy and epoxy composites are shown in Figure 4.36. The TGA and DTGA thermograms of neat epoxy show thermal decomposition of neat epoxy at 381°C. Two thermal transitions of ST-SF/epoxy composite were in a range of 200-550°C. The first transition was observed as a shoulder peak with an initial decomposition around 214 °C attributed to thermal decomposition of silk fabric existing in the composites (Srihanam, Srisuwan and Simchure, 2009). The second transition of ST-SF/epoxy composites in the range of 200-550°C corresponding to thermal decomposition of the epoxy and the decomposition peak was approximately at 378°C.

The thermograms of glass fabric/epoxy composite shows one decomposition transition as a peak at 381°C due to thermal decomposition of epoxy. In addition, epoxy decomposition was also observed as a shoulder peak at temperature higher than 381°C.

Three thermal transitions of Kevlar/epoxy composite were in a range of 220-650°C. The first peak was observed around 390°C attributed to thermal decomposition of epoxy in the composites. The second peak was observed at 433°C due to thermal decomposition of interfacial epoxy where epoxy reacted with NH₂ groups of Kevlar fabric (Cai and Yu, 2011). The third peak was observed at 590°C attributed to thermal decomposition of Kevlar fabric existing in the composites (Cai and Yu, 2011). Thermal decomposition temperature of neat epoxy, ST-SF/epoxy composite, glass fabric/epoxy composite and Kevlar fabric/epoxy composite are summarized in Table 4.20. The thermal stability of ST-SF/epoxy composite was lower than that of the epoxy composite reinforced with glass and Kevlar fabric. The

epoxy composites prepared with 3 different fabrics contained two different microstructures of epoxy matrix. Ones located at fabric-epoxy interface called interface epoxy. Another located far away from the fabric surface called bulk epoxy. However, the decomposition of interfacial epoxy was more pronounced in the epoxy composites reinforced with glass and Kevlar fabrics.



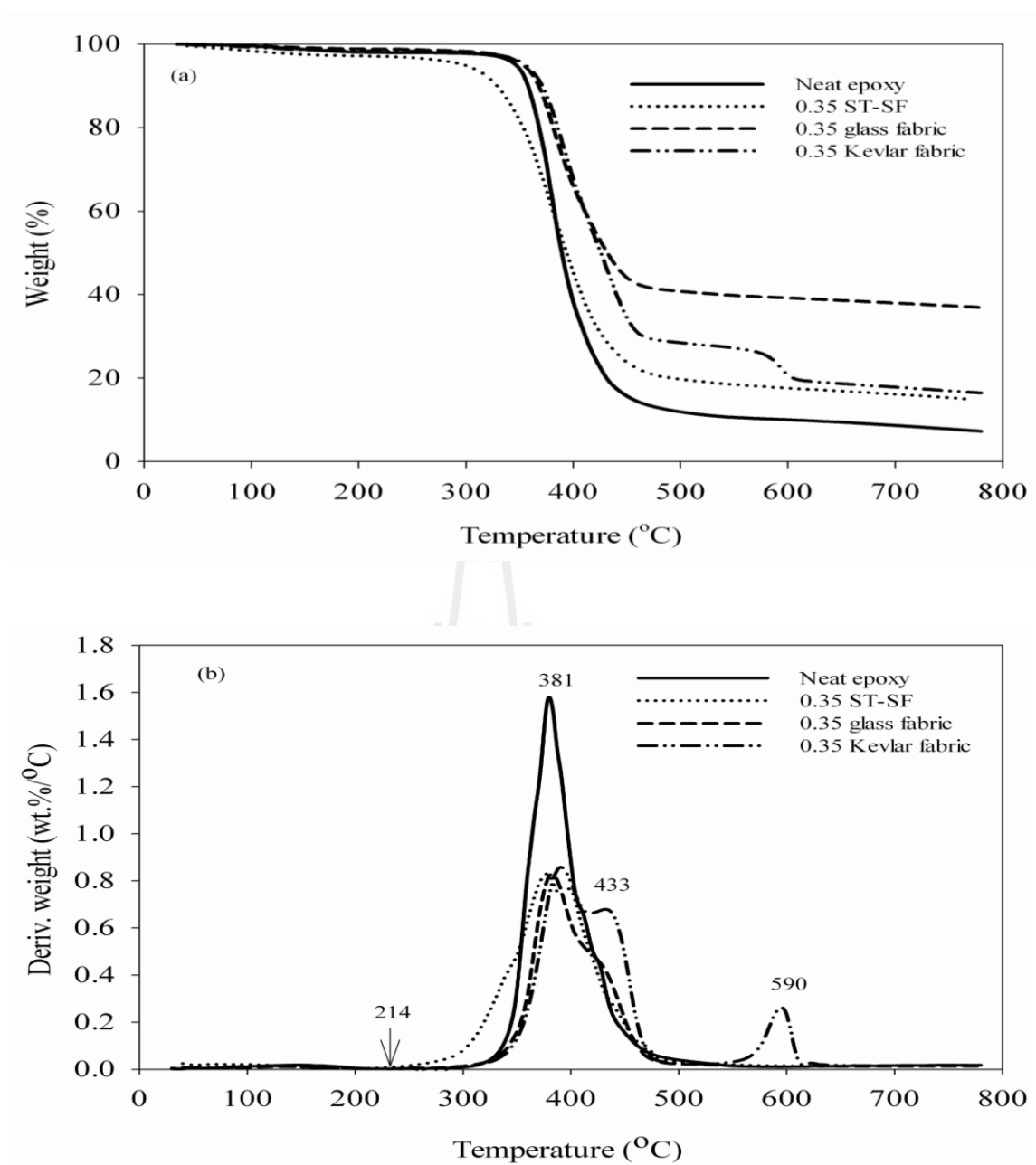


Figure 4.36 TGA (a) and DTGA (b) curves of neat epoxy and epoxy composites prepared with ST-SF, glass fabric and Kevlar fabric at weight fraction of 0.35.

Table 4.20 Thermal decomposition (T_d) of neat epoxy and epoxy composites prepared with ST-SF, glass fabric and Kevlar fabric at fabric fraction of 0.35.

Materials	Fabric decomposition (°C)	Epoxy decomposition (°C)
Neat epoxy	-	381.0 (peak)
ST-SF/epoxy composite	214.0 (initial decomposition)	378.0 (peak)
glass fabric/epoxy composite	-	381.0 (peak)
Kevlar fabric/epoxy composite	590.0 (peak)	390.0, 433.0 (peak)

DSC curves of neat epoxy, ST-SF/epoxy composite, glass fabric/epoxy composite and Kevlar fabric/epoxy composite before post curing are shown in Figure 4.37. The curing temperature of ST-SF/epoxy composite, glass fabric/epoxy composite and Kevlar fabric/epoxy composite were higher than that of neat epoxy. The curing temperature of ST-SF/epoxy composite and glass fabric/epoxy composite were approximately the same. However, the curing temperature of ST-SF/epoxy composite was higher than that of Kevlar fabric/epoxy composite. Curing temperature of neat epoxy and epoxy composites prepared with ST-SF, glass fabric and Kevlar fabric at fabric fraction of 0.35 before post curing are summarized in Table 4.21.

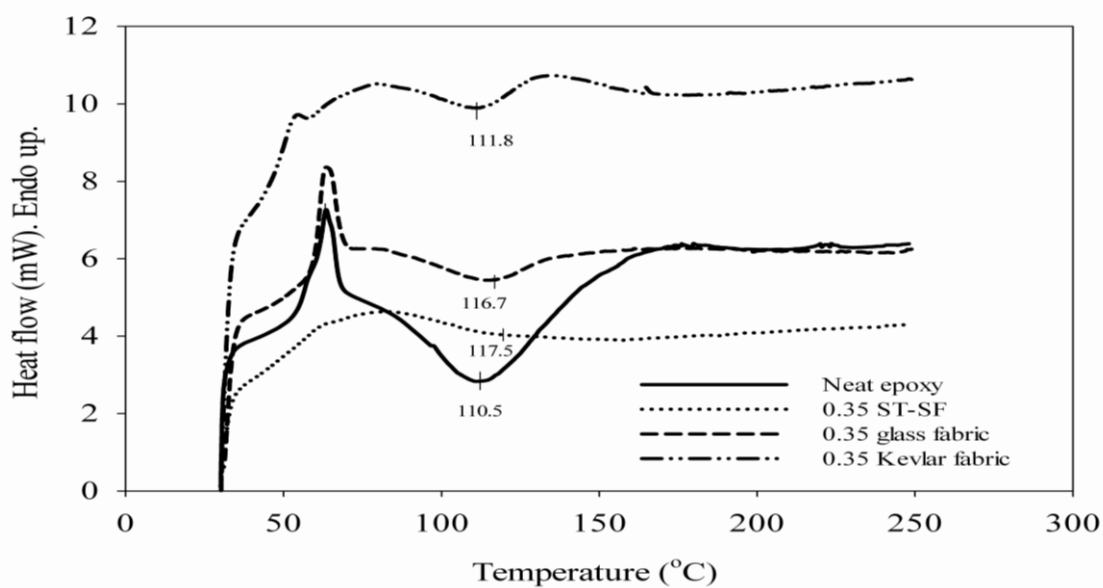


Figure 4.37 DSC curves of neat epoxy and epoxy composites prepared with ST-SF, glass fabric and Kevlar fabric at fabric fraction of 0.35 before post curing.

Table 4.21 Curing temperatures (T_{cure}) of neat epoxy and epoxy composites prepared with ST-SF, glass fabric and Kevlar fabric at fabric fraction of 0.35 before post curing.

Material	T_{cure} (°C)
Neat epoxy	110.5
ST-SF/epoxy composite	117.5
Glass/epoxy composite	116.7
Kevlar/epoxy composite	111.8

For post cured neat epoxy and epoxy composites, their DSC curves from the first heating scan and the second heating scan are shown in Figure 4.38. From the first heating DSC curves, glass transition temperature of neat epoxy and glass fabric/epoxy composite was observed as an endotherm peak. On the other hand, glass transition temperatures of ST-SF/epoxy composite and Kevlar fabric/epoxy composite appeared as a shift of the baseline. Glass transition temperature of ST-SF/epoxy composite, glass/epoxy composite and Kevlar fabric/epoxy composite with the weight fraction of 0.35, obtained from the first and the second heating scan are shown in Table 4.22. Glass transition temperature after post curing of ST-SF/epoxy composite, obtained from the first heating scan, was higher than that of glass fabric/epoxy composite and much higher than that of Kevlar/epoxy composite, as summarized in Table 4.22.

Glass transition temperature from the second heating scan of ST-SF/epoxy composite was higher than that of glass fabric/epoxy composite and much higher than that of Kevlar fabric/epoxy composite. However, glass transition temperature from the second heating scan of neat epoxy and epoxy composite was higher than glass transition temperature obtained from the first heating scan. These because epoxy gained more reaction between amide curing agent and epoxide ring. The fully curing was obtained in the second heating scan.

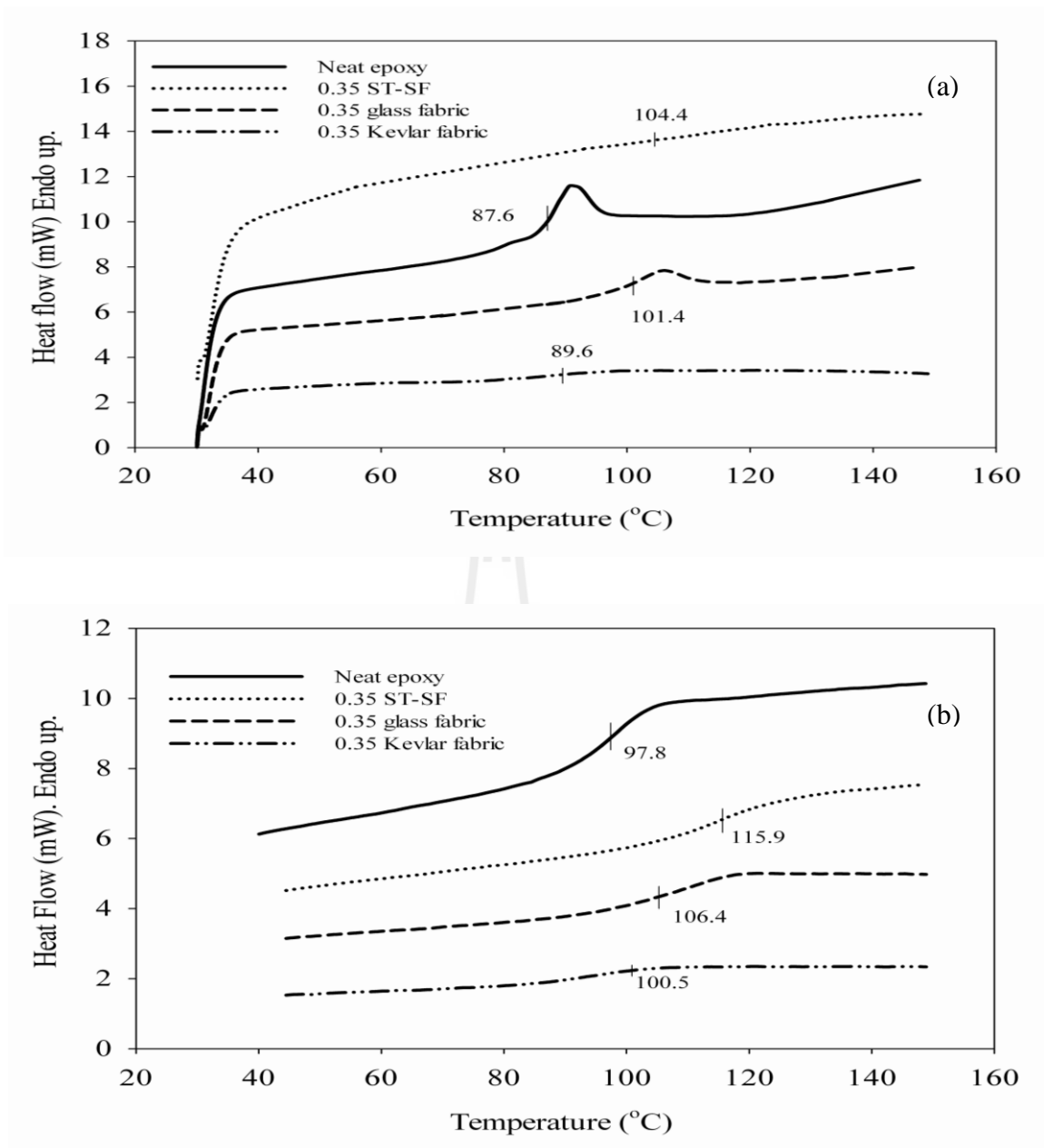


Figure 4.38 DSC curves neat epoxy and epoxy composites prepared with ST-SF, glass fabric and Kevlar fabric at fabric fraction of 0.35 from the first heating scan (a) and from the second heating scan (b).

Table 4.22 Glass transition temperature (T_g) of ST-SF/epoxy composite, glass fabric/epoxy composite and Kevlar fabric/epoxy composite with the weight fraction of 0.35, obtained from the first and the second heating scan.

Material	T_g (°C) 1 st heating scan (°C)	T_g (°C) 2 nd heating scan
Neat epoxy	87.6	97.8
ST-SF/epoxy composite	104.4	115.9
glass/epoxy composite	101.4	106.4
Kevlar/epoxy composite	89.6	100.5

4.4.3 Fracture surface morphology of the composites.

For ST-SF/epoxy composite, radial striation running from one fabric to another fabric surface and also smooth mirror zone were observed from fracture surface, as depicted in Figure 4.39 (a). This indicated that ST-SF/epoxy composite still fractured in a brittle manner. For glass fabric/epoxy composite and Kevlar fabric/epoxy composite, the smooth surface of epoxy matrix next to the fabric was observed, as seen in Figure 4.39 (b-c).

The SEM micrograph of silk fiber on fracture surface of ST-SF/epoxy composite showed that individual silk fibers located inner the silk bundle was broken, not the fibers located outer fiber bundle closely contacting to epoxy matrix, as depicted in Figure 4.40 (a). For glass fiber of glass fabric/epoxy composite, the glass fiber was brittlely broken under impact loading test, as depicted in Figure 4.40 (b).

Kevlar fabric/epoxy composite underwent large deformation before rupture under impact test and Kevlar fiber broke into microfibrill, as shown in Figure 4.40 (c).

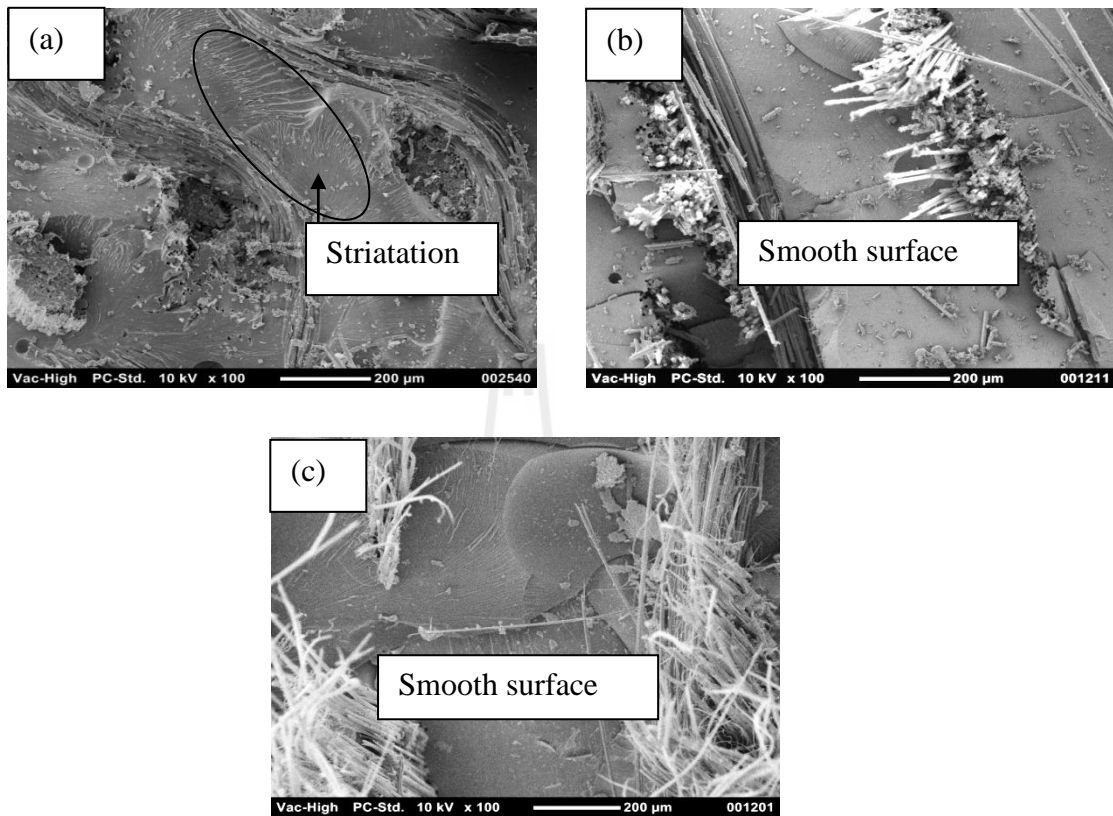


Figure 4.39 SEM micrographs of epoxy composites with (a) 0.35 ST-SF, (b) 0.35 glass fabric, and (c) 0.35 Kevlar fabric at a magnification of x100.

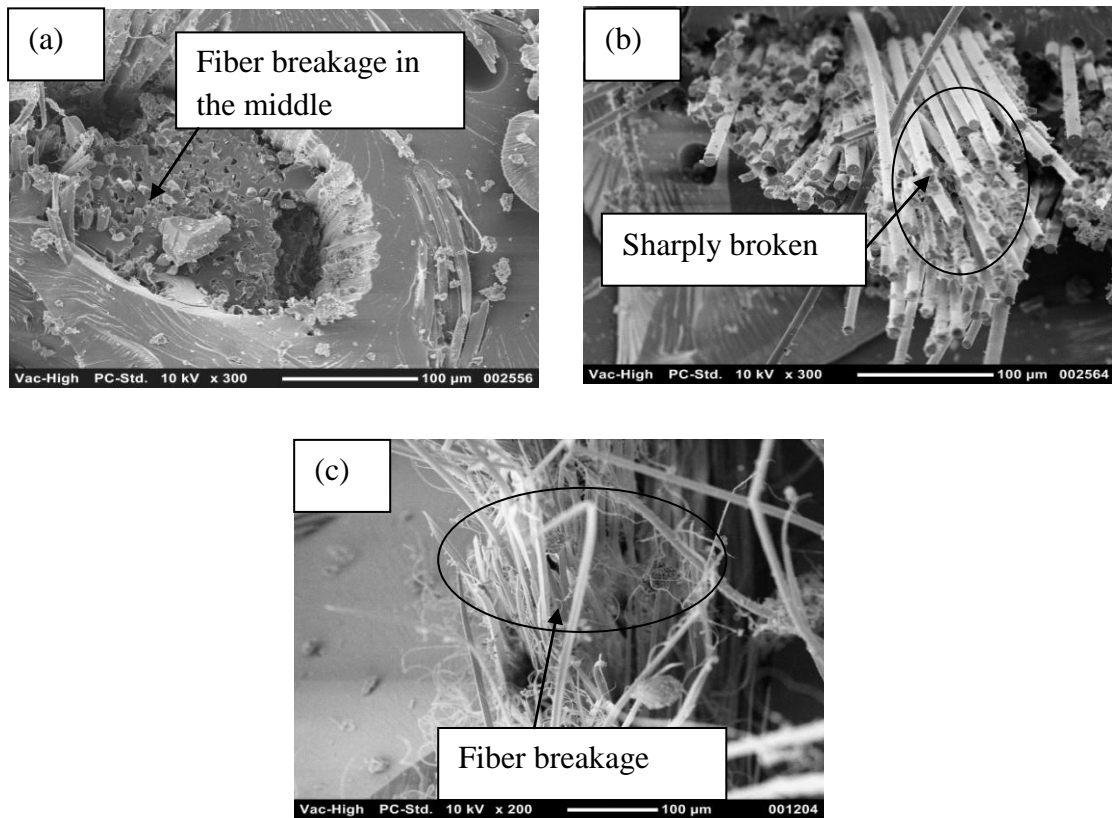


Figure 4.40 SEM micrographs of epoxy composites with (a) 0.35 ST-SF, (b) 0.35 glass fabric and (c) 0.35 Kevlar fabric at a magnification of x300, x300 and x200, respectively.

CHAPTER V

CONCLUSIONS

For UT-SF fabric, tensile properties of the fabric in warp and weft direction were not much different. After silane treatment, normalized tensile strength and normalized toughness of ST-SF was higher than those of UT-SF. Thermal stability of ST-SF was better than that of UT-SF. It was confirmed by FT-IR and XRF spectrometry that APTES deposited onto ST-SF surface. In addition, ST-SF surface was rougher than UT-SF surface. The molecular conformation of ST-SF did not changed after the silane treatment.

In comparison, normalized modulus of elasticity of Kevlar fabric and glass fabric were higher than that of UT-SF and ST-SF. Normalized tensile strength of Kevlar fabric was higher than that of silk fabric and glass fabric. However, normalized toughness of ST-SF was higher than that of Kevlar fabric and glass fabric. The thermal stability of Kevlar and glass fabric was higher than that of UT-SF and ST-SF. In addition, the glass fabric surface and Kevlar fabric surface were smooth.

For UT-SF/epoxy composite, the mechanical properties including Young's modulus, tensile strength, impact strength, flexural modulus and flexural strength of UT-SF/epoxy composites tended to increase with increasing UT-SF weight fraction over 0.18. However, tensile strength, elongation at break, impact strength, flexural strength, flexural strain at break of neat epoxy were higher than those of UT-SF/epoxy composites. HDT of UT-SF/epoxy composite decreased at UT-SF weight fraction was higher than 0.18. Curing temperature (T_{cure}) of UT-SF/epoxy

composite increased with increasing UT-SF content. In addition, glass transition temperature (T_g) after post curing obtained from the first and the second heating scan of UT-SF/epoxy composites decreased with increasing UT-SF content. The first thermal decomposition of UT-SF/epoxy composites was initially occurred at 229-266°C. The second decomposition of UT-SF/epoxy composites were approximate at 380-383°C. However, this decomposition peak became boarder as increasing UT-SF content. The UT-SF/epoxy composite broke in a brittle manner. However, the size of a mirror zone minimized with increasing UT-SF content.

For ST-SF/epoxy composite, Young's modulus, tensile strength, impact strength, flexural modulus and flexural strength of ST-SF/epoxy composites increased with increasing ST-SF content. The mechanical properties, Young's modulus, tensile strength, flexural modulus and flexural strength, of ST-SF/epoxy composites were insignificantly different from those of UT-SF/epoxy composites. Impact strength of ST-SF/epoxy composite was higher than that of UT-SF/epoxy composite. HDT of ST-SF/epoxy composite was slightly higher than that of UT-SF/epoxy composite. T_{cure} of ST-SF/epoxy composite was lower than that of UT-SF/epoxy composite whereas T_g after post curing obtained from the first and the second heating scan of ST-SF/epoxy composite was higher than that of UT-SF/epoxy composite. The initial decomposition temperature of ST-SF within ST-SF/epoxy composite was lower than that within UT-SF/epoxy composite. However, epoxy decomposition temperature of ST-SF/epoxy composite was not significantly different from that of UT-SF/epoxy composite. In addition, the interfacial adhesion between ST-SF and epoxy matrix was better than that that between UT-SF and epoxy matrix. ST-SF/epoxy composite still broke in a brittle manner.

Young's modulus, tensile strength, impact strength, flexural modulus and flexural strength of ST-SF/epoxy composite were lower than those of glass fabric/composite and Kevlar fabric/composite. HDT of ST-SF/epoxy composite was comparable to that of glass fabric/epoxy composite but higher than that of Kevlar/epoxy composite. T_{cure} of ST-SF/epoxy composite and glass fabric/epoxy composite was approximate the same. However, the T_{cure} of ST-SF/epoxy composite was higher than that of Kevlar/epoxy composite. T_g of ST-SF/epoxy composite after post curing obtained from the first and the second heating scan was higher than that of glass fabric/epoxy composite and much higher than that of Kevlar/epoxy composite. In addition, the thermal stability of ST-SF/epoxy composite was lower than that of the epoxy composite reinforced with glass and Kevlar fabric.

For glass fabric/epoxy composite and Kevlar fabric/epoxy composite, the smooth surface of epoxy matrix next to the fabric was observed. Silk fibers locating inside the silk bundle broke, and fibers locating outside fiber bundle adhered very well closely contacting to epoxy matrix. For glass fabric/epoxy composite, the glass fiber was brittlely broken under impact loading test. In addition, the Kevlar fiber within Kevlar fabric/epoxy composite underwent large deformation before rupture under impact test and Kevlar fiber broke into microfibril.

REFERENCES

- Alagar, M., Ashok Kumar, A., Mahesh, K. P. O., and Dinakaran, K. (2000). Studies on thermal and morphological characteristics of E-glass/Kevlar 49 reinforced siliconized epoxy composites. **Eur. Polym. J.** 36: 2449-2454.
- Alavudeen, A., Thiruchitrambalam, M., Venkateshwaran, N., and Athijayamani, A. (2011). Review of natural fiber reinforced woven composite. **Rev. Adv. Mater. Sci.** 27: 146-150.
- Allred, R., and Roylance, D. (1983). Transverse moisture sensitivity of aramid/epoxy composites. **J. Mater. Sci.** 18: 652-656.
- Alman, G. H., Digz, F., Jaluba, C., Calabro, T., Horam, R. L., Chen, J., *et al.* (2003). Silk-based biomaterials. **Biomaterials.** 24: 401-416.
- Asi, O. (2009). Effect of different woven linear densities on the bearing strength behaviour of glass fiber reinforced epoxy composites pinned joints. **Compos. Struct.** 90: 43-52.
- Aziz, M. E. (2004). **A Study on The Effect of Hardener on The Mechanical Properties of Epoxy Resin.** Iraq Ministry of Higher Education and Scientific Research University of Technology, Baghdad.
- Bayraktar, O., Malay, O., Ozgarip, Y., and Batigun, A. (2005). Silk fibroin as a novel coating material for controlled release of theophylline. **Eur. J. Pharm. Biopharm.** 60: 373-381.

- Benzler, B. (1999). Crosslinking and degree of cure of thermosetting materials by Differential Scanning Calorimetry (DSC). **Information for users of Mettler Toledo thermal analysis systems.**
- Bini, E., Knight, D. P., and Kaplan, D. L. (2004). Mapping domain structures in silks from insects and spiders related to protein assembly. **J. Mol. Biol.** 335: 27-40.
- Byung, C. K., Sang, W. P., and Dai, G. L. (2008). Fracture toughness of the nano-particle reinforced epoxy composite. **Compos. Struct.** 86: 69–77.
- Calventus, Y., Montserrat, S., and Hutchinson, J. M. (2001). Enthalpy relaxation of non-stoichiometric epoxy-amine resins. **Polymer.** 42: 7081-7093.
- Cheng, H., and Kai, S. (1998). Easyare finishing of silk fabrics with a novel multifunctional epoxide. Part 1. **J. Soc. Dyers Colour.** 114: 359-362.
- Chow, W. S. (2007). Water absorption of epoxy/glass fiber/organo-montmorillonite nanocomposites **Express. Polym. Lett.** 1: 104-108.
- Costa, C. C., Calado, V. M. A., and Tavares, F. W. (2005). A Study of Viscoelastic Response of A Bisphenol A Derived epoxy. **2nd Mercosur Congress on Chemical Engineering, 4th Mercosur Congress on Process Systems Engineering, Brazil.**
- Craven, J. P., Cripps, R., and Viney, C. (2000). Evaluating the silk/epoxy interface by means of the Microbond Test. **Composites Part A.** 31: 653-660.
- Cristaldi, G., Latteri, A., Recca, G., and Cicala, G. (2010). Woven fabric engineering (PP 317-342). In P. D. Dubrovski (eds)., **Composites Based on Natural Fibre Fabrics.** Catania: Sciyo.

- D'Almeida, J. R. M., Menezes, G. W. D., and Monteiro, S. N. (2003). Ageing of the DGEBA/TETA epoxy system with off-stoichiometric compositions. **Mat. Res.** 6: 415-420.
- d'Almeida, J. R. M., and Monteiro, S. N. (1998). The influence of the amount of hardener on the tensile mechanical behavior of an epoxy system. **Polym. Adv. Technol.** 9: 216-221.
- Davarpanah, S., Mahmoodi, N. M., Arami, M., Bahrami, H., and Mazaheri, F. (2009). Environmentally friendly surface modification of silk fiber: Chitosan grafting and dyeing. **Appl. Surf. Sci.** 255: 4171-4176.
- Day, R. J., Hewson, K. D., and Lovell, P. A. (2002). Surface modification and its effect on the interfacial properties of model aramid-fibre/epoxy composites. **Compos. Sci. Technol.** 62: 153-166.
- Eakkanalaksamee, T. (2005). **Liquid fuel from co-processing of plastic waste.** Mahidol University, Bangkok.
- Gañan, P., Garbizu, S., Llano-Ponte, R., and Mondragon, I. (2005). Surface modification of sisal fibers: Effects on the mechanical and thermal properties of their epoxy composites. **Polym. Compos.** 26: 121-127.
- George, J., Ivens, J., and Verpoest, I. (1999). Surface modification to improve the impact performance of natural fibre composites. **12th International Conference on Composite Materials (ICCM 12)**, Paris, France.
- George, J., Sreekala, M. S., and Thomas, S. (2001). A review on interface modification and characterization of natural fiber reinforced plastic composites. **Polym. Eng. Sci.** 41: 1471-1485.

- George, J., and Verpoest, J. I. I. (1999). Mechanical properties of flax fibre reinforced epoxy composites. **Angew. Makromol. Chem.** 272: 41-45.
- Gosline, J. H., Guerette, P. A., Ortlepp, C. S., and Savage, K. N. (1999). The mechanical design of spider silks: from fibroin sequence to mechanical function. **J. Exp. Biol.** 202: 3295–3303.
- Goud, G., and Rao, R. N. (2011). Effect of fibre content and alkali treatment on mechanical properties of Roystonea regia-reinforced epoxy partially biodegradable composites. **Bull. Mater. Sci.** 34: 1575-1581.
- Guduri, B. R., and Luyt, A. S. (2006). Mechanical and morphological properties of carbon fiber reinforced–modified epoxy composites. **J. Appl. Polym. Sci.** 101: 3529-3536.
- Guo, F., Zhang, Z.-Z., Liu, W.-M., Su, F.-H., and Zhang, H.-J. (2009). Effect of plasma treatment of Kevlar fabric on the tribological behavior of Kevlar fabric/phenolic composites. **Tribol. Int.** 42: 243-249.
- Hakimi, O., Knight, D. P., Knight, M. M., Grahn, M. F., and Vadgama, P. (2006). Ultrastructure of insect and spider cocoon silks. **Biomacromolecules.** 7: 2901-2908.
- Hakimi, O., Knight, D. P., Vollrath, F., and Vadgama, P. (2007). Spider and mulberry silkworm silks as compatible biomaterials. **Composites Part B.** 38: 324-337.
- He, J., Jia, G., Cui, S., Wang, S., and Gao, Y. (2010). Chemical modification of Bombyx mori silk with calcium-salt treatment and subsequent glycerin triglycidyl ether crosslinking. **J. Appl. Polym. Sci.** 118: 3260-3268.

- Jensen, R. E., Palmese, G. R., and McKnight, S. H. (2006). Viscoelastic properties of alkoxy silane-epoxy interpenetrating networks. **Int. J. Adhes. Adhes.** 26: 103-115.
- Jiang, Z., Gyurova, L. A., Schlarb, A. K., Friedrich, K., and Zhang, Z. (2008). Study on friction and wear behavior of polyphenylene sulfide composites reinforced by short carbon fibers and sub-micro TiO₂ particles. **Compos. Sci. Technol.** 68: 734-742.
- Jin, F.-L., and Park, S.-J. (2012). Thermal properties of epoxy resin/filler hybrid composites. **Polym. Degrad. Stab.** 97: 2148-2153.
- Kanchanomai, C., and Rattananon, S. (2008). Effects of loading rate and thickness on mixed-mode I/II fracture toughness of thermoset epoxy resin. **J. Appl. Polym. Sci.** 109: 2408-2416.
- Kanchanomai, C., Rattananon, S., and Soni, M. (2005). Effects of loading rate on fracture behavior and mechanism of thermoset epoxy resin. **Composites Part B** 24: 886-892.
- Keusch, S., and Haessler, R. (1999). Influence of surface treatment of glass fibres on the dynamic mechanical properties of epoxy resin composites. **Composites Part A** 30: 997-1002.
- Khan, M. M. R., Tsukada, M., Gotoh, Y., Morikawa, H., Freddi, G., and Shiozaki, H. (2010). Physical properties and dyeability of silk fibers degummed with citric acid. **Bioresour. Technol.** 101: 8439-8445.
- Ku, H., Wang, H., Pattarachaiyakoop, N., and Trada, M. (2011). A review on the tensile properties of natural fiber reinforced polymer composites. **Composites Part B.** 42: 856-873.

- Kweon, H., Park, S., Ye, J., Lee, Y., and Cho, C. (2001). Preparation of semi-interpenetrating polymer networks composed of silk fibroin and poly(ethylene glycol) macromer. **J. Appl. Polym. Sci.** 80: 1848-1853.
- Lee, H., and Neville, K. (1967). **Handbook of Epoxy Resins**. New York: McGraw-Hill.
- Lee, S. M., Cho, D., Park, W. H., Lee, S. G., Han, S. O., and Drzal, L. T. (2005). Novel silk/poly(butylene succinate) biocomposites: the effect of short fibre content on their mechanical and thermal properties. **Compos. Sci. Technol.** 65: 647-657.
- Lefevre, T., Paquet-Mercier, F., Lesage, S., Rousseau, M.-E., Bedard, S., and Pezolet, M. (2009). Study by Raman spectromicroscopy of the effect of tensile deformation on the molecular structure of Bombyx mori silk. **Vib. Spectrosc.** 51: 136-141.
- Lettieri, M., and Frigione, M. (2010). Natural and artificial weathering effects on cold-cured epoxy resins. **J. Appl. Polym. Sci.** 119: 1635-1645.
- Lewin, M., and Pearce, E. (eds). (1998). **Handbook of fiber chemistry**. New York: Marcel Dekker.
- Li, G., Liu, H., Li, T., and Wang, J. (2012). Surface modification and functionalization of silk fibroin fibers/fabric toward high performance applications. **Mater. Sci. Eng. C.** 32: 627-636.
- Li, G., Zhang, C., Wang, Y., Li, P., Yu, Y., Jia, X., *et al.* (2008). Interface correlation and toughness matching of phosphoric acid functionalized Kevlar fiber and epoxy matrix for filament winding composites. **Compos. Sci. Technol.** 68: 3208-3214.

- Li, Y., Mai, Y.-W., and Ye, L. (2000). Sisal fibre and its composites: a review of recent developments. **Compos. Sci. Technol.** 60: 2037-2055.
- Liu, Q., and Hughes, M. (2008). The fracture behaviour and toughness of woven flax fibre reinforced epoxy composites. **Composites Part A.** 39: 1644-1652.
- Liu, Y.-L., Wei, W.-L., Hsu, K.-Y., and Ho, W.-H. (2004). Thermal stability of epoxy-silica hybrid materials by thermogravimetric analysis. **Thermochim. Acta.** 412: 139-147.
- Loh, K. M. K., and Tan, C. K. W. (2011). **Natural Silkworm-Epoxy Resin Composite for High Performance Application.** Singapore: InTech.
- Mallick, P. K. (Ed.). (1997). **Composites engineering handbook.** New York: Marcel Dekker.
- May, C. A. (1988). **Epoxy Resins: Chemistry and Technology.** New York: M. Dekker.
- May, C. A., and Tanaka, Y. j. a. (1973). **Epoxy resins; chemistry and technology.** Edited by Clayton A. May and Yoshio Tanaka. New York: M. Dekker.
- Meyers, M. A., Chen, P.-Y., Lin, A. Y.-M., and Seki, Y. (2008). Biological materials: Structure and mechanical properties. **Prog. Mater Sci.** 53: 1-206.
- Mika, T. F., and Bauer, R. S. (1988.). "Curing Agents and Modifiers." in **Epoxy Resins Chemistry and Technology.** New York: Marcel Dekker, Inc.
- Minoshima, K., Maekawa, Y., and Komai, K. (2000). The influence of vacuum on fracture and fatigue behavior in a single aramid fiber. **Int. J. Fatigue** 22: 757-765.
- Mondrel, M., Truudy, K., Kumar, S. N., and Kumar, V. (2007). Scanning electron microscopic study on the cross sections of cocoon filament and degummed

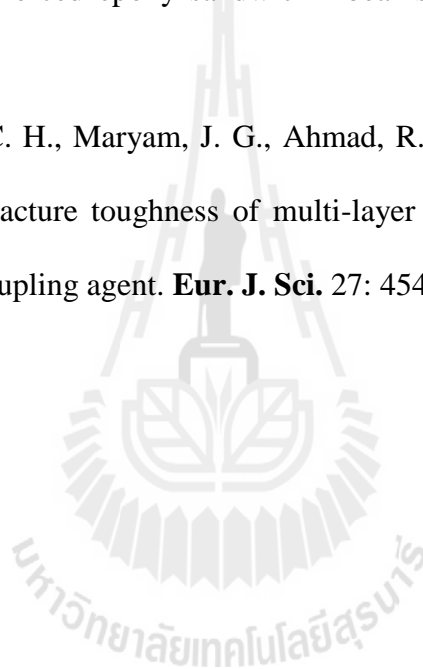
- fiber of different breeds/hybrids of mulberry silkworm, *Bombyx mori* Linn. **J. Entomol.** 4: 362-370.
- Murphy, A. R., John, P. S., and Kaplan, D. L. (2008). Modification of silk fibroin using diazonium coupling chemistry and the effects on hMSC proliferation and differentiation. **Biomaterials.** 29: 2829-2838.
- Mustata, F., and Bicu, I. (2001). Rheological and thermal behaviour of DGEBA/EA and DGEHQ/EA epoxy systems crosslinked with TETA. **Polym. Test.** 20: 533-538.
- Odegard, G. M. B., and Yopadhyay, A. (2011). Physical aging of epoxy polymers and their composites. **J. Polym. Sci., Part B: Polym. Phys.** 49: 1695-1716.
- Okutan, B., Aslan, Z., and Karakuzu, R. (2001). A study of the effects of various geometric parameters on the failure strength of pin-loaded woven-glass-fiber reinforced epoxy laminate. **Compos. Sci. Technol.** 61: 1491-1497.
- Pérez-Rigueiro, J., Viney, C., Llorca, J., and Elices, M. (2000). Mechanical properties of single-brin silkworm silk. **J. Appl. Polym. Sci.** 75: 1270-1277.
- Pérez-Rigueiro, J., Viney, C., Llorca, J., and Elices, M. (2000). Mechanical properties of silkworm silk in liquid media. **Polymer** 41: 8433-8439.
- Plangsangmas, L., Mecholsky, J. J., and Brennan, A. B. (1999). Determination of fracture toughness of epoxy using fractography. **J. Appl. Polym. Sci.** 72: 257-268.
- Plaza, G. R., Corsini, P., Pérez-Rigueiro, J., Marsano, E., Guinea, G. V., and Elices, M. (2008). Effect of water on *Bombyx mori* regenerated silk fibers and its application in modifying their mechanical properties. **J. Appl. Polym. Sci.** 109: 1793-1801.

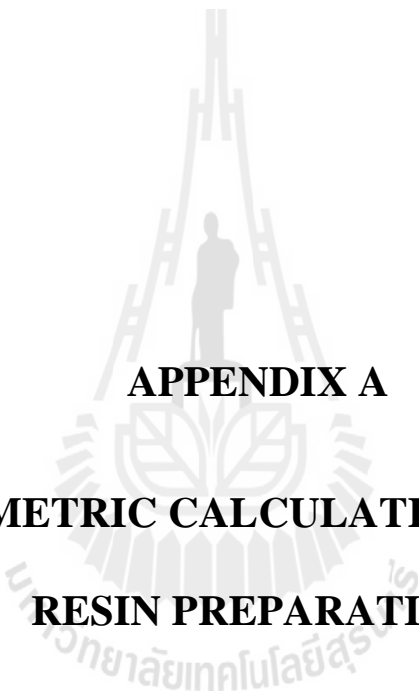
- Poza, P., Perez-Rigueiro, J., Elices, M., and Llorca, J. (2002). Fractographic analysis of silkworm and spider silk. **Eng. Fract. Mech.** 69: 1035-1048.
- Priya, S. P., and Rai, S. K. (2011). Impact, compression, density, void content, and weight reduction studies on waste silk fabric/epoxy composites. **J. Reinf. Plast. Compos.** 24: 1605-1610.
- Priya, S. P., Ramakrishna, H. V., Rai, S. K., and Rajulu, A. V. (2005). Tensile, flexural, and chemical resistance properties of waste silk fabric-reinforced epoxy laminates. **J. Reinf. Plast. Compos.** 24: 643-648.
- Reddy, N., and Yang, Y. (2010). Structure and properties of cocoons and silk fibers produced by *Hyalophora cecropia*. **J. Mater. Sci.** 45: 4414-4421.
- Robinson, E. J., Douglas, E. P., and Mecholsky, J. J. (2002). The effect of stoichiometry on the fracture toughness of a liquid crystalline epoxy. **Polym. Eng. Sci.** 42: 269-279.
- Rochardjo, H. S. B., Komotori, J., Shimizu, M., and Miyano, Y. (1997). Effects of the fiber content on the longitudinal tensile fracture behavior of uni-directional carbon/epoxy composites. **J. Mater. Process. Technol.** 67: 89-93.
- Rong, M. Z., Zhang, M. Q., Liu, Y., Yang, G. C., and Zeng, H. M. (2001). The effect of fiber treatment on the mechanical properties of unidirectional sisal-reinforced epoxy composites. **Compos. Sci. Technol.** 61: 1437-1447.
- Rosu, D., Cascaval, C. N., Mastata, F., and Ciobanu, C. (2002). Cure kinetic of epoxy resins study by non-isothermal DSC data. **Thermochim. Acta.** 383: 119-127.
- Sgriccia, N., Hawley, M. C., and Misra, M. (2008). Characterization of natural fiber surfaces and natural fiber composites. **Composites Part A.** 39: 1632-1637.

- Shen, Y., Johnson, M. A., and Martin, D. C. (1998). Microstructural Characterization of *Bombyx mori* Silk Fibers. **Macromol.** 31: 8857-8864.
- Sirichaisit, J., Brookes, V. L., Young, R. J., and Vollrath, F. (2003). Analysis of structure/property relationships in silkworm (*Bombyx mori*) and spider dragline (*Nephila edulis*) silks using Raman spectroscopy. **Pak. J. Biol. Sci.** 4: 387-394.
- Sonwalkar, T. N. (1993). **Hand book of silk technology**. New Delhi: Wiley Eastern.
- Srihanam, P., Srisuwan, Y., and Simchure, W. (2009). Characteristics of silk fiber with and without sericin component: A comparison between *Bombyx mori* and *Philosamia ricini* silks. **Pak. J. Biol. Sci.** 12: 872-876.
- Suay Antón, J. J., Gómez Ribelles, J. L., Monleón Pradas, M., and Arnau Izquierdo, G. (1999). Anhydride and diamine epoxy–Kevlar composites: thermal and dynamic-mechanical properties. **Polym. Adv. Technol.** 10: 615-619.
- Tanaka, T., Magoshi, J., Magoshi, Y., Ichi Inoue, S., Kobayashi, M., Tsuda, H., *et al.* (2002). Thermal properties of *Bombyx mori* and several wild silkworm silks. Phase transition of liquid silk. **J. Therm. Anal. Calorim.** 70: 825-832.
- Tanaka, Y., and Bauer, R. S. (1988). "Curing Reactions." in **Epoxy Resins Chemistry and Technology**. New York: Marcel Dekker, Inc.
- Tang, L.-G., and Kardos, J. L. (1997). A review of methods for improving the interfacial adhesion between carbon fiber and polymer matrix. **Polym. Compos.** 18: 100-113.
- Tomoyuki, H., and Shaul, M. (2007). Vibrational-exciton couplings for the Amide I, II, III, and A Modes of Peptides. **J. Phys. Chem. B.** 111: 11032-11046.

- Ude, A. U., Ariffin, A. K., Sopian, K., Arifin, A., and Azhari, C. H. (2010). The impact damage response of plain woven natural silk/epoxy laminated composite plates. **IJEST** 2: 128-140
- Vepari, C., and Kaplan, D. L. (2007). Silk as a biomaterial. **Prog. Polym. Sci.** 32: 991-1007.
- Wetze, B., Rosse, P., Houpw, F., and Fond Freddrid, K. (2006). Epoxy nanocomposites – fracture and toughening mechanisms. **Eng. Fract. Mech.** 73: 2375–2398.
- Wu, S. R., Sheu, G. S., and Shyu, S. S. (1996). Kevlar fiber–epoxy adhesion and its effect on composite mechanical and fracture properties by plasma and chemical treatment. **J. Appl. Polym. Sci.** 62: 1347-1360.
- Xie, Y., Hill, C. A. S., Xiao, Z., Militz, H., and Mai, C. (2010). Silane coupling agents used for natural fiber/polymer composites: A review. **Composites Part A.** 41: 806-819.
- Yang, B., Kozey, V., Adanur, S., and Kumar, S. (2000). Bending, compression, and shear behavior of woven glass fiber-epoxy composites. **Composites Part B.** 31: 715-721.
- Yongzhong, W., Hyeon-Joo, K., Gordana, V.-N., and David, L. K. (2006). Stem cell-based tissue engineering with silk biomaterials. **Biomaterials.** 27: 6064–6082.
- Yue, C. Y., and Padmanabhan, K. (1999). Interfacial studies on surface modified Kevlar fibre/epoxy matrix composites. **Composites Part B.** 30: 205-217.
- Zhang, Z., and Evans, D. (2003). Investigation of fracture properties of epoxy at low temperatures. **Polym. Eng. Sci.** 43: 1071-1080.

- Zhao, F. M., and Takeda, N. (2000). Effect of interfacial adhesion and statistical fiber strength on tensile strength of unidirectional glass fiber/epoxy composites. Part I: experiment results. **Composites Part A**. 31: 1203-1214.
- Zhao, R., and Luo, W. (2008). Fracture surface analysis on nano-SiO₂/epoxy composite. **Mater. Sci. Eng. A**. 483-484: 313-315.
- Zhou, G., Forbes, A. J., and Foster, N. (1999). Static behaviour of preconditioned glass-fibre-reinforced epoxy sandwich I-beams. **Compos. Sci. Technol.** 59: 963-973.
- Zulkifli, R., Azhari, C. H., Maryam, J. G., Ahmad, R. L., and Abu, B. S. (2009). Interlaminar fracture toughness of multi-layer woven silk/epoxy composites treated with coupling agent. **Eur. J. Sci.** 27: 454-462.





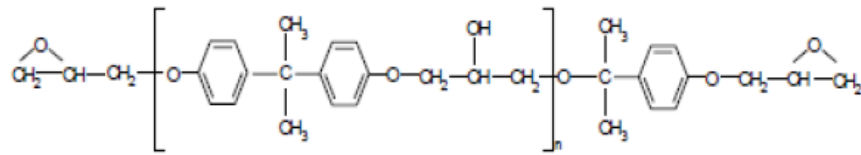
APPENDIX A

STOICHIOMETRIC CALCULATION FOR EPOXY

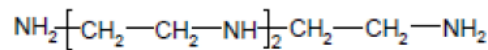
RESIN PREPARATION

Example of a stoichiometric calculation

Epoxy resin: Diglycidyl ether of bisphenol A (DGEBA)



Amine curing agent: Triethylene tetramine (TETA)



Molecular weight of amine:

6 carbon	= 6x12 =	72	(g/mol)
4 nitrogens	= 4x14 =	56	(g/mol)
18 hydrogen	= 18x1 =	18	(g/mol)
Molecular weight	=	<u>146</u>	(g/mol)

Amine hydrogen equivalent weight of amine (AHEW), which is the molecular weight of the amine divided by the number of the active hydrogens, following equation (1).

$$\text{AHEW} = \frac{\text{molecular weight of amine}}{\text{number of active hydrogens}} \dots\dots\dots(1)$$

There are 6 amine active hydrogens functionally reactive with an epoxy group. Therefore, AHEW of TETA = $146 \text{ (g/mol)}/6\text{(equivalents/mol)} = 24.3 \text{ g/ equivalents}$.

Epoxy equivalent weight (EEW), molecular weight of epoxy molecule divided by the number of epoxy group, following equation (2). Where, AHEW and EEW are available from the manufacturer (Thomas and Puckett, 1997).

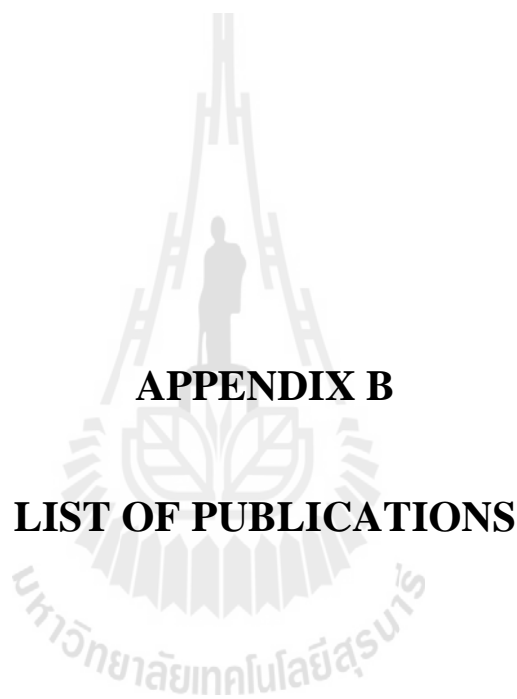
$$\text{EEW} = \frac{\text{molecular weight of epoxy}}{\text{number of epoxy groups}} \dots\dots\dots(2)$$

If, DGEBA has molecular weight of 368 g/mol and there are 2 epoxy groups. Therefore, EEW of DGEBA = $368 \text{ (g/mol)}/2\text{(equivalents/mol)} = 184 \text{ g/ equivalents}$.

The calculation for the amount of added amine, per hundred parts of the epoxy resin (phr), is simply shown in equation (3):

$$\text{phr} = \frac{\text{AHEW}}{\text{EEW}} \times 100 \dots\dots\dots(3)$$

$$\text{Therefore; phr} = \frac{24.3 \text{ g/equivalents}}{184 \text{ g/eqivalents}} \times 100 = 13.2$$



APPENDIX B

LIST OF PUBLICATIONS

มหาวิทยาลัยเทคโนโลยีสุรนารี

List of Publications

Chaisomkul, N., Suppakarn, N., and Sutapun, W. (2010). Mechanical properties and morphology of epoxy composite reinforced by silk fabric. In **Proceeding of Pure and Applied Chemistry International Conference 2010**. (pp 415-418), Bangkok, Thailand.

Chaisomkul, N., Suppakarn, N., and Sutapun, W. (2011). Study of *B. Mori* silk fabric and *B. Mori* silk reinforced epoxy composite. **Adv. Mater. Res.** 410: 329-332.



Mechanical Properties and Morphology of Epoxy Composite Reinforced by Silk Fabric

N. Chaisomkul^{1,2}, N. Suppakarn^{1,2} and W. Sutapun^{1,2*}

¹ School of Polymer Engineering, Institute of Engineering, Suranaree University of Technology, Nakorn Ratchasima 30000, Thailand

² Center of Petroleum, Petrochemical and Advanced Materials, Chulalongkorn University, Bangkok 10330, Thailand

*E-mail: wimonlak@sut.ac.th, Tel: +66-44-224435

Abstract: In this work, silk (*Bombyx mori*) fabric was used as an alternative reinforcement for epoxy (diglycidyl ether of bisphenol-A, DGEBA) composite. The untreated silk fabric (UT-SF)/epoxy composites were prepared by lamination. The content of UT-SF was 0-30 wt%. Mechanical properties, including flexural properties, impact property and heat distortion temperature (HDT) of neat epoxy and the epoxy composites were investigated. Thermal properties of the neat epoxy and the epoxy composites were investigated by the thermogravimetric analysis (TGA) and differential scanning calorimetry (DSC). In addition, morphology of fracture surface of neat epoxy and UT-SF/epoxy composites were examined. It was found that the flexural modulus of epoxy composites did not significantly change with increasing UT-SF content. The flexural strength of the composites was lower than that of neat epoxy. The epoxy composite prepared with 30 wt% UT-SF had impact strength higher than that of epoxy composite prepared with UT-SF lower than 30 wt%. The HDT of epoxy composites increased with increasing fabric content but decreased at 30 wt% UT-SF. The Tg and Tc of UT-SF/epoxy composite were lower than those of neat epoxy. Thermal decomposition of epoxy composites was not significant by different from that of neat epoxy. The neat epoxy, 15 wt% UT-SF/epoxy composite, and 30 wt% UT-SF/epoxy composite were fractured in a brittle manner.

Introduction

Silk is a biopolymer with good mechanical properties and biodegradability [1,2]. Several species of silk spinning insects exist in nature, including caterpillars and spiders. However, silk thread spun by the larvae of silkworm, *Bombyx mori* (*B. mori*), is of practical importance as a source of textile grade fibers [3]. *Bombyx mori* fibers consist primarily of two components, fibroin and sericin [4-6]. Fibroin is the structural protein of silk fiber whereas sericin is the water soluble proteinaceous glue that serves to bond the fibers together. The removal of gum and natural coloring known as degumming will be performed before fiber spinning and textile preparing [7,8]. Some of researchers have reported that woven fabric silk reinforced polymer composite has been used as structural materials for solar car body due to their cost and weight advantages [9,10]. Some physical properties of *B. mori* silk is shown in table 1. The woven silk fabric reinforced epoxy resin is a potential alternative for the man made fiber/epoxy composites [11]. In this work, the silk fabric was used as a reinforced material for an epoxy composite. Mechanical properties (flexural, impact and HDT), thermal properties (DSC and TGA) and

morphology of neat epoxy and silk fabric reinforced epoxy resin were determined.

Table 1 Some physical properties of *B. mori* silk [12]

Properties	Density (g/m ³)	Young's modulus (GPa)	Tensile strength (MPa)	Elongation at break (%)
<i>B. mori</i> silk	1.3-1.8	16	650-750	18-20

Materials and Methods

Materials: The *Bombyx mori* silk fabric was purchased from Housewife group of tumbol Sompoi, Aumphur Rasrisalai, Sisaket Thailand. Diglycidyl ether of bisphenol-A, DGEBA (YD127), with epoxy equivalent weight of 180-187 g/eq was purchased from Thai Organics Chemical Co., Ltd. Triethylenetetramine (TETA), a curing agent, having amine hydrogen equivalent weight of 146 g/eq was purchased from Vista Co., Ltd. The BYK A560 defoamer, for degassing epoxy system, was purchased from Coloshal International Co., Ltd.

Sample preparation: The *Bombyx mori* silk fabric was cut into a square shape of 30 cm x 30 cm and dried in an oven at 110°C for 12 hr to remove moisture. This silk fabric was named UT-SF.

The DGEBA and TETA were mixed by the weight ratio of 100:13.2. The 0.015 cm³ of BYK-A560 was then added into the DGEBA before mixed with TETA. Silk fabric was soaked in the degassed DGEBA for 24 hr before composite preparation. The epoxy composites were prepared by lamination technique with UT-SF content in a range of 10-30 wt%. The epoxy composites were cured at room temperature for 24 hr before post cured in an oven at 110°C for 6 hr. The composites were then cut with a saw to prepare the test specimens for composite characterizations.

Composite characterization: Flexural properties of neat epoxy and UT-SF/epoxy composites were tested according to ASTM D790 using an Instron universal testing machine (model 5569, load cell of 50 kN). The specimen was examined under a span length of 96 mm and a crosshead speed of 2.65 mm/min. At least five specimens were tested for each composition of epoxy composite.

Unnotched Izod impact strength of neat epoxy and UT-SF/epoxy composites were evaluated on Atlas testing machine (BPI) following ASTM D256. The pendulum energy of 2.7 J was used. At least five specimens were tested and the average impact strength were calculated.

Heat distortion temperature (HDT) of neat epoxy and UT-SF/epoxy composites were evaluated on heat distortion temperature instrument (HDV 1 Manual DTVL/VICAT) in accordance with ASTM D648 under a stress of 0.455 MPa with a span length of 100 mm and a heating rate of 2°C/min.

Thermogravimetric analyzer (TA Instrument SDT, 2960) and differential scanning calorimetry (PYRIS Dimond, DSC7) were employed for thermal analysis of neat epoxy and UT-SF/epoxy composites. For TGA analysis, after post cured, neat epoxy and UT-SF/epoxy composites were investigated with a heating rate of 20°C/min under a nitrogen atmosphere. For DSC analysis, neat epoxy before and after post cured and UT-SF/epoxy composites before post cured were examined with a heating rate of 20°C/min under a nitrogen atmosphere. The UT-SF/epoxy composite were prepared as epoxy-coated UT-SF for analyzing by DSC.

The morphology of fracture surface of neat epoxy and UT-SF/epoxy composites obtained from flexural testing were investigated by scanning electron microscope, SEM (JSM 6400), with an accelerating voltage of 10 kV. The samples were coated with gold to avoid charging under an electron beam.

Results and Discussion

The Flexural properties of neat epoxy and epoxy composites are shown in Figure 1. The flexural modulus of epoxy composites did not significantly change with increasing UT-SF content. The flexural strength of neat epoxy and epoxy composite decreased with increasing UT-SF content. However, the flexural modulus and flexural strength tended to increase when the UT-SF was increased to 30 wt%.

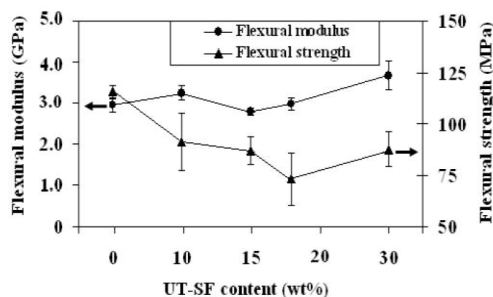


Figure 1 Plot of flexural modulus and flexural strength of neat epoxy and UT-SF/epoxy composites as a function of UT-SF content.

The impact properties of neat epoxy and epoxy composites are shown in Figure 2. The impact strength of the neat epoxy was higher than that of UT-SF/epoxy composites. As weight fraction of UT-SF was increased from 10 wt% to 20 wt%, the impact strength of epoxy composite decreased. However, increasing UT-SF content to 30 wt% led to the improvement of impact strength of the composite upto 10 kJ/m². At UT-SF content lower than 30 wt%, the specimen breaking was initiated by the propagation of voids within the epoxy matrix and at fabric-epoxy interface under impact stress. Nevertheless, at UT-SF of 30 wt%, the fabrics were closely packed by which this made the fabrics absorbing more impact energy. The silk fabric, itself, was able to absorb more impact energy than epoxy resin. As a result, the epoxy composite prepared with 30 wt% UT-SF had impact strength higher than that of epoxy composite prepared with UT-SF lower than 30 wt%. The HDT of neat epoxy and epoxy composite increased with increasing fabric content but it decreased at UT-SF content of 30 wt%, as shown in Table 2.

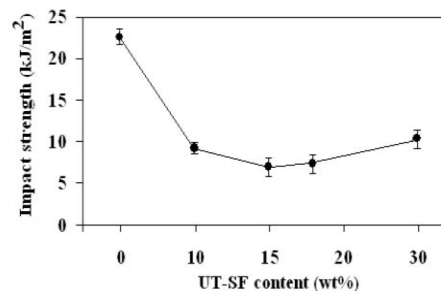


Figure 2 Plot of impact strength of neat epoxy and UT-SF/epoxy composites as a function of UT-SF content.

Table 2 HDT of neat epoxy and UT-SF/epoxy composites at various content of UT-SF.

Properties	Fabric content (wt%)				
	0	10	15	18	30
HDT (°C)	83.7	79.2	91.1	99.8	93.2

The TGA and DTGA curve of UT-SF, neat epoxy after post cured, and UT-SF/epoxy composites after post cured are shown in Figure 3. The TGA and DTGA thermogram of neat epoxy show one transition at 381°C attributed to thermal decomposition of neat epoxy. The thermograms of silk fabric show two transitions in a range of 30°C-800°C. The first transition was observed around 66°C attributed to the evaporation of water and the second transition was observed from 250°C-450°C corresponded to thermal decomposition of the silk fabric. Two thermal transitions of UT-SF/epoxy composites was in a range of 30°C-800°C. The first transition of UT-SF/epoxy composites was observed from 220°C-340°C attributed

to thermal decomposition of silk fabric existing in UT-SF/epoxy composite. It was observed as a shoulder peak at the fabric content of 30 wt%. However, at lower UT-SF content this transition was hardly observed because it was combined with the transition peak of epoxy decomposition. The second transition of UT-SF/epoxy composites was observed from 350°C-450°C corresponded to the thermal decomposition of epoxy and the decomposition peaks were approximately at 381°C.

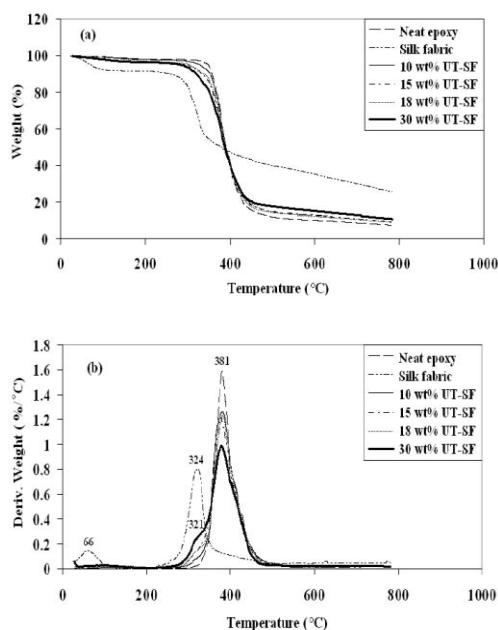


Figure 3 TGA (a) and DTGA curve (b) of neat epoxy and UT-SF/epoxy composites (heating rate of 20 °C/min under N₂ atmosphere).

The DSC curves of neat epoxy and silk fabric coated with epoxy are shown in figure 4. The DSC curve of neat epoxy before post cured shows glass transition temperature (T_g) at 58.4°C and exothermic peak, as a result of cross-linking reaction of epoxy at 117.7°C (T_c). The DSC curve of neat epoxy after post cured at 110°C for 6 hr shows T_g at 98°C and small exothermic peak at 130°C. This indicated that some epoxide groups were not undergone ring opening reaction during the post curing process. After post cured, T_g of neat epoxy was 40°C higher than that of neat epoxy before post cured. The DSC curve of epoxy-coated UT-SF shows T_g at 54.9°C and exothermic peak at 113.4°C. The DSC curve of silk fabric shows only one endothermic peak at 75°C attributed to the evaporation of water, however, this endothermic peak was not observed from the DSC curve of epoxy-coated silk fabric. The lower in T_c and T_g of the epoxy coated on UT-SF indicated that UT-

SF retarded the curing reaction of epoxy at interface even though it was the amide-rich region.

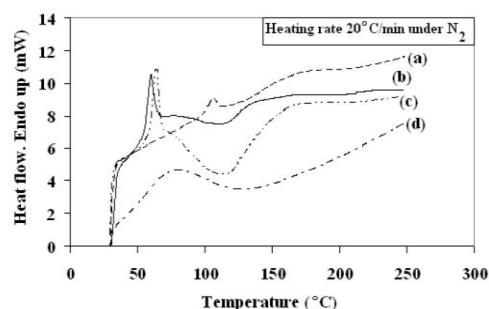


Figure 4 Plot of DSC curve of: (a) neat epoxy after post cured at 110 °C 6 hr, (b) epoxy-coated silk fabric before post cured (c) neat epoxy before post cured, and (d) silk fabric.

The SEM micrograph of neat epoxy shows that it was broken in a brittle manner. Radial striations are observed on fracture surface; the intersection of the striations indicates the fracture initiation site as shown in Figure 5(a). Small radial striations are found in the region which was mirror zone [13].

For 15 wt% UT-SF/epoxy composite, the radial striations running from one fabric surface to another fabric surface, smooth mirror zone and fabric-matrix delamination are observed. In addition, crack propagation are observed along fabric surface. These indicated that the 15 wt% UT-SF/epoxy composite was broken in a brittle manner as shown in Figure 5(b).

The radial striation running from one fabric surface to another fabric surface and smooth mirror zone were also observed in 30 wt% UT-SF/epoxy composite. Even though the delamination was observed at fabric-epoxy interface, the large delamination did not occur as in 30 wt% UT-SF/epoxy composite. In addition, the composites contained no crack in the matrix region. These indicated that the 30 wt% UT-SF/epoxy composite was, as well, broken in a brittle manner, as shown in figure 5(C).

Conclusions

The flexural modulus of epoxy composite did not significantly change with increasing UT-SF content. The flexural strength and impact strength of the composites was lower than that of neat epoxy. The epoxy composite prepared with 30 wt% UT-SF had impact strength and flexural strength higher than that of epoxy composites prepared with UT-SF lower than 30 wt%. The flexural strength and impact strength tended to increase at UT-SF content of 30 wt%. The HDT of epoxy composites increased with increasing fabric content but decreased at 30 wt% UT-SF. The T_g and T_c of epoxy coated on silk fabric were lower than

those of neat epoxy. This indicated that UT-SF retarded the curing reaction of epoxy at interface. Thermal decomposition of epoxy composites was not significantly different from that of neat epoxy. The neat epoxy, 15 wt% UT-SF composites, and 30 wt% UT-SF composite were fractured in a brittle manner.

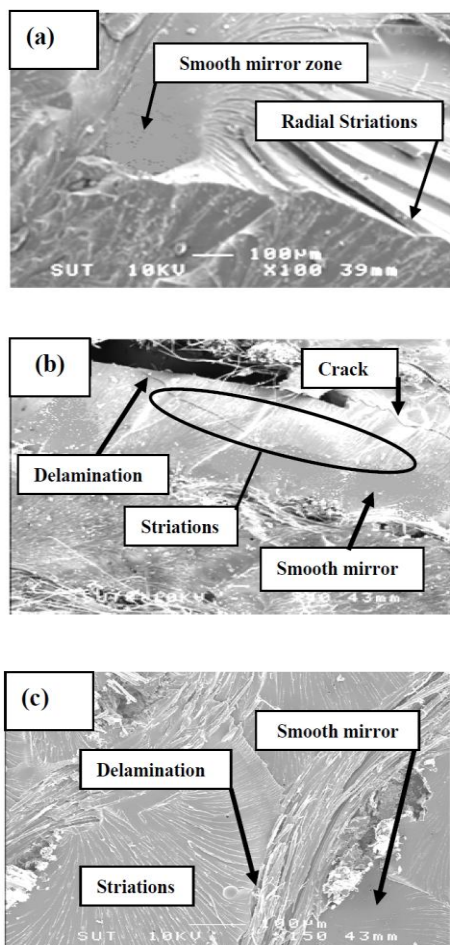


Figure 5 SEM micrographs of neat epoxy and UT-SF/epoxy composites; (a) neat epoxy at a magnification of 100x, (b) 15 wt% UT-SF/epoxy composite at a magnification of 40x, and (c) 30 wt% UT-SF/epoxy composite at a magnification of 150x.

Acknowledgements

The authors would like to express their thanks to Suranaree University of Technology and Center for Petroleum, Petrochemicals, and Advanced Materials for financial support.

References

- [1] H.J. Jin, J. Park, R. Valluzzi and D.L. Cebe, *Biomacromolecules*, **5** (2004), pp. 711-717.
- [2] H.-Y. Cheung, K.-T. Lau, Y.-F. Paw, Y.-Q. Zhao and D. Hui, *Composites Part B*, **41** (2009) pp. 223-228.
- [3] Md.M.R. Khan, H. Morikawa, Y. Gohto, M. Miura, Z. Ming, Y. Sato and M. Iwasa, *Biomacromolecules*, **42** (2008), pp. 264-270.
- [4] Y. Shen, M.A. Jhonson and D.C. Martin, *Macromol.* **31** (1998), pp. 8857-8864.
- [5] H. Zhang, J. Magoshi, M. Becker, J.Y. Chen and R. Matsunaga, *J. Appl. Polym. Sci.* **86** (2002), pp. 1817-1820.
- [6] M.A. Meyers, P.-Y. Chen, A.Y.-M. Lin and Y. Seki, *Mater. Sci.* **53** (2008), pp 201-206
- [7] G. Freddi, R. Mossotti and R. Innocenti., *Biotechnol.* **106** (2003), pp. 106-112.
- [8] D. Sargunamani and N. Selvakumar, *Polym. Degrad. Stab.* **91** (2006), pp. 2644-2653.
- [9] R. Zulkifli, C.H. Azhari, M.J. Ghazali, A.R. Ismail and A.B. Sulong, *Eur. J. Sci.* **27** (2009), pp.454-462.
- [10] A.U. Ude, A.K. Ariffin, K.Sopian and C. H. Azhari, *J. Eng. Appl. Sci.* **5** (2010), pp 75-87.
- [11] W. Sutapun, P. Rossapol, S. Keaw-on and D. Kittilurkul, Proceeding of The 2nd International Conference Advances in Petrochemicals and Polymer, (2007) BC-22.
- [12] J. Perez-Rigueir, C. Viney, J. Llorca and M. Elices, *J. Appl. Polym. Sci.* **75** (2000), pp. 1270-1277.
- [13] R. Zhao and W. Lao, *Mater. Sci. Eng., A*, **483-484** (2008), pp 313-315.

Advanced Materials Research Vol. 410 (2012) pp 329-332
 Online available since 2011/Nov/29 at www.scientific.net
 © (2012) Trans Tech Publications, Switzerland
 doi:10.4028/www.scientific.net/AMR.410.329

STUDY OF *B. Mori* SILK FABRIC AND *B. Mori* SILK REINFORCED EPOXY COMPOSITE

N. Chaisomkul^{1,2,a}, N. Suppakarn^{1,2,b} and W. Sutapun^{1,2,c}

¹ School of Polymer Engineering, Institute of Engineering, Suranaree University of Technology,
 Nakorn Ratchasima 30000, Thailand

² Center for Petroleum, Petrochemical and Advanced Materials, Chulalongkorn University,
 Bangkok 10330, Thailand

^aChaisomkul_na@hotmail.com, ^bnitinat@sut.ac.th, ^cwimonlak@sut.ac.th

Keywords: *B. mori* silk, Silk/epoxy composite, Natural fiber/epoxy composite.

Abstract. In this work, degummed (*Bombyx mori*) silk fabric was used as a bio-reinforcement for epoxy composite. The silk fabric was in a form of plain weaving with 177 ends/10 cm x 201 picks/10 cm. The degummed silk fabric (dSF)/epoxy composites were prepared by hand lay-up with dSF weight fraction of 0.18-0.35. The dSF was characterized using a universal testing machine (UTM) and a thermogravimetric analyzer (TGA). Mechanical properties including tensile properties, and impact property of neat epoxy and epoxy composites were investigated using a UTM and an impact testing machine, respectively. Thermal properties of neat epoxy and dSF/epoxy composites were investigated using a TGA. In addition, morphology of fracture surface of neat epoxy and dSF/epoxy composite were examined via a scanning electron microscope. Tensile strength of dSF was not significantly dependent in direction, was 537.1 N in warp direction, and 555 N in weft direction. In addition, dSF decomposed at 324°C under nitrogen atmosphere. The tensile strength and impact strength of the neat epoxy were higher than those of dSF/epoxy composites. However, tensile strength and impact strength tended to increase with increasing dSF content. On the other hand, Young's modulus was improved by addition of dSF. The dSF/epoxy composites still fractured in a brittle manner.

Introduction

Silk is a biopolymer with good mechanical properties and biodegradability [1]. Several species of silk spinning insects exist in nature, including caterpillars and spiders. Practically, silk thread spun by silk worm larvae of *Bombyx mori* (*B. mori*), is a good source of textile grade fiber [2]. *B. mori* fiber consists primarily of two components, fibroin and sericin [3,4]. Fibroin is the structural protein of the fiber and sericin is the water soluble proteinaceous glue that serves to bond the fibers together. The removal of the sericin known as degumming is performed before fiber spinning and textile preparing [5,6]. Besides its esthetic appearance, tensile strength of the silk fiber (0.2-0.9 N/tex) falls in that range of synthetic reinforcement (0.8-1.8 N/tex) used for epoxy composite such as glass fiber and kevlar fiber [7, 8]. Nevertheless, elongation at break of silk fiber (17-20%) is much higher than that of synthetic fiber (2-4%) [7,8]. Composite reinforcement is employed in several geometrical forms such as woven, braided, knitted, chopped strand mat etc. [9]. According to its mechanical properties and availability, the woven silk fabric must be a good alternative reinforcement for epoxy composite. In this work, degummed (*B. mori*) silk fabric was used as a bio-reinforcement for epoxy composite.

Materials and Methods

Materials. The degummed *B. mori* silk fabric (plain weaving with 177 ends/10cm x 201 picks/10cm) was purchased from Housewife group of Tumbol Sompoi, Aumphur Rasrisalai, Sisaket Thailand. Diglycidyl ether of bisphenol-A, DGEBA (YD127), with epoxy equivalent weight of 180-187 g/eq, was purchased from Thai Organics Chemical Co., Ltd. Triethylenetetramine

(TETA), a curing agent, having amine hydrogen equivalent weight of 146 g/eq was purchased from Vista Co., Ltd. The BYK A560 defoamer, for degassing epoxy system, was purchased from Coloshal International Co., Ltd.

Silk fabric preparation. The degummed silk fabric (dSF) was cut into a square shape of 30 cm x 30 cm for composite preparation and dried in an oven at 110°C for 12 hr to remove moisture.

Composite preparation. First, the 0.015 cm³(cal.) of BYK A560 was added into DGEBA and then the DGEBA was degassed for 24 hr before mixed with TETA. The DGEBA and TETA were mixed by the weight ratio of 100:13.2. The neat epoxy and epoxy composite were prepared by hand lay-up. The composite was made with dSF weight fraction of 0.18-0.35. The neat epoxy and epoxy composites were cured at room temperature for 24 hr before post cured in an oven at 110°C for 6 hr. The neat epoxy and epoxy composites were then cut for test specimen preparation prior to composite characterization.

Material characterization. Tensile properties of dSF, 10 cm x 15 cm, were tested in warp and weft direction according to ASTM D5034 using a universal testing machine (Lloyds, Model LR-5K). The specimen was examined under a crosshead speed of 300 mm/min with load cell of 5kN.

Tensile properties of neat epoxy and dSF/epoxy composite were determined in accordance with ASTM D 5083 under a universal testing machine (Instron model 5569). The specimen was tested in uniaxial tension at a crosshead speed of 5 mm/min with load cell of 50 kN.

Unnotched Izod impact strength of neat epoxy and dSF/epoxy composites were evaluated on Atlas testing machine (BPI) following ASTM D256 using pendulum energy of 2.7 J.

Thermogravimetric analyzer (TA Instrument SDT, 2960) was employed for thermal analysis of silk fiber, neat epoxy and dSF/epoxy composites with a heating rate of 20°C/min under a nitrogen atmosphere.

The fracture surface morphology of neat epoxy and dSF/epoxy composites obtained from tensile test were investigated using scanning electron microscope, SEM (JSM 5410LV), with an accelerating voltage of 15 kV.

Results and Discussion

The tensile strength and elongation at break of plain weaving dSF are listed in Table 1. Tensile strength (TS) and elongation at break (EB) of silk fabric in warp direction and weft direction of dSF were not significantly different. The TS was in a range of 537-555 N and the EB was in a range of 15-16%. The tensile properties of neat epoxy and epoxy composites are shown in Fig. 1. The tensile modulus of epoxy composites increased with increasing weight fraction of dSF. Tensile strength of neat epoxy was higher than those of epoxy composites and tensile strength of the composites increased with increasing weight fraction of dSF. The impact property of neat epoxy and epoxy composites is shown in Fig. 2. Impact strength of neat epoxy was higher than those of dSF/epoxy composites. Nevertheless, the impact strength of epoxy composites increased with increasing dSF content.

Table. 1 Tensile strength of plain weaving degummed silk fabric.

Testing direction	Tensile strength* (N)	Elongation at break (%)
Warp (177 ends/10 cm)	537±0.95	15.22±0.57
Weft (201 picks/10cm)	555±1.26	16.08±0.86

* Tensile strength: tensile force at break.

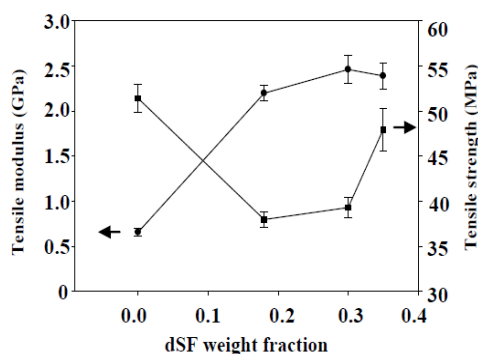


Figure 1. Tensile modulus and strength of neat epoxy and epoxy

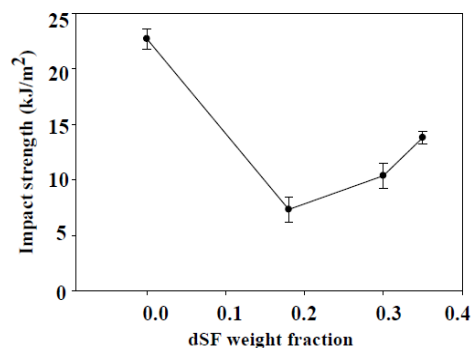


Figure 2. Impact strength of neat epoxy and epoxy composites.

The TGA and DTGA curves of dSF, neat epoxy and dSF/epoxy composites are shown in Fig 3. The thermograms of dSF show two transitions in a range of 30-800°C. The first transition was observed around 66°C attributed to the evaporation of water and the second transition was observed at 324°C due to thermal decomposition of silk fibroin [10, 11]. The TGA and DTGA thermogram of neat epoxy show one transition at 381°C attributed to thermal decomposition of neat epoxy. Two thermal transitions of dSF/epoxy composites were observed. The first transition of dSF/epoxy composites was observed around 220-340°C attributed to thermal decomposition of silk fabric existing in dSF/epoxy composite. However, this composition peak was observed as a shoulder peak for epoxy composites prepared with 0.30 and 0.35 dSF. In addition, at dSF content of 0.18, this transition was hardly observed because the peak was combined with the peak of epoxy decomposition. The second transition of dSF/epoxy composites was observed from 350-450°C corresponded to the thermal decomposition of epoxy and the decomposition peaks were approximately observed at 381°C.

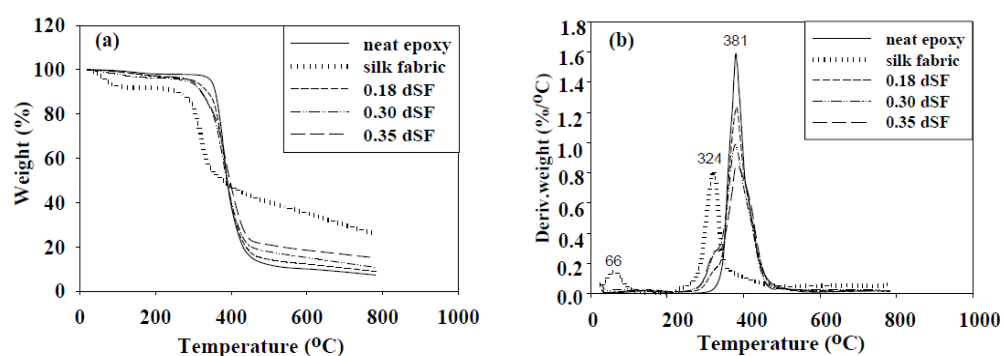


Figure 3. TGA (a) and DTGA curves (b) of neat epoxy and dSF/epoxy composites.

The fracture surface of neat epoxy contained radial striations and a mirror zone, as observed in its SEM micrograph shown in Fig. 4(a). The intersection of striations was a initiation site for fracture [12,13]. The radial striations and a mirror zone were the evidence that neat epoxy fractured in a brittle manner.

For dSF/epoxy composites, radial striations running from one fabric surface to another fabric surface and also smooth mirror zone were observed from the fracture surface as depicted in Fig. 4(b) and Fig. 4(c). It meant that the dSF/epoxy composites fractured in a brittle manner, as well. However, the size of a mirror zone was minimized with increasing dSF content, as seen in Fig. 4 (a-c), resulting in increase of the impact strength of the composites prepared with 0.30 and 0.35

dSF. In addition, the large delamination was observed on fracture surface of a dSF/epoxy composites prepared with 0.18 and 0.35 dSF, as shown in Fig 4(b,c).

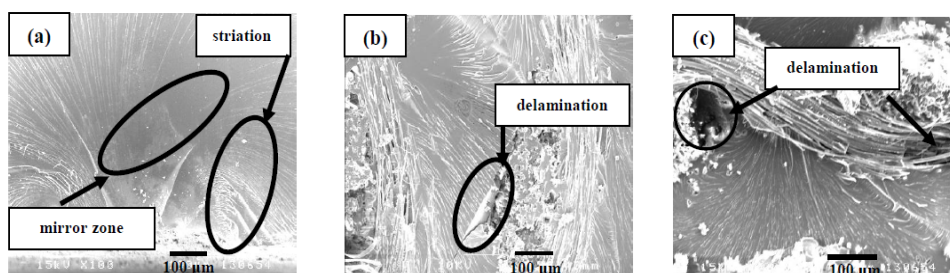


Figure 4. SEM micrographs of neat epoxy and dSF/epoxy composites at a magnification of 100; (a) neat epoxy, (b) dSF/epoxy composite with 0.18 dSF, and (c) dSF/epoxy composite with 0.35 dSF.

Conclusions

The tensile strength of dSF in warp and weft direction were not different and in a range of 537-555 N. In addition, dSF decomposed at 324°C under a nitrogen atmosphere. The tensile strength and impact strength of neat epoxy was higher than those of dSF/epoxy composites. However, tensile strength and impact strength tended to increase with increasing dSF content. On the other hand, Young's modulus was improved by addition of dSF. The dSF/epoxy composites still fractured in a brittle manner.

Acknowledgements

The authors would like to express their thanks to Suranaree University of Technology and Center of Petroleum, Petrochemicals and Advanced Materials for financial support, and Queen Sirikit Sericulture Center (Nakornratchasima) for providing LLOY UTM instrument.

References

- [1] H. J. Jin, J. Park, R. Valluzzi and D. L. Cebe: *Biomacromolecules*. Vol. 5 (2004), p. 711.
- [2] M. D. M. R. Khan, H. Morikawa, Y. Gohto, M. Miura, Z. Ming, Y. Sato and M. Iwasa: *Biomacromolecules*. Vol. 42 (2008), p. 264.
- [3] Y. Shen, M. A. Jhon son and D. C. Martin: *Macromol*. Vol 31 (1998), p. 8858.
- [4] M. A. Meyers, P.-Y. Chen, A. Y.-M. Lin and Y. Seki: *Mater. Sci*. Vol. 53 (2008), p 201.
- [5] G. Freddi, R. Mossotti and R. Innocenti: *Biotechnol*. Vol. 106 (2003), p. 106.
- [6] D. Sargunamani and N. Selvakumar: *Polym. Degrad. Stab*. Vol. 91 (2006), p. 2644.
- [7] R. Zulkifli, C. H. Azhari, M. J. Ghazali, A. R. Ismail and A. B. Sulong: *Eur. J. Sci*. Vol. 27 (2009), p.454.
- [8] P. K. Mallick: *Composites Engineering Handbook* (Marcel Dekker Publications, New York 1997).
- [9] K. K. Chawala: *Composite Materials* (Marcel Dekker Publications, New York 1998).
- [10] Reddy and Yang: *J. Mater. Sci*. Vol. 45 (2010), p. 17.
- [11] Srihanam, Srisuwan and Simchure: *Int. J. Chem. Technol*. Vol. 2 (2010), p. 23.
- [12] R. Zhao and W. Lao: *Mater. Sci. Eng., A*. Vol. 483-484 (2008), p. 313.
- [13] Almeida and Monteiro: *Polymer. Adv. Tech*. Vol. 9 (1998), p. 21

BIOGRAPHY

Miss Nattida Chaisomkul was born on July 24, 1985 in Roi-Et, Thailand. She earned her Bachelor's Degree in Polymer Engineering from Suranaree University of Technology (SUT) in 2007. After that, she then continued her Master's degree in Polymer Engineering at School of Polymer Engineering, Institute of Engineering, Suranaree University of Technology. During her master's degree study, she presented two poster presentations entitle: "**Mechanical properties and morphology of epoxy composite reinforced by silk fabric**" at the Pure and Applied Chemistry International Conference 2010 (PACCON 2010) in Bangkok, Thailand and "**Study Of *B. Mori* silk fabric and *B. Mori* silk reinforced epoxy composite**" at Processing and Fabrication of Advanced Materials XX (PFAM XX 2011) in Hong Kong, China.

